INFORMATION TO USERS

This manuscript has been reproduced from the microfilm master. UMI films the text directly from the original or copy submitted. Thus, some thesis and dissertation copies are in typewriter face, while others may be from any type of computer printer.

The quality of this reproduction is dependent upon the quality of the copy submitted. Broken or indistinct print, colored or poor quality illustrations and photographs, print bleedthrough, substandard margins, and improper alignment can adversely affect reproduction.

In the unlikely event that the author did not send UMI a complete manuscript and there are missing pages, these will be noted. Also, if unauthorized copyright material had to be removed, a note will indicate the deletion.

Oversize materials (e.g., maps, drawings, charts) are reproduced by sectioning the original, beginning at the upper left-hand corner and continuing from left to right in equal sections with small overlaps. Each original is also photographed in one exposure and is included in reduced form at the back of the book.

Photographs included in the original manuscript have been reproduced xerographically in this copy. Higher quality 6" x 9" black and white photographic prints are available for any photographs or illustrations appearing in this copy for an additional charge. Contact UMI directly to order.

UMI

A Bell & Howell Information Company
300 North Zeeb Road, Ann Arbor MI 48106-1346 USA
313/761-4700 800/521-0600

UNIVERSITY OF ALBERTA

Development of Microlens Technology

by

Huy Tran The Nguyen ©

A thesis submitted to the Faculty of Graduate Studies and Research in partial fulfillment of the requirements for the degree of **Master of Science**

Department of Electrical and Computer Engineering

Edmonton, Alberta

Fall 1997

National Library of Canada

Bibliothèque nationale du Canada

Acquisitions and Bibliographic Services

Acquisitions et services bibliographiques

395 Wellington Street
Ottawa ON K1A 0N4
Canada

395, rue Wellington
Ottawa ON K1A 0N4
Canada

Your file Votre référence

Our file Notre référence

The author has granted a non-exclusive licence allowing the National Library of Canada to reproduce, loan, distribute or sell copies of this thesis in microform, paper or electronic formats.

L'auteur a accordé une licence non exclusive permettant à la Bibliothèque nationale du Canada de reproduire, prêter, distribuer ou vendre des copies de cette thèse sous la forme de microfiche/film, de reproduction sur papier ou sur format électronique.

The author retains ownership of the copyright in this thesis. Neither the thesis nor substantial extracts from it may be printed or otherwise reproduced without the author's permission.

L'auteur conserve la propriété du droit d'auteur qui protège cette thèse. Ni la thèse ni des extraits substantiels de celle-ci ne doivent être imprimés ou autrement reproduits sans son autorisation.

0-612-22649-2

Canada

UNIVERSITY OF ALBERTA

Library Release Form

Name of Author: Huy Tran The Nguyen

Title of Thesis: Development of Microlens Technology

Degree: Master of Science

Year this Degree is granted: 1997

Permission is hereby granted to the University of Alberta Library to reproduce single copies of this thesis and lend or sell such copies for private, scholarly, or scientific research purposes only.

The author reserves all other publication and other rights in association with the copyright in the thesis, and except as hereinbefore provided, neither the thesis nor any substantial portion thereof may be printed or otherwise reproduced in any material form whatever without the author's prior written permission.

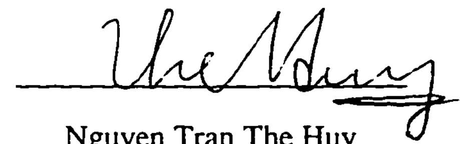

Nguyen Tran The Huy

6503-93A Ave, Edmonton

Alberta, Canada, T6B 0X1.

Date: June 27, 1997

UNIVERSITY OF ALBERTA

Faculty of Graduate Studies and Research

The undersigned certify that they have read, and recommended to the Faculty of Graduate Studies and Research for acceptance, a thesis entitled

"Development of Microlens Technology"

submitted by **Nguyen Tran The Huy** in partial fulfillment of the requirements for the degree of **Master of Science**.

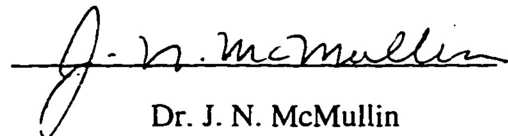

Dr. J. N. McMullin

Supervisor

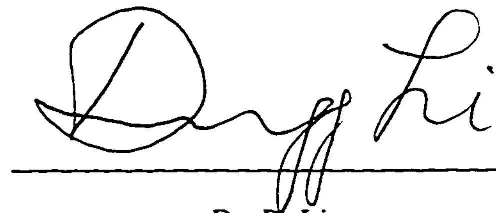

Dr. D. Li

Mechanical Eng.

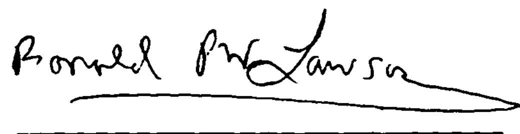

Dr. R. P. W. Lawson

Elec. and Comp. Eng.

Date: 23 June 1997

Dedicated to my relatives and friends.

ABSTRACT

This thesis describes work done to improve the dispensed polymer microlens technology developed at TRLabs (Edmonton). The shape of a dispensed polymer lens is determined by surface tension and adhesion of the polymer to the substrate. The properties of eleven different polymers were measured. By using dispensed polymer microlenses as etching masks, the fabrication of fused silica and silicon microlenses was investigated. A process that allows the control of F# (lens focal length/lens diameter) for a certain microlens design was developed. In microlens testing, methods for the effective use of a laboratory Mach-Zehnder interferometer were developed. Some attempts to reduce microlens wave aberration were made experimentally.

Acknowledgement

This work has been influenced directly and indirectly by a number of individuals. Therefore, I would like to take this opportunity to express my sincere thanks to every one of them for their support in all aspects.

First of all, I would like to thank my supervisor, Dr. J. N. McMullin, for recruiting me to work on this project and for letting me become a TRLabs student. His guidance during the project has helped me learn more about how to improve myself further.

I would like to thank the members of my examining committee, Dr. J. N. McMullin, Dr. R. P. W. Lawson and Dr. D. Li, for reviewing this thesis. It was an honor for me to be encouraged and advised by Dr. R. I. MacDonald and Dr. B. P. Keyworth who especially gave me support for my work at AMC. My special thanks are also extended to Dino Corazza for his invaluable assistance in many aspects related to my work.

I also wish to thank Graham McKinnon, Jim Broughton, Glen Fiztpatrick, Tran Tran and all the staff at AMC for technical assistance as well as for being encouraging. In addition, I would like to thank Dr. Beatrys Lacquet, a visiting professor from South Africa, for being willing to discuss some problems which occurred in my work.

My thanks are also expressed to my colleagues at TRLabs for their helpful advice in different moments. I would like to thank Lorin Mabbott, Jonathan Holzman for preparing some samples, Rajkumar Nagarajan, Yong Zheng, Sing Cheng, Dave Boertjes, Sheldon Walklin, Alan Hnatiw, Reza Paiam, Erik Johnson and a number of other students of HyPIC and TRLabs for their input at various times.

I would like to thank my parents, my relatives and all my friends who have always supported me physically and mentally and have been very patient with me.

Finally, I would like to acknowledge TRLabs for their financial support and the administration staff for their assistance without which this work would not have been possible.

Table of Contents

1. INTRODUCTION 1
1.1 The History of Microlenses 1
1.1.1 Single Microlenses 1
1.1.2 Microlens Arrays 2

1.2 Applications 5
1.2.1 Free-Space Optical Bus 6
1.2.2 VCSEL Package 7
1.2.3 Free-Space Optoelectronic Switch 7

1.3 Project Objective and Overview 9

2. POLYMER MICROLENS FABRICATION 10
2.1 The Theory of Liquid Lens Formation 10
2.2 The Dispensing Technique 15
2.3 Measurements of Various Optical Polymers 21
2.4 Discussion 27

3. GLASS AND SILICON MICROLENS FABRICATION 28
3.1 Reactive Ion Etching 29
3.1.1 Basic Concepts 29
3.1.2 Process Control Parameters 32

3.2 Preliminary Investigations 33
3.2.1 Analysis of Etched Shapes 33
3.2.2 Initial Etch 36
3.2.3 Scanning Accuracy with the Profilometer 40
3.2.4 The Role of Cleaning Process 41

3.3 Process Control 46
3.3.1 F# and Selectivity Analysis 46
3.3.2 Etch Recipe Characterization 48

3.4 Discussion 52

4. MICROLENS TESTING 53
4.1 Overview on Microlens Measurements 53

4.2 Mach-Zehnder Interferometer 54
4.2.1 Main Concepts 54
4.2.2 Set up Requirements 59

4.3 Test Procedures 63
4.3.1 Diameter 63
4.3.2 Focal Length and Spot Size 65
4.3.3 Interferogram Generation and Interpretation 68

4.4 Summary 70

5. INVESTIGATION OF MICROLENS ABERRATION 71
5.1 Gravity Effect Tests 71
5.1.1 Aberrations in the Transition Region 72
5.1.2 Aberration of Large Diameter Microlenses...72
5.2 Etch Selectivity Effect Tests 75
6. CONCLUSION.. 78
REFERENCES 80
APPENDIX I 85
APPENDIX II 90
APPENDIX III 92

List of Tables

Table 2.1: Specifications of spherical dispensed polymer microlenses. 20

Table 3.1: Dispensing parameters for initial etched samples 38

Table 3.2: Lens characteristics comparison. 43

Table 3.3: Estimated and measured F#s of quartz microlenses 47

Table 3.4: Examples of guessed recipes...47

Table 4.1: Conversion factor for diameter measurement. 65

Table I.1: Measurement results for various polymers...87

Table III.1: Zoom lens VZM 0.7× – 4.5×. 93

Table III.2: Microobjectives...93

Table of Figures

Figure 1.1: Scanning Electron Microscope (SEM) pictures of part of a dispensed polymer spherical microlens array 5
Figure 1.2: Dispensed polymer microlenses used in "extractor card" 6
prototyping 6
Figure 1.3: Dispensed polymer microlenses used in VCSEL packaging 7
Figure 1.4: Dispensed polymer microlenses used in free-space switch 8
Figure 2.1: The analysis of drop shape 12
Figure 2.2: Dimensions of dispensed polymer lenses 14
Figure 2.3: The principal illustration of dispensing set up 16
Figure 2.4: Defining the surface of dispensing 17
Figure 2.5: A sequence of dispensing 18
Figure 2.6: Dispensing stage set up 19
Figure 2.7: Multiple layer dispensed polymer microlenses of F# = 1.3 19
Figure 2.8: Anamorphic lens 20
Figure 2.9: Scanned cylindrical profiles of NOA 63 22
Figure 2.10: Scanned cylindrical profiles of NOA 65 23
Figure 2.11: Scanned cylindrical profiles of NOA 68 24
Figure 2.12: The relation between contact angle and lens size of polymers 26
NOA 63, 65, 68 26
Figure 3.1: Basic low pressure processes of plasma etching 30
Figure 3.2: The effect of plasma-enhanced chemical reaction on etch rate 31
Figure 3.3: Illustration of anisotropic (directional) etch 32
Figure 3.4: Transferring dispensed polymer microlens patterns into substrate by RIE 34
Figure 3.5: Etched lens formed by RIE process 34
Figure 3.6: Partially etched profiles scanned with profilometer 35
Figure 3.7: Dispensed polymer microlenses which were initially etched 37
Figure 3.8: SEM pictures of the initially etched quartz sample 39
Figure 3.9: Corning 7059F glass was not etched by RIE 40
Figure 3.10: The effect of scanning speed on the accuracy 41
Figure 3.11: The first completely etched quartz microlens array 43
Figure 3.12: Damaged etched surfaces before surface correction 44
Figure 3.13: No thermal effect on cylindrical polymer surface by baking; Magnification 153× 44
Figure 3.14: Microscope pictures of similar microlens arrays between damaged surfaces (a) and corrected surfaces (b) 45
Figure 3.15: Polymer partially stripped after having been partially etched 50
Figure 3.16: The effect of O_2-flow on etch selectivity 51
Figure 3.17: The effect of plasma power on substrate etch rates 51
Figure 4.1: The operation principle of a Mach-Zehnder interferometer 55
Figure 4.2: Concepts of light waves 56
Figure 4.3: Interference of two plane waves 56
Figure 4.4: Interference of non-plane waves with a plane wave 57
Figure 4.5: The effect of perfect lenses for plane waves 58
Figure 4.6: The effect of a nonperfect lens on plane wave 58
Figure 4.7: The schematic layout of the Mach-Zehnder interferometer 60
Figure 4.8: Two actual views of the schematic layout in Fig. 4.7 without components 10, 11 and 12 61
Figure 4.9: Measurement configurations with Mach-Zehnder interferometer 62

Figure 4.10: Positions for lens diameter measurement. 64
Figure 4.11: Set up for diameter measurement with IPLab software. 64
Figure 4.12: Set up for focal length measurement...65
Figure 4.13: the concept of focal point. 66
Figure 4.14: Positions for focal length measurement. 67
Figure 4.15: Display fringe patterns in interferogram generation procedure.................69
Figure 5.1: Wave aberration of polymer lenses in the transition range. 73
Figure 5.2: Severe wave aberration of large polymer (NOA 63) lenses......................74
Figure 5.3: Large polymer lenses dispensed on polymer film(NOA 63 on NOA 63).......75
Figure 5.4: Effect of etch selectivity on wave aberration of quartz microlenses............76

List of Abbreviations

AMC	Alberta Microelectronics Center
CCD	charge-coupled device
CITR	Canadian Institute for Telecommunications Research
CVD	chemical vapor deposition
GRIN	gradient-index or graded index
IC	integrated circuit
LED	light-emitting-diode
MFC	mass flow controller
MTF	modulation transfer function
NOA	Norland Optical Adhesive
PMMA	Polymethyl methacrylate
PSF	point spread function
RIE	reactive ion etching
SEM	scanning electron microscope
TRLabs	Telecommunications Research Laboratories
UV	ultra-violet
VCSEL	vertical cavity surface emitting laser

List of Symbols

θ, α	The static contact angle
γ	Surface tension
r	radial coordinate
Z	The dimensionless z-coordinate
b	The radius of curvature at the liquid drop vertex
g	The gravity acceleration
ρ	density
h	The height of the microlens
n	Refractive index
F#	f-number of lenses
W	The width of the cylindrical microlens
S	The selectivity
D, ∅	The diameter of the microlens
f	The paraxial focal length of the microlens
I	Light intensity
λ	Wavelength
NA	The numerical aperture of lenses
WA	Wave aberration
NG	Negative gravity
PG	Positive gravity

1. INTRODUCTION

The revolution in telecommunications has made photonics become a multi-disciplinary field. The goals of researchers in the field are to look for different types of components, component technology and device structures right up to the system level to fulfill the required demands of the industry. One of the important functions is the coupling of laser light into optical fibers and waveguides. There are other applications which have also motivated researchers to look for effective fabrication techniques of microlenses and microlens arrays. This chapter will give a brief view on the history of microlenses, the project objective and the outline of the thesis.

1.1 THE HISTORY OF MICROLENSES

Various types of microlenses have been developed for the growing demands of modern technology. At first, only methods for the fabrication of microlenses on the endfaces of single-mode fibers were reported. Following these, different techniques were successively developed for combination lens-coupling, microlens arrays, and integrated microlenses. Accordingly, different microlens fabrication methods such as photolithography, chemical etching, thermal melting, mechanical polishing have been developed. The following subsection describes some of the highlights of this development adapted from Ref. 1, pages 149-214.

1.1.1 Single Microlenses

The starting point is the idea of integrating a microlens between a light source and a fiber. In 1972, L. G. Cohen and M. V. Schneider first presented the idea of using a microlens to substantially improve the coupling efficiency. They were the first to apply photolithography, which is commonly used in integrated circuit (IC) technology, to make hemispherical and hemicylindrical microlenses. Later, the fabrication processes were simplified by P. D. Bear and modified by K. S. Lee and F. S. Barnes.

In 1974, L. G. Cohen and M. V. Schneider also proposed the concept of making a lens on the emitting surface of the laser diode. Subsequently, integrated lenses have been widely employed for the coupling between light-emitting-diodes (LEDs) and optical fibers.

In 1981, P. Kayoun et al. reported a method for the fabrication of conical microlenses by etching the fiber in a hydrofluoric acid solution. Since the etching rate is high in the cladding region and low in the core of the fiber, after etching the fiber end becomes conical. In 1982, G. Eisenstein and D. Vitello proposed another, better etchant solution for this process.

D. Kato was the first to publish a paper on making use of the surface tension of the melting glass that directly gives rise to the spherical surface for the construction of microlens. His invention led to the development of a tapered fiber with a hemispherical end. In late 1981, the first hemiellipsoidal microlens was made by H. Sakaguchi et al. by mechanical polishing the fiber ends into quadrangular pyramids followed by melting them with an arc discharge. After that, other integrated lenses were also reported by S. Mukai et al. in 1985, and by N. Walpole et al. in 1987.

With advances in semiconductor technology, laser diodes and laser diode arrays are being found increasingly in high-tech applications as well as in everyday products because of their properties such as low price, small size, and arrayed form. Edge-emitting laser diodes have been used as cheap, reliable light sources. For high-precision applications, however, their astigmatic beams with elliptically shaped mode profiles must be converted into nonastigmatic and spherical laser beams by using collimating micro-optics or optical elements that can compensate for the different diameters of the emitted laser beam [2, 3]. This operation can be performed by various types of elements in a suitable geometry, e.g. astigmatic gradient-index (GRIN) collimators. The development of microlens arrays is described in the next section.

1.1.2 Microlens Arrays

For more than a decade, a number of ways of exploiting available technology for fabricating microlens arrays have been developed. Numerous types of microlens arrays were reported successively by M. Oikawa et al. in 1981, K. Iga et al. in 1982, Y. Ishihara and K. Tanikagi in 1982, G. D. Khoe et al. in 1982, N. F. Borreli et al. in 1985 and Z. D. Popovic et al. in 1985 [1, p 279-310]. Planar microlens arrays can be used in multiple imaging systems for applications such as optical computing, matrix-vector multiplication, optical interconnection, pattern recognition, and optical image processing.

In recent years, free-space optical interconnects have been investigated for interconnections between compact arrays of laser sources and detectors capable of high bit rate operation, processors on different boards, and for the development of multi-channel optical buses or backplanes in high speed computers and switches. Because of their free-space pathways these structures use light beams in place of electrical signals and may have large advantages over their conventional electrical counterparts. These features include higher interconnect density, immunity from electromagnetic interference, large channel capacities, architectural freedom in partitioning the functionality of the chips and better thermal management [4].

In general, microlenses, analogous to microelectronic structures and in conjunction with them, are key components towards highly integrated, compact laser systems. They also are of increasing interest for applications of laser technology in other fields not directly related to the communications industry such as bar code scanners and copiers.

Thin film microlens arrays can be produced with the help of simple fabrication procedures such as vapor deposition techniques [5]. Using this technology, and by changing the mask geometry and/or the composition and number of layers, one can design various types of micro-optical components. Linear and 2D-arrays (two-dimensional arrays) of cylindrical lenses can be deposited with laser drilled elliptical holes as microscopic array masks. Micro-optical thin-film arrays can also be deposited on flexible and heat-resistant

polymer substrates. Arrays of up to 1000 elements consisting of single layers (SiO_2) or multilayers (SiO_2 and HfO_2, alternating) can be manufactured by using these techniques.

The ion-exchange process in glass is a well-developed method for the fabrication of gradient-index microlenses as well as for waveguides [3]. First of all, the glass substrate is masked by a metal layer and then deposited into a bath of molten salt of a monovalent ion. The exchange of these ions with sodium ions in the glass substrate usually causes a change in the refractive index, the color of the glass, the volume (and therefore the strain tensor), but it may also destroy the structure of the glass. The diffusion response is variable due to the dependence of the exchange process on certain parameters. The index profiles are varied with glass types, different types of exchange pairs, mask design, and the parameters of the exchange process, e.g. the temperature or the ion concentration. The exchange process may also be assisted by an electrical field. However, the exact chemical behavior during an exchange process in glass is unknown.

The Na-Ag ion-exchange process used for fabrication of GRIN microelements [2] is another example. The index distribution is formed by a diffusion process. In the lateral direction the distribution is influenced by a metal mask, which shields certain areas of the glass against diffusion during the process. Astigmatic microlenses can be fabricated by using elliptic mask apertures.

Polymethyl methacrylate (PMMA) microlens arrays can be formed by patterning an array of cylindrical columns with the help of deep-UV lithography. In a N_2 atmosphere, the substrate carrying the PMMA columns is contacted to a hot plate for a short time and the resulting PMMA column array is then melted to form a microlens array.

When glass or semiconductor microlenses are desired, the previous approach can be used to form the photoresist patterns. Then, these patterns can be transferred into the substrate such as glass, silicon by reactive ion etching (RIE) [6-9]. Laser ablation can also be used to pattern mesas for reflow and glass microlenses can be deposited directly on substrate by vapor deposition through shadow mask. In general, methods using

photolithography are not suitable for rapid prototyping of lens arrays with arbitrary focal length and pitch.

Recently, a unique technique which can be used to fabricate dispensed polymer microlenses has been invented at Telecommunications Research Laboratories (TRLabs) based in Edmonton, Alberta, Canada and has also been patented. This technique makes it possible to extend the work in the area of micro-optics for a wide range of applications. It is an extremely simple and inexpensive technique, but can be used to fabricate cylindrical and spherical microlenses of excellent quality and high uniformity [10]. It is also potentially adaptable to different curable liquids. Figure 1.1 shows part of an array. Lenses made by this method have shown diffraction limited characteristics for diameters up to 600 μm and wave aberration limited behavior for diameters over 600 μm (Chapters 2, 4). The F# range of 0.9 to 30 (Chapters 2, 3) can be reached with the variation of focal length within an array limited to ± 2% [11].

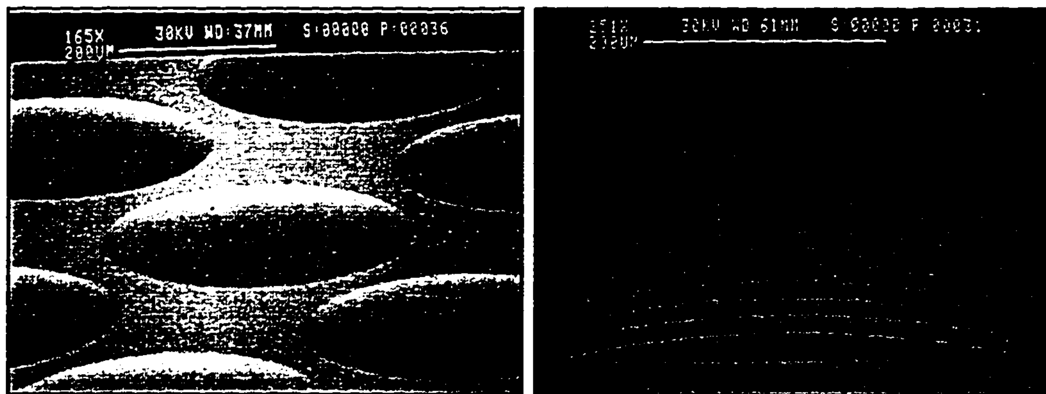

Figure 1.1 Scanning Electron Microscope (SEM) pictures of part of a dispensed polymer spherical microlens array [10].

1.2 APPLICATIONS

Some applications using microlenses developed at TRLabs will be described in this section.

1.2.1 Free-Space Optical Bus

One of the programs of the Canadian Institute for Telecommunications Research (CITR) is the development of a free-space parallel optical bus. A beam extractor card for this project was developed at TRLabs [12].

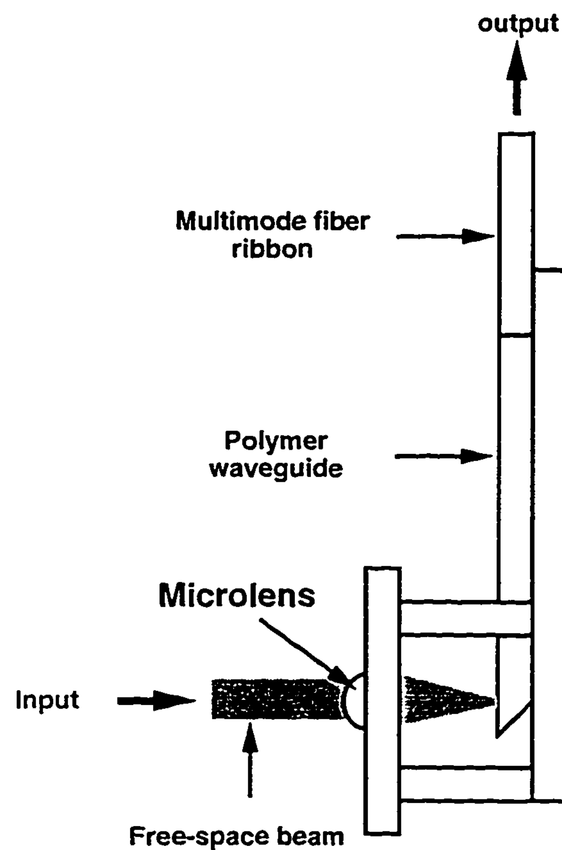

Figure 1.2 Dispensed polymer microlenses used in "extractor card" prototyping [12].

The principal function of the extractor card is to intercept free-space collimated beams from an optical backplane and couple them into polymer waveguides for distribution to photodetectors or fibers. The structure of this card is illustrated in Fig. 1.2. The key components required for this card are a dispensed polymer microlens array used to focus

the collimated beams to tight spots, and low-loss polymer waveguides with 45° reflective end facets used for signal routing.

1.2.2 VCSEL Package

Figure 1.3 (adapted from [11]) shows the principle of a vertical cavity surface emitting laser (VCSEL) package which uses a linear array of dispensed polymer microlenses. The average coupling efficiency in this application was 47.5% ± 5% which is the best reported in the literature so far [11].

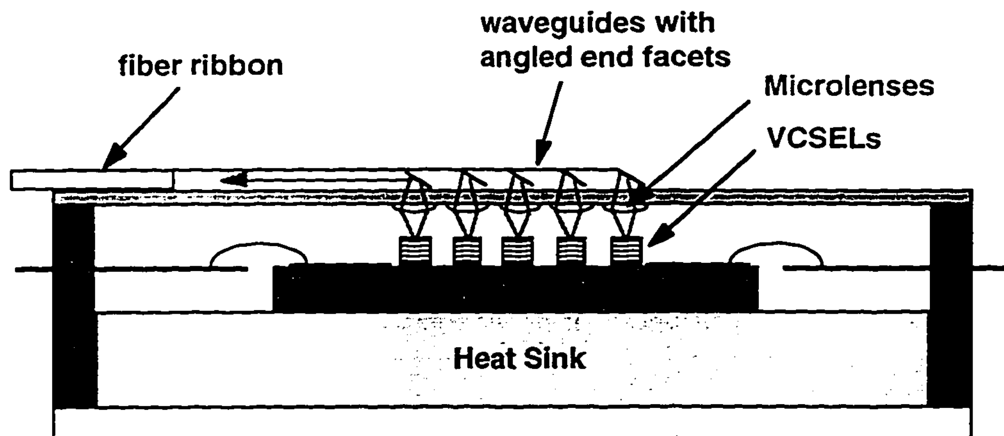

Figure 1.3 Dispensed polymer microlenses used in VCSEL packaging [11].

1.2.3 Free-Space Optoelectronic Switch

Another example of an application of dispensed polymer microlenses is their use in the architecture of a 3×3 free-space switch whose functional representation is illustrated in Fig. 1.4 (adapted from [13]). This design is one of the developments for future optoelectronic switching modules in fibre-optic communications because it can be used to control the distribution of the optical inputs 1, 2, 3 to the photodetectors of the electrical outputs A, B, C (Fig. 1.4(a)). In this configuration, the most important element is the focusing and beam splitting element (Fig. 1.4(b)).

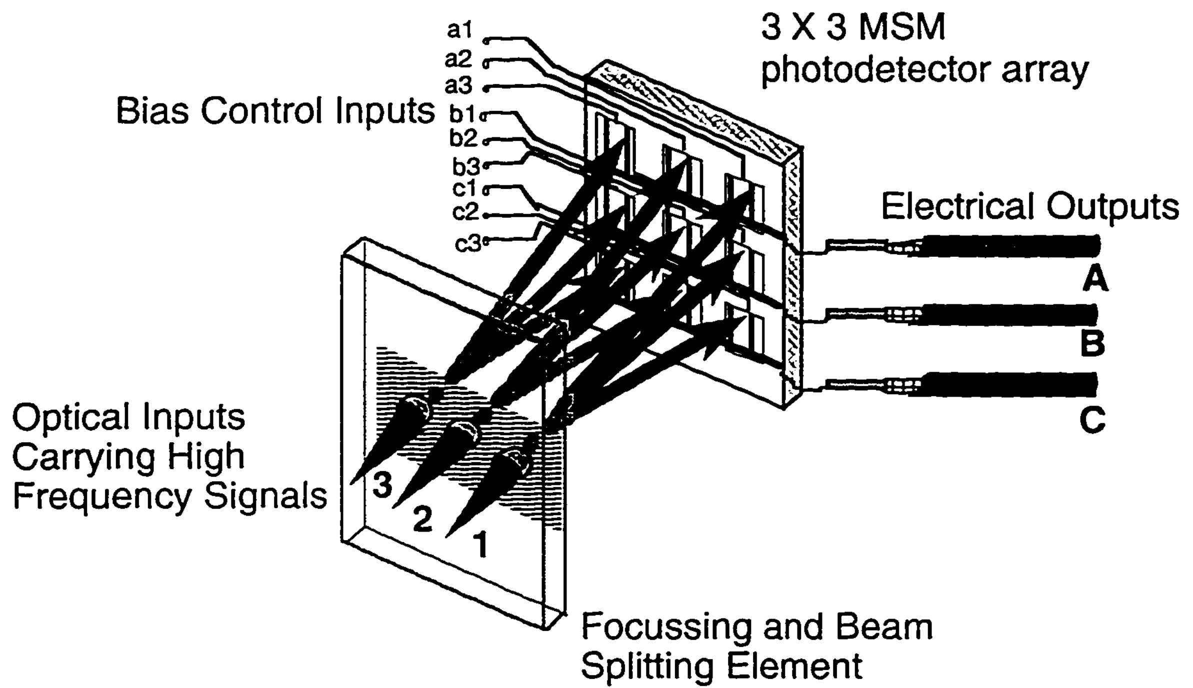

(a) Microlenses in free-space switch.

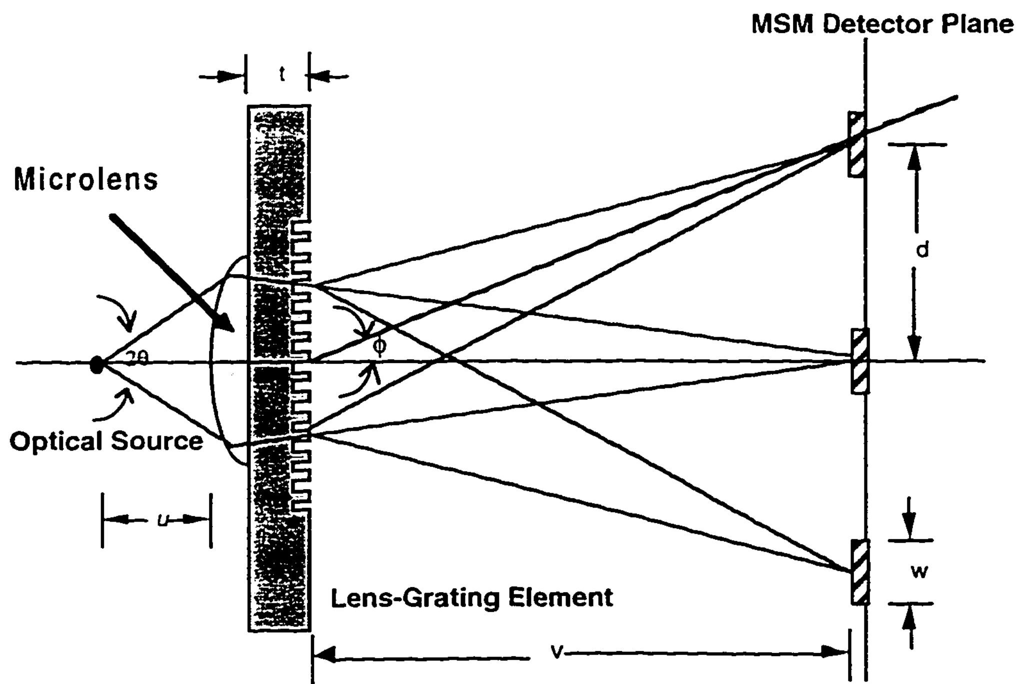

(b) Microlens function in beam focusing and splitting element.

Figure 1.4 Dispensed polymer microlenses used in free-space switch [13].

1.3 PROJECT OBJECTIVE AND OVERVIEW

Dispensed polymer microlenses have shown a number of advantages that are attractive to research and industrial interests. Therefore, the objective of this project is the continuation of work already started in the area of polymer micro-optics. The goals of this project are:

1. **Develop ways of fabricating lenses of arbitrary diameter and focal length with reduced aberrations using a wide range of materials.**
2. **Develop the fabrication process of microlenses in glass and silicon using dispensed polymer mask.**
3. **Develop methods of microlens testing using a laboratory Mach-Zehnder interferometer.**

This work started with a study of the formation of liquid lenses on solid substrate surfaces and with investigating properties of different dispensed optical adhesives. Then, a process was developed to allow transfer dispensed polymer microlens patterns into quartz and silicon substrates by using reactive ion etching (RIE). Since lens testing is an important part of this project, a standard measurement procedure has been implemented to allow effective use of a bulk optics Mach-Zehnder interferometer. Finally, the experimental investigations of some effects on wave aberrations were carried out with this very useful tool.

In this thesis, Chapter 2 gives a description of the TRLabs dispensing technique used to make polymer microlenses and shows measurement results obtained from various optical polymers. Chapter 3 is an account of the development of a process to transfer the dispensed polymer lens shapes into fused silica and silicon. Chapter 4 describes a number of measurement procedures developed which use a Mach-Zehnder interferometer. The two effects of gravity and etch selectivity on wave aberration of microlenses are investigated experimentally in Chapter 5. Chapter 6 presents a summary on the work done and concludes with some suggestions for further development.

2. POLYMER MICROLENS FABRICATION

The dispensed polymer microlens technology has been established but needs to be extended to the point that it can be adapted to a wide range of practical applications. To achieve this goal a significant amount of characterization work for the dispensing process needs to be done. The properties of both spherical and cylindrical dispensed polymer microlenses depend on many parameters that affect the final shapes of ultraviolet light-cured (UV-cured) dispensed volumes of liquid optical adhesives. If separated from all curing effects, it is well known that characteristics of these liquid lenses are dominated by surface tension and other related fluid phenomena which have not yet been accurately modeled [14]. Therefore, only an empirical characterization approach seems practical at the present time. This chapter reviews some basic theoretical aspects of liquid lens formation on substrate surfaces, describes the dispensing technique mentioned in Chapter 1, and presents some measurements of various dispensed polymers.

2.1 THE THEORY OF LIQUID LENS FORMATION

Theoretically, the formation of liquid lenses can be predictable with the knowledge of parameters such as surface tension, liquid viscosity and substrate type. Like other liquids, after a volume of an optical adhesive is placed on a substrate surface, this volume, without any further external influence, will undergo a sequence of dynamic changes. These start with wetting and spontaneous spreading over the solid substrate surface until a mechanical equilibrium in the system is reached.

The liquid shape of the adhesive in equilibrium is determined by hydrostatic pressures, surface tensions of a three-phase substrate/polymer/air system and gravity (negligible for very small lenses). However, for ideal substrate surfaces (absolutely smooth and uniform) and without the effect of gravity, these equilibrium shapes are determined by dynamic (before equilibrium state) and static (at the equilibrium state) contact angles between the polymer surface and the substrate. Therefore, one can predict the

characteristics of polymer lenses by using the knowledge of these angles if curing does not have significant effects on the final shape of the lens.

While the characteristics of static contact angles are well modeled in the literature [14-19], those of dynamic contact angles and the time of reaching equilibrium are not. Although it is independent of gravity, the static contact angle always shows hysteresis caused by the existence of numerous metastable states for system having three-phase (solid/liquid/vapor) boundaries. Therefore, for most practical materials the apparent macroscopic static contact angle is not unique [14, 15, 18]. The metastable states are the result of surface heterogeneity, surface roughness, or surface deformity etc.

Theoretically, the relation between static contact angle and the surface tension of a liquid is given in [15-23] by Young's equation as

$$\cos\theta = \frac{\gamma_{sv} - \gamma_{sl}}{\gamma_{lv}} \tag{2.1}$$

where

γ = surface tension.

θ = the static contact angle.

sv, sl, lv represent the interfaces solid/vapor, solid/liquid and liquid/vapor.

A modification of Equation (2.1) was derived by Gibbs as

$$\cos\theta = \frac{\pi_{s/l} - \pi_{s/v}}{\gamma_{l/v}} \tag{2.2}$$

where

$$\pi_{s/l} = \gamma_{s/o} - \gamma_{s/l} \tag{2.3}$$

$$\pi_{s/v} = \gamma_{s/o} - \gamma_{s/v} \tag{2.4}$$

s/l, s/v and γ are defined as above while s/o is designated for solid/vacuum interface. $\pi_{s/l}$ measures the tendency of the liquid to spread and $\pi_{s/v}$ opposes the spreading of the liquid. Similarly, $\gamma_{l/v}$ measures the tendency of the drop to contract under surface tension forces.

The contact angle θ, can also be expressed mathematically by the competition between adhesive and cohesive forces as

$$\cos\theta = \frac{2W_a}{W_c} - 1 \qquad (2.5)$$

where the work of adhesion W_a for equilibrium is the reversible work required to separate a unit area of liquid from a solid and can be given by

$$W_a = \gamma_{l/v}\,(1 + \cos\theta). \qquad (2.6)$$

The work of cohesion, on the other hand is a measure of molecular interactions of molecules of the same kind and is given by

$$W_c = 2\gamma_{l/v}. \qquad (2.7)$$

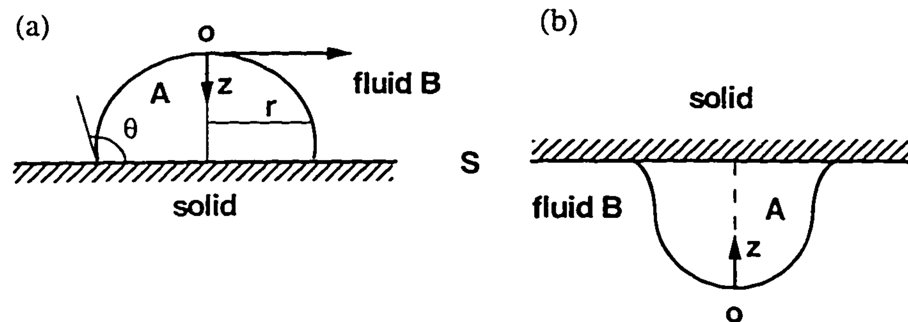

Figure 2.1 The analysis of drop shape.

More than a century ago, Bashforth and Adams [19] investigated the apparent equilibrium shapes of the fluid interface for a drop of fluid A placed on a solid S which is otherwise in contact with fluid B (Fig. 2.1). They were the first to carry out a numerical solution for this shape and established tables relating the size and shape of liquid drops to the surface tension. Later, these tables were extended for a wider range of sessile drop (Fig. 2.1(a)) and pendant drop (Fig. 2.1(b)) conditions [19]. The materials must be chosen so that A is denser than B and does not spread spontaneously on S. At the final equilibrium position, two factors that determine the shape of the fluid interface are gravity and

interfacial tension. Gravity favors a large diameter drop of small height while the interfacial tension favors a smaller drop of greater height where the surface area is minimized. The actual drop shape reflects a balance between these two effects.

Using dimensionless coordinates $Z = (z/b)$ and $R = (r/b)$, one can describe the drop shape with a second-order ordinary differential equation that cannot be solved analytically, except for certain limiting cases. This equation is given in [15, 19] as follows:

$$\frac{Z''}{\left[1 + (Z')^2\right]^{3/2}} + \frac{Z'}{R\left[1 + (Z')^2\right]^{1/2}} = 2 + \beta Z \tag{2.8}$$

where
$$\beta = (\rho_A - \rho_B)\, g b^2/\gamma \tag{2.9}$$

$Z = Z(R)$ and its derivatives taken with respect to R.

r = the radial coordinate in the horizontal plane (Fig. 2.1(a)).

z = z-coordinate of the interested point with respect to vertex O (Fig. 2.1(a)).

b = the radius of curvature at the drop vertex.

γ = liquid surface tension.

g = the gravitational acceleration.

ρ_A = density of fluid A.

ρ_B = density of fluid B.

$\beta > 0$ for sessile drop and $\beta < 0$ for pendant drop.

With respect to R, the boundary conditions for Equation (2.8) are $Z(0) = 0$ and $Z'(0) = 0$. This is the basis for the theoretical analysis of the shape of dispensed polymer droplets. However, to a good approximation, one can assume small lenses to be spherical caps. In deed, these shapes will be the solutions of Equation (2.8) if $g = 0$.

In practice, f/number (F# = focal length/diameter) is a variable which is often used to describe a lens. Therefore, analytical relations between the F# of a small lens and its

dimensions should be useful. Optically, the paraxial (very close to axis) focal length of a thin plano-convex lens is given by

$$f = \frac{R}{n-1} \tag{2.10}$$

where R is the radius of curvature of the profile in paraxial region and n is the refractive index of the lens material. Then the $F\#_p$ of a polymer microlens is given by

$$F\#_p = \frac{R_p}{(n_p - 1)D} = \frac{1}{(n_p - 1)D}\left(\frac{h_p}{2} + \frac{D^2}{8h_p}\right) = \frac{1}{2(n_p - 1)\sin\alpha_p} \tag{2.11}$$

where the dimensions are illustrated in Fig. 2.2 as

R_p = the radius of curvature of polymer microlens.

D = diameter of the polymer microlens.

h_p = the height of the polymer microlens.

n_p = the refractive index of the polymer.

α_p = the contact angle of polymer lens.

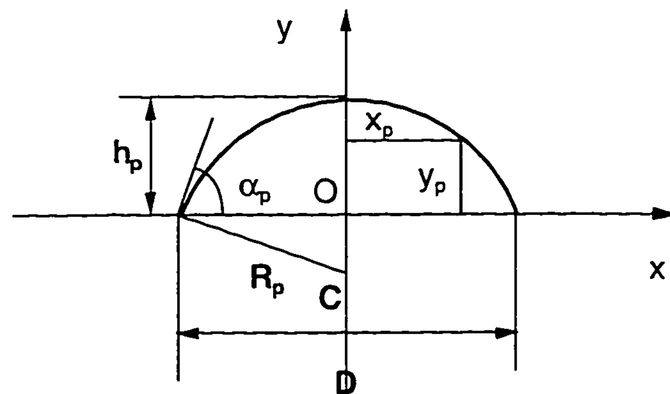

Figure 2.2 Dimensions of dispensed polymer lenses.

Equation (2.11) allows one to determine F#s of dispensed polymer microlenses whose refractive index is given when contact angles or dimensions are known.

The liquid lens formation described above along with necessary control equipment is exploited at TRLabs to fabricate UV-cured polymer microlenses. Details of this technique will be described next.

2.2 THE DISPENSING TECHNIQUE

The UV-cured polymer microlenses used in the applications described in Section 1.2 were made by a dispensing technique which is too complicated to be modeled accurately. Unlike the theory in last section, there are so many unknowns that affect dispensing results. This complexity, which is beyond the scope of this thesis, involves such problems as the forming of a liquid volume at the needle tip, the wetting of substrates, the separating and forming of liquid traces or droplets on solid surface which move dynamically before coming to an equilibrium shape. Further studies on these issues are given in [14-23].

In practice, the process of microlens fabrication needs to be so controlled that requirements on designed parameters such as lens sizes (diameters for spherical lenses; widths and length for cylindrical lenses), pitches (distance between array elements), F#s and diffraction-limited quality can be met. For the dispensing technique, varying parameters such as dispensing pressure, time (for spherical), speed (for cylindrical), height (the minimal gap set from needle tip to substrate surface) and the inner diameter of the needle can be used to control the lens size. However, F#s and diffraction-limited quality are more difficult to control because they depend on the dispensed liquid shapes which are affected by a number of other parameters described in the previous section.

The set up which can be used to dispense different types of liquid optical adhesives is illustrated schematically in Fig. 2.3. In this system, a pressurized syringe containing liquid optical adhesive is used to dispense traces or to deposit precisely controlled droplets of liquid optical adhesives for cylindrical or spherical microlenses, respectively. The apparatus is controlled by a computer and monitored on a TV screen by a microscope

equipped with a charge-coupled device (CCD) camera as an imaging system. If an array of lenses is desired, then the technique will be used as a step-and-repeat process. The appropriate pressure from a dry air supply is set manually and the substrate is held on top of a vacuum chuck. The timing of open connection from dry air supply to the syringe through the pressure delivery unit and the motion of XYZ actuator with preset patterns are controlled by a computer via a control board.

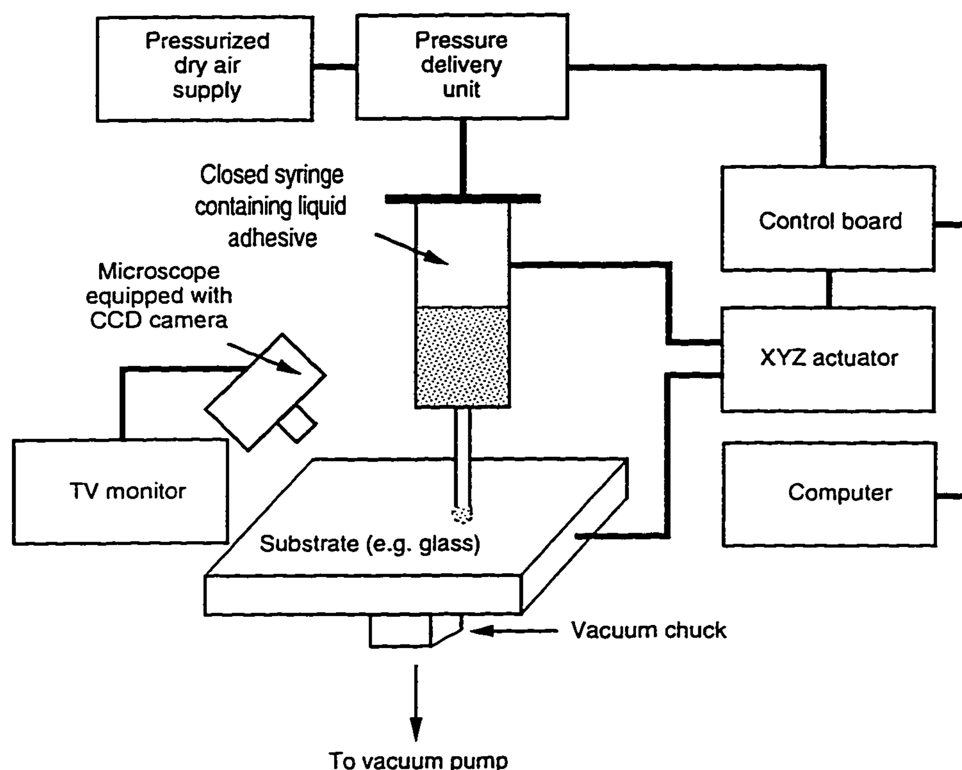

Figure 2.3 The principal illustration of dispensing set up.

Commonly used substrates for dispensed polymer microlenses are: (a) Corning 7059F glass plates coated with a thin layer of SiO_2 deposited by chemical vapor deposition (CVD) at the Alberta Microelectronics Center (AMC), (b) quartz plates and (c) polished silicon wafers. Before dispensing, a substrate cleaning process begins by blowing on both sides of it with dry nitrogen to remove dust particles. Then the substrate is placed inside a spinner and its dial is set to maximum speed for thirty seconds. While the substrate is being

spun, it is cleaned for thirty seconds with methanol, then for the same time with acetone. This cleaning technique cannot be used to prepare samples for etching as is discussed in the next chapter. After cleaning, the substrate is placed on the dispensing stage and blown with dry nitrogen again to be ready for dispensing.

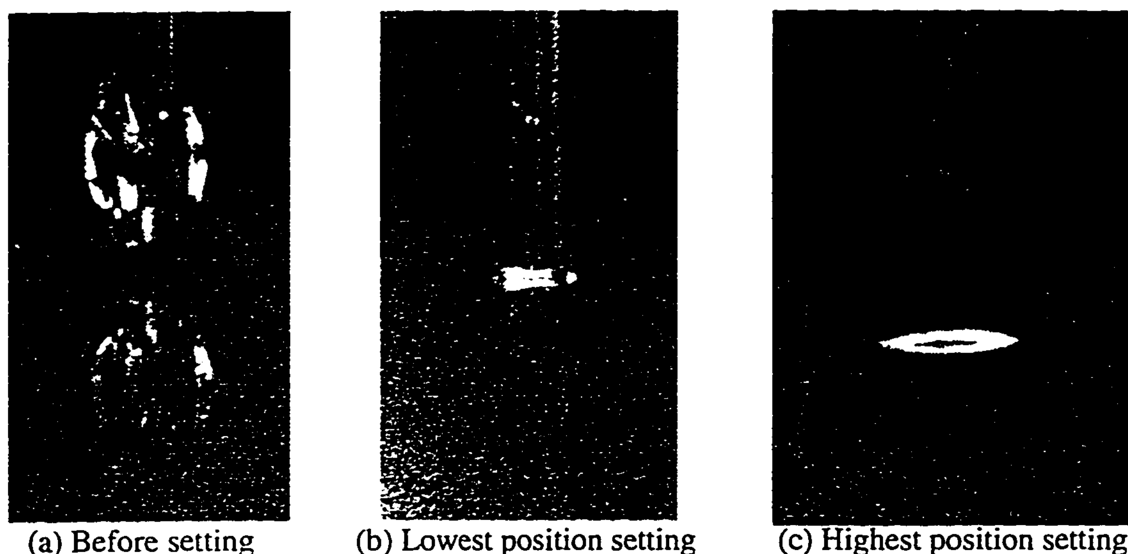

(a) Before setting (b) Lowest position setting (c) Highest position setting

Figure 2.4 Defining the surface of dispensing.

The liquid adhesive volume dispensed is controlled by choosing different combinations of apparatus parameters such as needle tip diameter, dispensing pressure, and dispensing time or speed. Then this amount of liquid adhesive is placed on the substrate surface by controlling the position and dispensing height. Figure 2.4 shows how the TV monitor may be used to determine the position and to set the maximum gap between the needle tip and the substrate surface during dispensing.

Fig. 2.5 shows a sequence of placing liquid polymer droplets on a substrate surface and the pictures in Fig. 2.6 show how the syringe, the microscope, the vacuum chuck, motorized actuators and substrate are arranged in the actual dispensing set up. The actual portion of dispensed polymer which stays on the surface and forms the lens depends on the nature of mechanical equilibrium or the balance of forces exerting on interfaces between the

dispensed polymer surface and all surfaces which are in contact with it in the system. Normally, dispensed liquid lenses are left covered for approximately thirty minutes before being cured with UV light so that uniform shapes close to equilibrium will result among all the lenses. Assuming a negligible effect of gravity, lens shapes are spherical for droplets, and cylindrical for traces. Circular lenses of diameters ranging from 2 to 5 mm were also made for the investigation of the effect of gravity which will be discussed in Chapter 5.

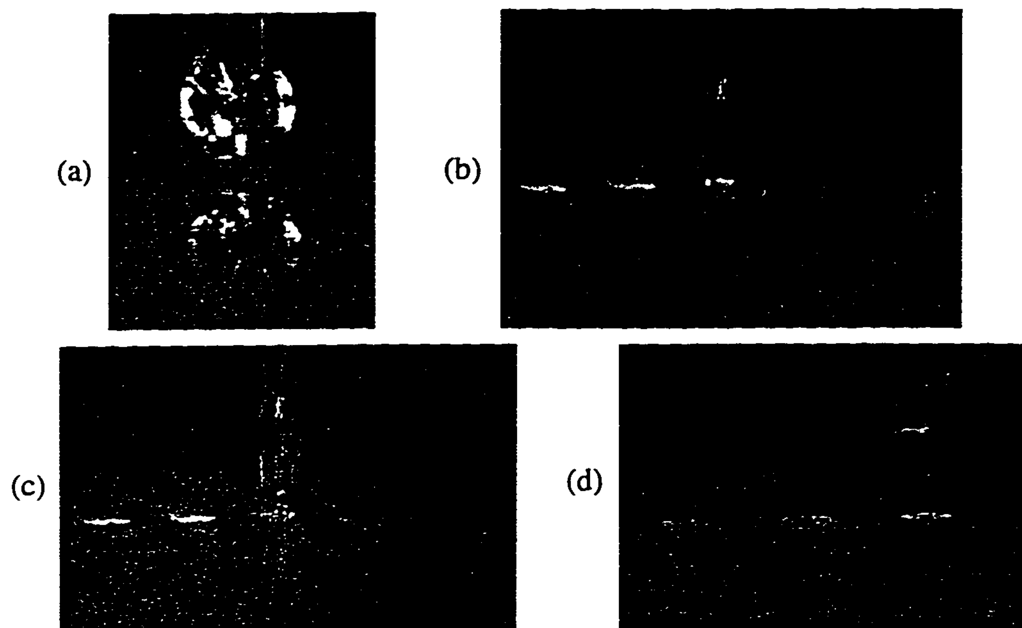

(a) Before polymer being placed; (b) Polymer being placed on substrate; (c) Polymer being separated; (d) Needle tip position after polymer dispensed.

Figure 2.5 A sequence of dispensing.

It has also been demonstrated at TRLabs that there are other capabilities of the dispensing technique such as the fabrication of astigmatic lenses [11] and the widening of the F# range of dispensed polymer microlenses [24]. Low F#s can also be made by stacking dispensed lenses. However, this technique undergoes the additional problem of axially aligning the layers. Fig. 2.7 shows a multiple layer lens. F#s can also be lowered slightly if liquid microlenses are cured immediately, but as with multiple layer lenses, it is

very difficult to prevent the needle tip from being clogged up in this process by reflected UV light. Astigmatic (or anamorphic) microlenses can be produced in such a way that small displacements either in x or y direction is applied to the needle tip during polymer being dispensed and Fig. 2.8 illustrates one lens made by this technique. This type of lens can be used in beam shaping applications.

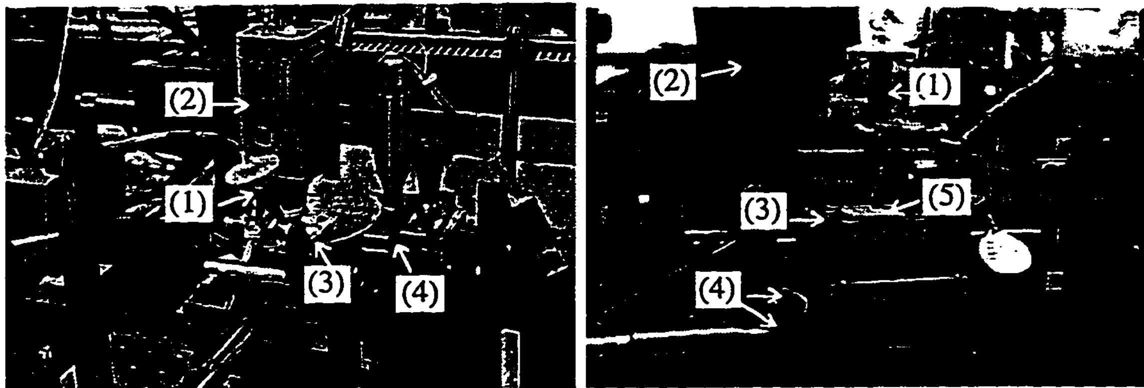

(a) For cylindrical lens fabrication. (b) For spherical lens fabrication.

(1). Syringe containing optical adhesive; (2). Microscope equipped with CCD camera; (3). Vacuum chuck; (4). Motorized actuator; (5). Substrate.

Figure 2.6 Dispensing stage set up.

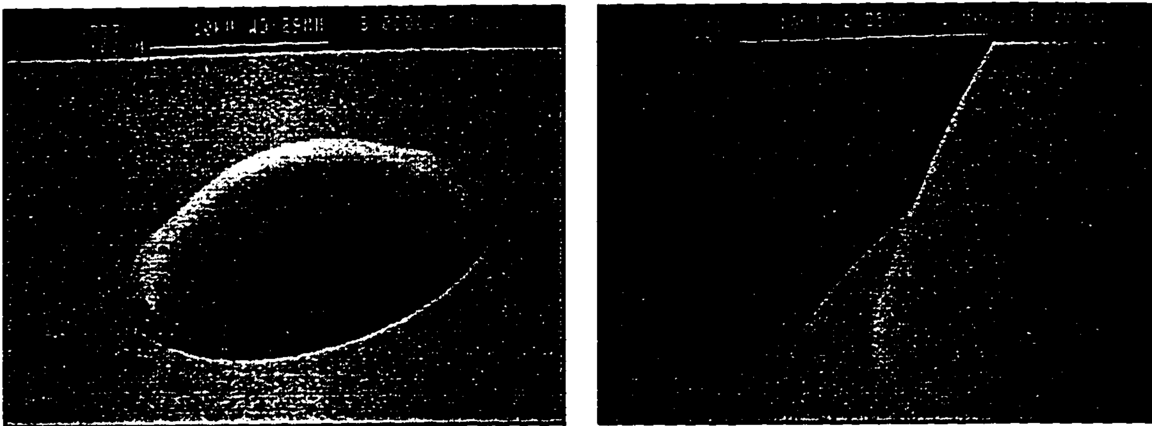

Figure 2.7 Multiple layer dispensed polymer microlenses of F# = 1.3.

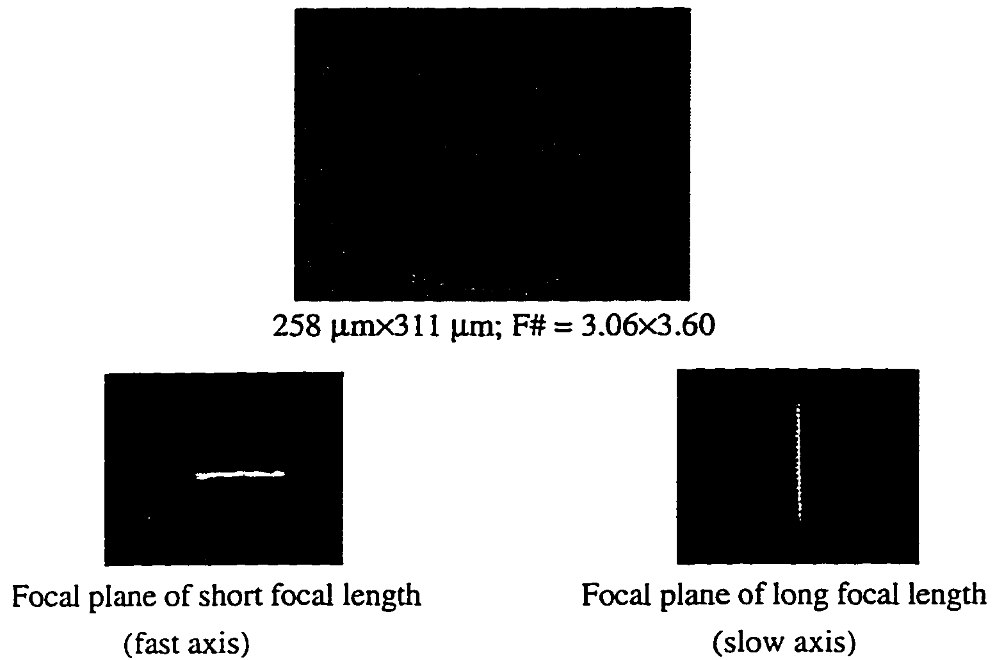

Figure 2.8 Anamorphic lens [11].

Table 2.1 gives a summary on up-to-date achievable specifications of spherical polymer microlenses made by dispensing.

Table 2.1 Specifications of spherical dispensed polymer microlenses.

PRELIMINARY SPECIFICATIONS	Min	Typical	Max	Units
Lens diameter (diffraction limited @ 850 nm)	70	-	600	μm
Lens diameter (spherical aberration limited @ 850 nm)	600	-	1500	μm
Lens spacing	150	250	60,000	μm
F/number	0.9	-	30	-
Transmission (400-1800 nm)	90	92	-	%
Array size (either dimension)	-	-	6	cm
Focal length variation within array	-	±1	±2	%
Placement error	-	±1	±2	μm

To reduce trial and error times in the dispensing process it is desirable to document standard data, especially those on properties of various dispensed optical polymers, required for different lens designs. The next section presents results of the measurements of contact angle for various polymers.

2.3 MEASUREMENTS OF VARIOUS OPTICAL POLYMERS

In Section 2.1, the contact angle between the polymer surface and the substrate is mentioned as one of the parameters that can be used to characterize dispensed polymer microlenses. Therefore, the knowledge of these angles of different optical polymers is essential for the fabrication of dispensed polymer microlenses from these materials.

The measured samples are cylindrical profiles dispensed on the surface of silicon wafers which are coated with CVD-SiO_2 and are believed to be similar to substrates of type (a) mentioned in Section 2.2. The dispensing height was set similarly as described in the previous section. The measured widths ranged approximately from 0.2 mm to 3 mm. For each kind of polymer, there are two sets of samples. One was made in such a way that after dispensing the substrate was covered for 30 minutes before curing and cured for 30 minutes with lenses facing up (positive gravity). The other set was covered and cured with lenses facing down (negative gravity) for the same times. The scanning results were acquired by using a profilometer available at AMC. Eleven different optical adhesives [25] were characterized:

- NOA 60, 61, 63, 65, 68, 81.
- OG 112, 113, 115, 116.
- UVO 114

Figures 2.9, 2.10, and 2.11 show the scans of three polymers NOA 63, 65 and 68. The rest of the scans can be found in Appendix I.

(a)

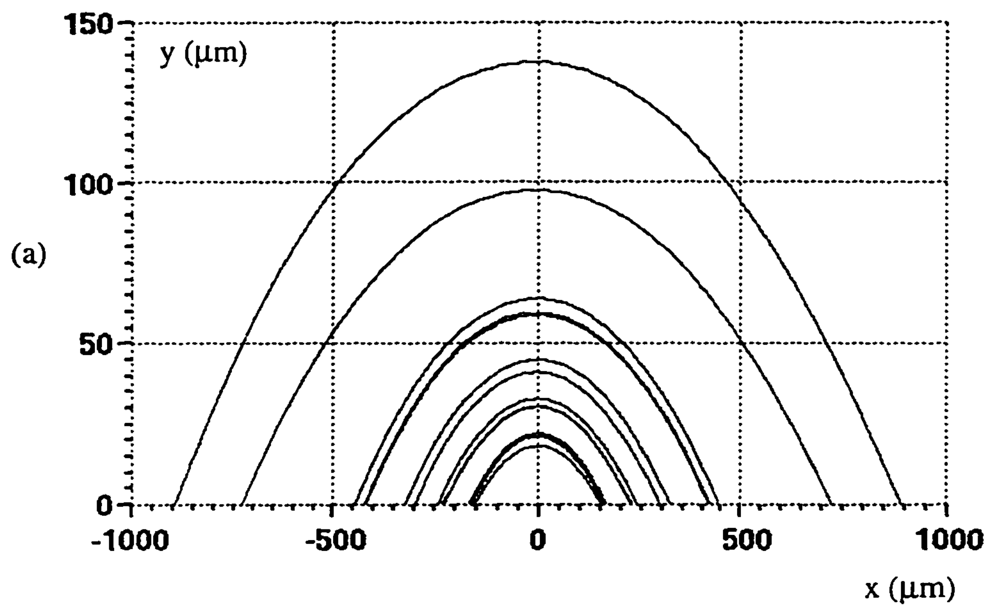

(b)

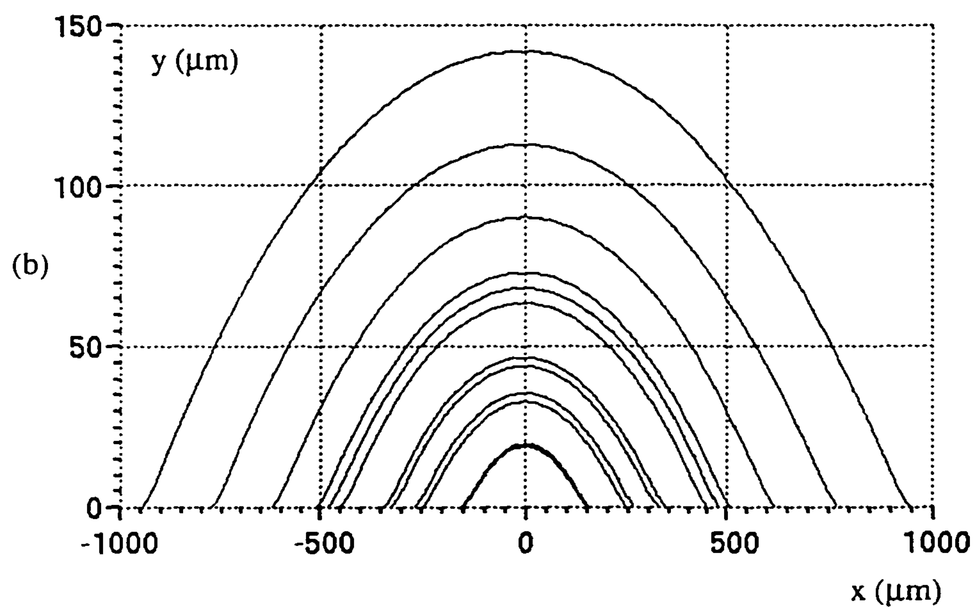

(a) Cured up side down (negative gravity).

(b) Cured right side up (positive gravity).

Figure 2.9 Scanned cylindrical profiles of NOA 63.

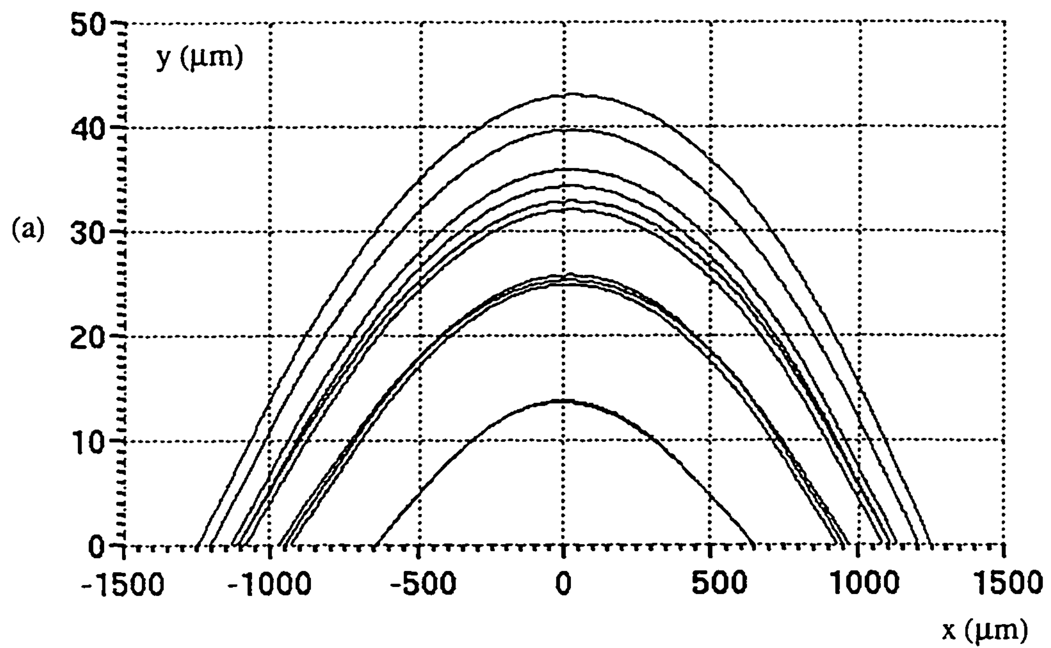

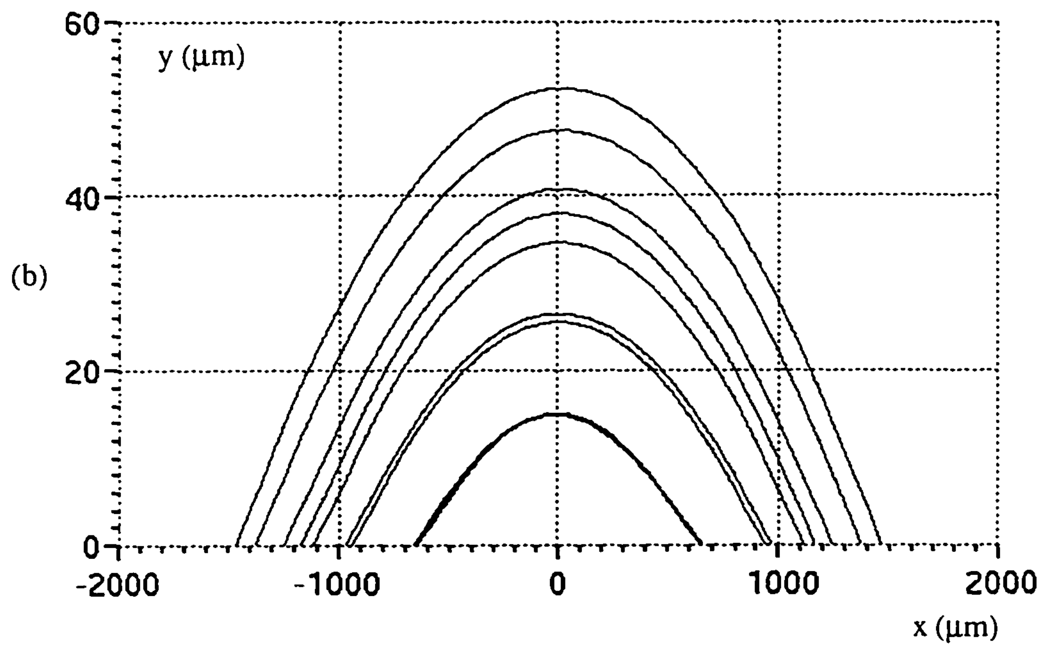

(a) Cured up side down (negative gravity).

(b) Cured right side up (positive gravity).

Figure 2.10 Scanned cylindrical profiles of NOA 65.

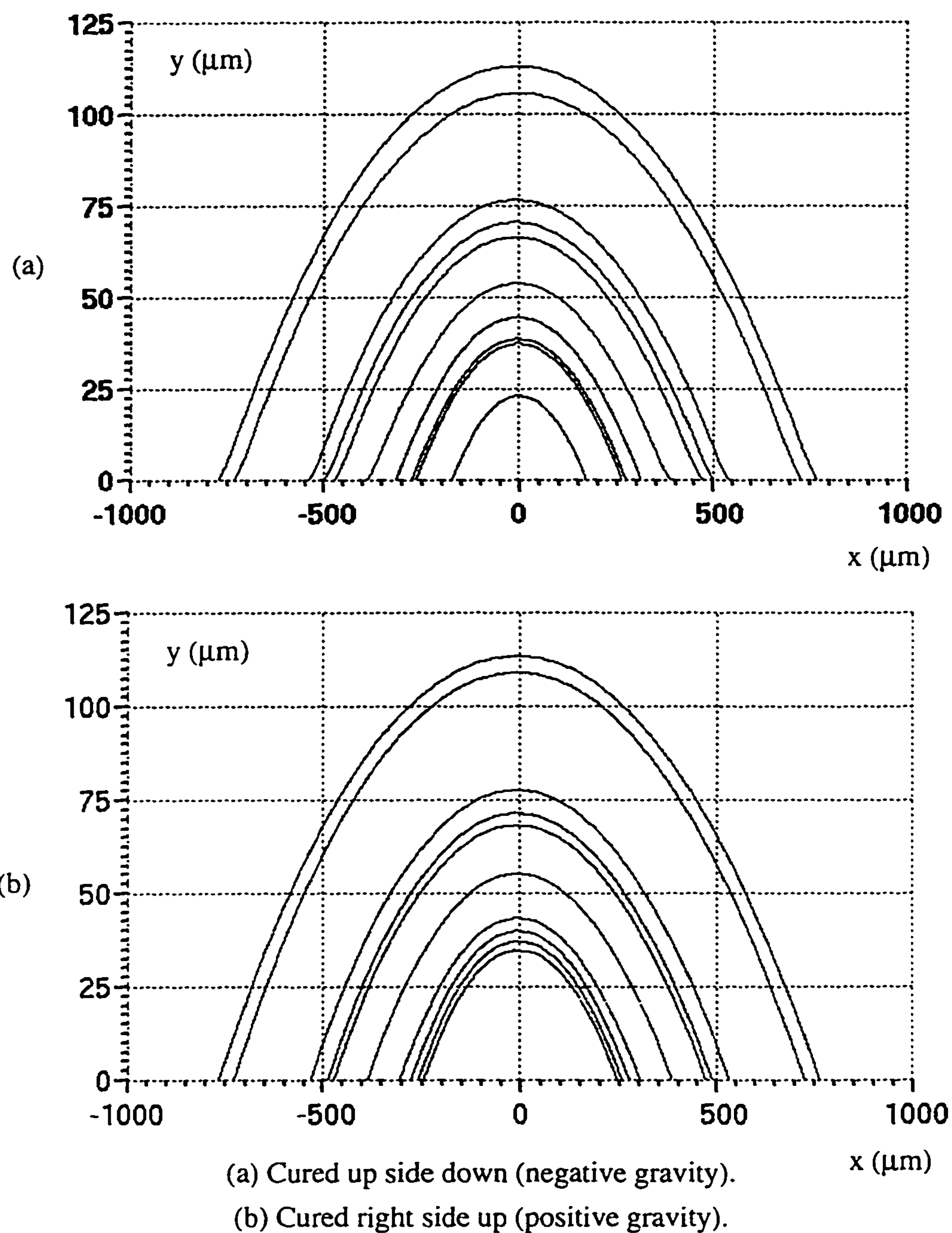

(a) Cured up side down (negative gravity).
(b) Cured right side up (positive gravity).

Figure 2.11 Scanned cylindrical profiles of NOA 68.

Although some of these samples were redone, their scanned profiles still showed wavy tops, perhaps due to quality nonuniformity of a particular batch of adhesives, variations of curing source etc. However, it is believed that the apparent contact angle is

still measurable despite this waviness. Another problem was the profile inconsistency of OG 113 samples which were repeated four times due to the unpredictable behavior of this material while curing. The first two samples were cured with the same method used for the other materials, but not all traces became polymer lenses even with an increase of curing time up to 60 minutes. Baking samples at 100°C for 60 minutes also did not make any difference. The final sample, which was cured immediately after dispensing (not applicable to negative gravity), shows non-constant scanned shapes of the adhesive which were probably still spreading dynamically. Otherwise, the majority of the scans show approximately constant shapes which characterize the combination of characteristics of the polymer properties and the dispensing conditions applied.

For profiles in this experiment, the computation of the angle that might give the most appropriate results for estimation of F#s by Equation (2.11) should be based on selective data points. Therefore, for each curve only the first and last ten percent (on the left and right side of the curve) of acquired data points were used to calculate different slopes of the curve. Then, the angle of the absolute maximum slope was calculated and these are given in Table I.1 of Appendix I.

The results seemed to show the effect of the order of dispensing because in each sample the smallest trace was dispensed first and the largest last. The average dispensing time for each sample was about 30 minutes. For further analysis, the values of these angles of polymers NOA 63, 65, 68 are shown in Fig. 2.12 with respect to half widths of lenses. These graphs show following trends:

1. The tendency for the angle to increase with the size of the lens. This might indicate that these liquid adhesives needed a longer time than 30 minutes to come to an equilibrium.
2. The lower the viscosity of the adhesive (e.g. lowest for NOA 65 of Fig. 2.12(b)), the faster its spreading (larger lens sizes) and the shorter time for equilibrium (less angle fluctuation and flatter curve tail).

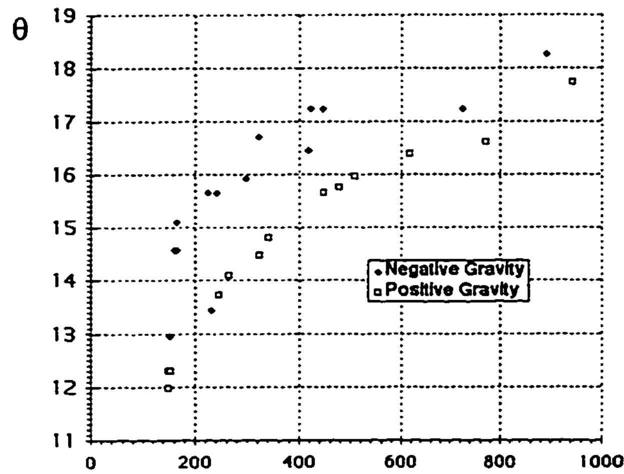

(a)

NOA 63

Viscosity 2000 cps

W/2 (µm)

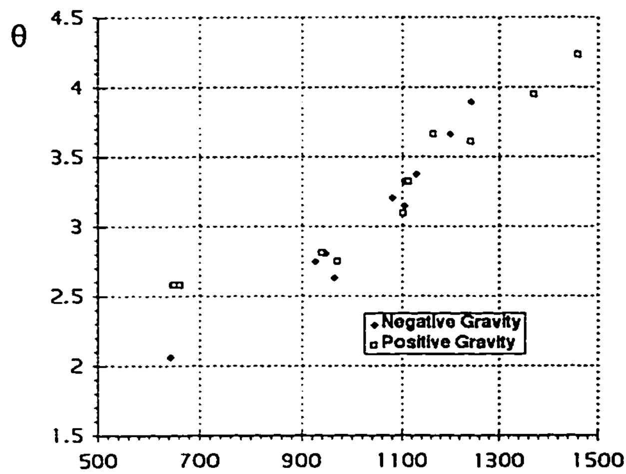

(b)

NOA 65

Viscosity 1200 cps

W/2 (µm)

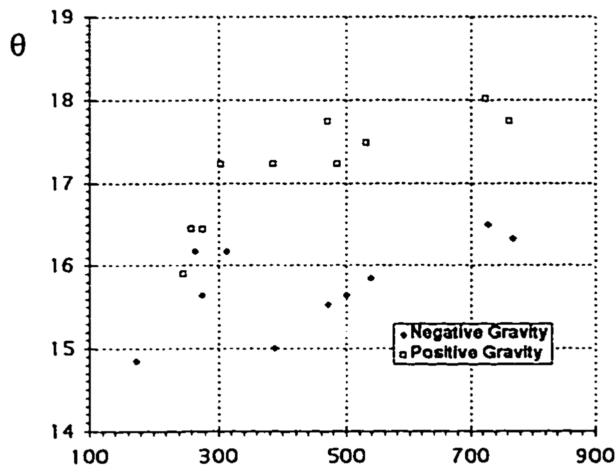

(c)

NOA 68

Viscosity 5000 cps

W/2 (µm)

θ - the calculated contact angle in degree; cps - centipoise; W/2 - half width of cylindrical lenses in micrometer.

Figure 2.12 The relation between contact angle and lens size of polymers NOA 63, 65, 68.

3. No clear difference between negative and positive gravity (theoretically, independent of gravity [15-18]).

2.4 DISCUSSION

The fabrication process of dispensed polymer microlenses which are suitable to a number of potential applications is reproducible. However, further characterization is required to make it adaptable to increasing demands. The theory of liquid lens formation has shown that the measurement of contact angle can be used to standardize the F# design. Consequently, a series of cylindrical microlens samples for eleven different optical adhesives was generated by the dispensing technique for this measurement. The acquired data that were used to calculate contact angles showed some irregularities caused by still unknown effects. These experimental results can be interpreted as follows:

1. The obtained contact angle of each polymer had a certain value range instead of being unique. The study of experimental results indicated that the dispensed adhesive of higher viscosity might need a longer time than 30 minutes to reach equilibrium. Adhesives of lower viscosity tend to spread faster than those of higher. Some adhesives appeared to be inappropriate to fabricating dispensed polymer microlenses, or experimental irregularities which were caused by some unknowns of nonideal dispensing and curing conditions need to be further investigated.
2. Another possible practical alternative is to characterize the fabrication process of both cylindrical and spherical dispensed polymer microlenses by measuring lens specifications such as size, F#, and quality for individually varied dispensing control parameters, substrate types, and types of adhesives.
3. Monitoring information might be used to automatically control the fabrication process.

3. GLASS AND SILICON MICROLENS FABRICATION

As the demand for microlens arrays has increased, a variety of microlens fabrication techniques have been developed. However, the photoresist and glass microlenses reported in [26-29], because of their high absorption coefficient, are not suitable to applications in optical communications with working wavelengths in the infrared (IR) region (1.3 or 1.55 μm). Polymer microlenses described in Chapter 2 do not have this problem, but unfortunately, telecommunications companies do not like anything with polymer in the package. Thus, one possible solution for this problem will be the use of silicon microlenses [6, 8] which can be produced by using one of the common dry etching techniques in microelectronics processing such as reactive ion etching (RIE) or ion-beam etching [7, 30]. These dry etching techniques can also be used to make glass or quartz microlenses that inherit the physical durability of a hard substrate compared to polymer lenses (photoresist and optical adhesive). In addition, dry etching will also add a degree of freedom to the design [8], namely the relative etch rates of the polymer and substrate, which can be used to modify the lens shape.

In this project, the fabrication of etched microlenses in quartz, CVD-SiO_2 and silicon has been investigated. Transferring photoresist microlenses into substrates by RIE always requires the use of a photolithographic process which generally consists of many time-consuming steps and might not be convenient for short turn-around design time. On the other hand, dispensed polymer microlenses have shown attractive characteristics such as their cost effectiveness, variability, high uniformity and excellent quality. Therefore, these microlenses should be considered as a masking material in transferring processes instead of the photoresist used by other workers [6-9, 30]. This replacement will be very advantageous if it can be controlled. This chapter will focus on using this approach to develop RIE processes for the fabrication of etched microlenses. First, it will be helpful if the nature of the RIE process is briefly described.

3.1 REACTIVE ION ETCHING

As a mode of plasma processing technology in which chemically reactive discharges are used to modify the surface properties of materials [31], RIE is vitally important to several of the largest manufacturing industries in the world. This technology provides unique ways for materials processing. For example, such small features can be generated that hundreds of them can be fit endwise within the width of a human hair. The introduction of plasma etching into manufacturing environments has been forced by the demands of microstructure fabrication technology [31, 32]. Being known as an effective technique which can provide a high precision anisotropic etching with minimum loss of the critical dimensions of desired patterns, RIE has been recently used to fabricate etched microlenses in glass and silicon [6-9].

Examining anisotropic etches involves the study of the fundamentals of plasma processing. Nevertheless, for the work of this project, only an understanding of the basic process is required. It is important to consider the entire set of processing requirements for a particular application. For pattern transfer, these might include requirements on etch rate, anisotropy, selectivity, uniformity across the substrate, surface quality, and process reproducibility. In terms of the commercial interest for certain quality requirements, the higher the etch rate the better because that in return will affect the cost effectiveness of production. This section will summarize basic concepts and process characteristics on dry etching that are crucial for the work of this project.

3.1.1 Basic Concepts

Etch mechanism: Basically, plasma etching can be thought of as a process in which a glow discharge is used to generate chemically reactive species such as atoms, radicals, ions from a relative inert molecular gas [32]. There are four basic low pressure plasma processes that can contribute to material removal from the surfaces in etching:

sputtering (Fig. 3.1(a)), pure chemical etching (Fig. 3.1(b)), ion energy driven etching (Fig. 3.1(c)), and ion inhibitor etching (3.1(d)).

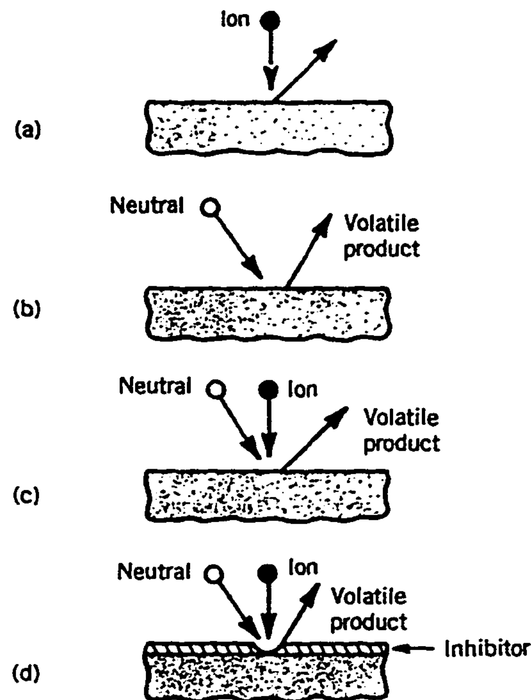

(a) sputtering. (b) pure chemical etching.
(c) ion energy driven etching (d) ion inhibitor etching

Figure 3.1 Basic low pressure processes of plasma etching.

RIE processes can be considered as ion-enhanced energy-driven etching, in which the combined effect of both etchant atoms and energetic ions in producing etch products is generated. An electric discharge supplies both etchants and energetic ions to the surface. The etch rate can generally be much larger than that produced by either pure chemical etching or by sputtering alone and it increases with increasing ion energy above a threshold energy of a few volts. As for pure chemical etching, in this process the etch product must be volatile. The etching is normally highly anisotropic because the energetic ions have a highly directional angular distribution when they strike the substrate. The detailed mechanism for etch product formation and the rate of formation are not well understood.

More details on related quantitative aspects such as plasma behavior, chemical reaction, chemical equilibrium, chemical kinetics and surface process etc. in plasma etching can be found in [31, 32] and especially in [33] for SiO_2 etching.

Etch rate: The etch rate in RIE processes is strongly affected by the plasma composition. Figure 3.2 (presented in [31, 32]) illustrates an example of the effect of a chemical reaction enhanced by plasma discharge on etch rate which is the measure of material removal per unit time. At first, the equilibrium chemical etch rate of silicon in the XeF_2 etchant gas is approximately 5 Å/min. Next, a drastical increase in etch rate is obtained by the addition of argon ion bombardment of the substrate (plasma-assisted). Finally, the last time period shows very low etch rate generated by physical sputtering of silicon by ion bombardment alone.

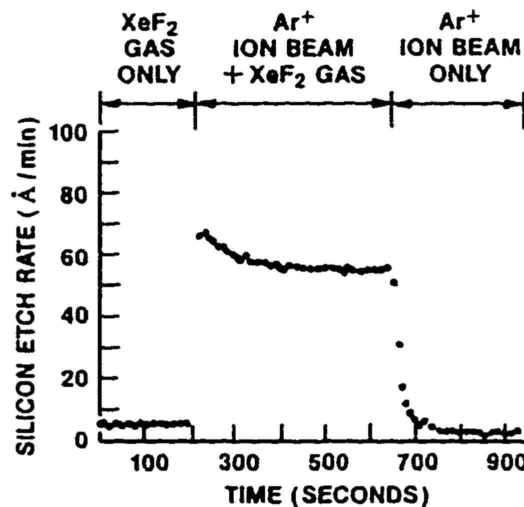

Figure 3.2 The effect of plasma-enhanced chemical reaction on etch rate.

Etch anisotropy: Anisotropic etch processes can faithfully transfer the mask patterns into substrate and can be easily produced by plasma processing. Figure 3.3 explains the concept of anisotropic or directional etch which has etch rates in z direction larger than the lateral (x and y) etch rates. The extreme case is the vertical etch (lateral etch rate is zero). If the lateral etch rates are not zero the anisotropy is quantitatively defined as

$$a = \frac{E_v}{E_h} \tag{3.1}$$

where E_v is the vertical etch rate and E_h is the horizontal etch rate.

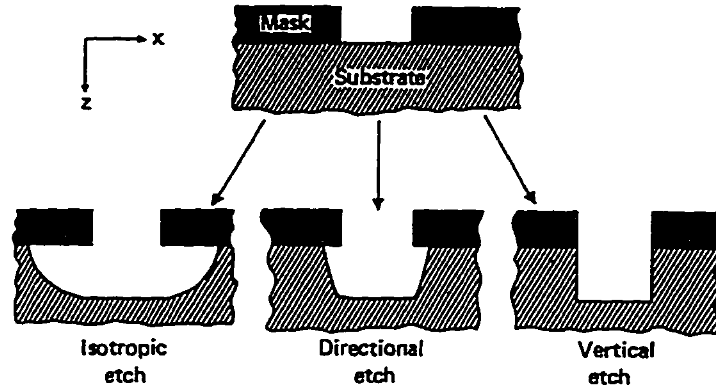

Figure 3.3 Illustration of anisotropic (directional) etch.

<u>Etch selectivity:</u>

In practice, the selectivity is used to quantitatively analyze the requirements of a simultaneous etch of different materials present in etching process. It is given by ratios of etch rates and in the next section it is taken as the ratio of substrate etch rate E_s to polymer etch rate E_p and is given by

$$S = \frac{E_s}{E_p} \tag{3.2}$$

3.1.2 Process Control Parameters

In plasma etching, the process control is very problematic because the number of parameters that affect the ultimate results is large [32]. The complexity of the problem is in the basic plasma physics and the consequences of plasma-surface interaction [31-33]. In general, this complexity gives a number of different ways to control processes, but it makes the problem of modeling become very difficult.

Basically, the parameters that determine the nature of processing plasma are excitation power, excitation frequency, gas flow rate, nature of discharge gas, reactor geometry, and pumping speed at the vacuum chamber. At the same time, plasma-surface interactions are affected by parameters such as surface geometry, surface temperature, the nature and potential of the surface. However, in practice with available gases such as O_2, CHF_3, CF_4, and SF_6 for the RIE system, the process control is based on varying:

1. The gas composition of selected species which are fed in to reactor chamber by setting the openings of mass flow controllers (MFC);
2. The pressure in the reactor chamber set by combination of roughing and turbo pumps;
3. The setting of the excitation power of the processing plasma.

In the process control, it is also necessary to estimate the required etching time which is principally determined by the thickness of removal, the nonuniformity factor due to thickness variation of etched features and vertical etch rate variations across the substrate surface.

3.2 PRELIMINARY INVESTIGATIONS

This section will describe work done in early stages of development of processes that allow the transfer of dispensed polymer microlens patterns into fused silica and silicon substrates by using RIE. The initial etch trials showed very encouraging results, but to get to the point that the developed processes can give the desired etch quality, it took some time to identify the cause of defects caused by an inappropriate cleaning process.

3.2.1 Analysis of Etched Shapes

A conceptual description of transferring dispensed polymer microlens patterns into substrates by using RIE is illustrated in Fig. 3.4. In this process, polymer microlenses are gradually etched away so that the same patterns will be formed into substrates as etched

microlenses whose characteristics are defined by the final etched shapes. Figure 3.5 describes qualitatively the effect of etch selectivity S on the formation of etched lens shapes (cross sections). Some examples shown in Fig. 3.6 are typical profiles of partially etched samples scanned with the Alpha Step 2000 profilometer.

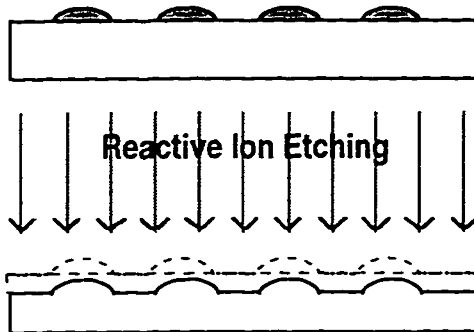

Figure 3.4 Transferring dispensed polymer microlens patterns into substrate by RIE.

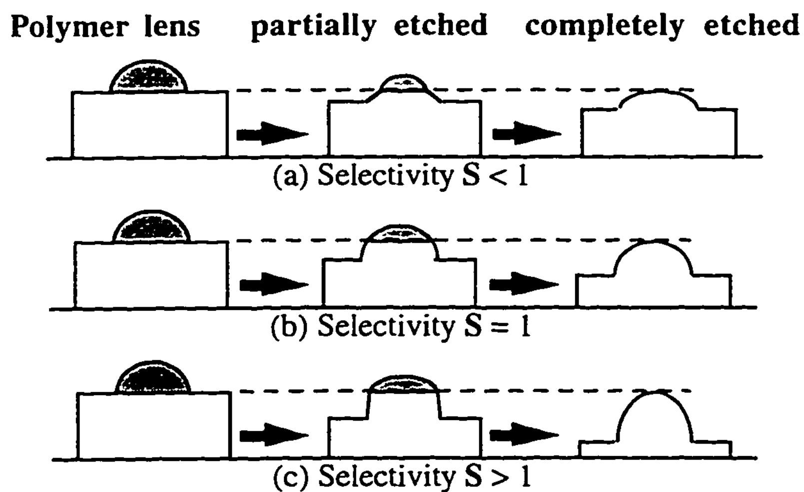

Figure 3.5 Etched lens formed by RIE process.

The analysis of etched shapes will become more useful for the RIE process control if it can be quantitatively described. Since the control of the RIE processing parameters can ultimately be converted into changes of etch rates and of etch selectivity S, the simplified analysis in this work will be based on following assumptions:

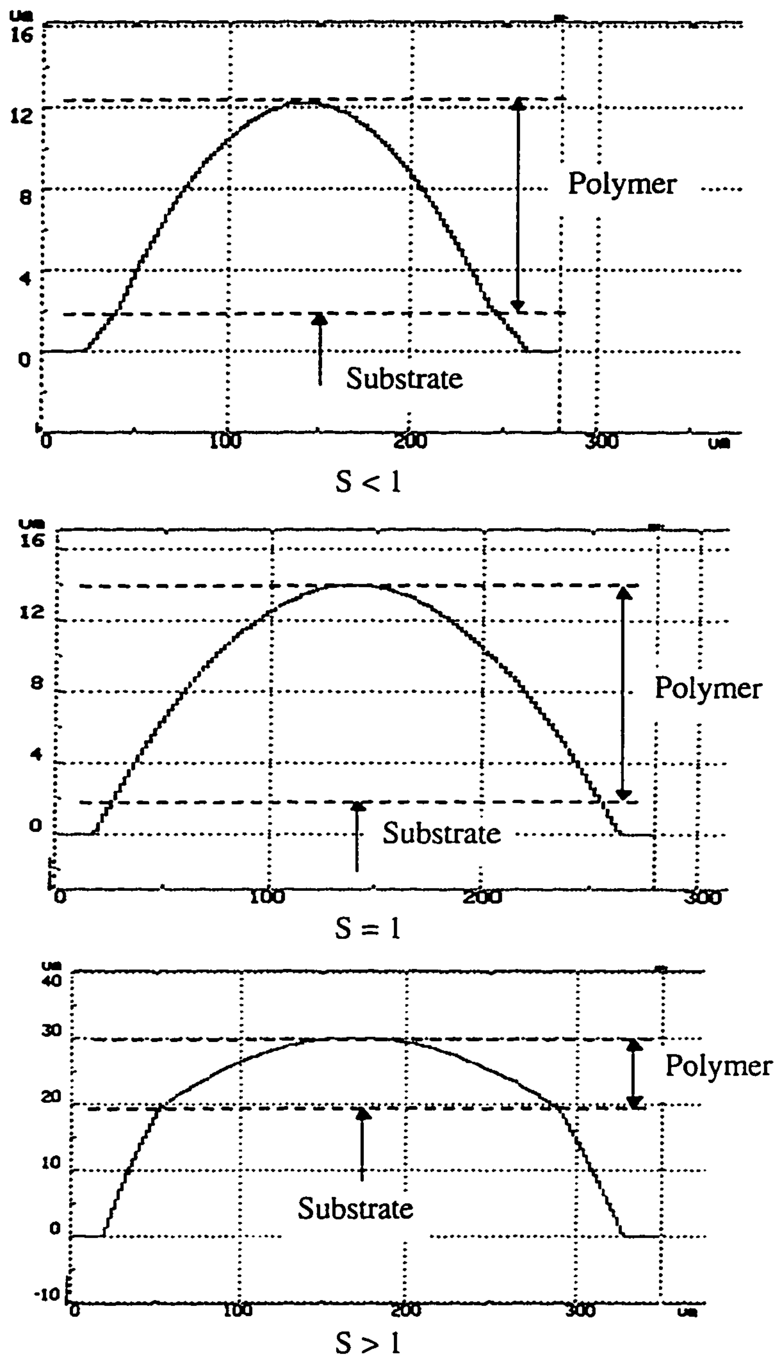

Figure 3.6 Partially etched profiles scanned with profilometer.

1. Polymer lenses have the ideal shapes that are defined by the surface tension between the dispensed polymer and the substrate for both spherical and cylindrical lenses. The effects of gravity are negligible.

2. The etch selectivity S is uniform over all the surface of the lens.

3. Lenses are formed by a highly anisotropic process. That means etched materials are removed mostly vertically and the change in lens diameter after the complete etch is negligible.

By using assumption 1 and coordinates defined in the previous chapter (see Fig. 2.2) the ideal polymer lens shape will have a cross section whose profile is mathematically given by

$$\left(\frac{x_p}{R_p}\right)^2 + \left(\frac{y_p - (h_p - R_p)}{R_p}\right)^2 = 1; -D/2 \leq x_p \leq +D/2 \text{ and } 0 \leq y_p \quad (3.3)$$

where
$$D = 2\sqrt{h_p(2R_p - h_p)} \quad (3.4)$$

and R_p, h_p, x_p, and y_p are defined in Fig. 2.2 of Chapter 2.

After etching, vertical distances will be scaled by a factor S. By substituting

$$y_p = y_s/S \quad (3.5)$$

and
$$x_p = x_s \quad (3.6)$$

where x_s, y_s are the profile coordinates of substrate lens, Equation (3.3) becomes

$$\left(\frac{x_s}{R_p}\right)^2 + \left(\frac{y_s - S(h_p - R_p)}{SR_p}\right)^2 = 1; -D/2 \leq x_s \leq +D/2 \text{ and } 0 \leq y_s \quad (3.7)$$

Equation (3.7) describes an arc of an ellipse and it shows the dependence of etched lens shapes on the etch selectivity S.

3.2.2 Initial Etch

Using dispensed polymer microlenses as masks in fabricating etched microlenses seems advantageous. An initial etch was done to examine whether or not it was feasible to transfer dispensed polymer microlens patterns into quartz and Corning 7059F glass substrates. Microlens patterns of different dispensed polymers were created on the

substrates and then were etched in the RIE chamber. The details of this work are summarized in the next paragraphs.

Sample preparation before etching: The first batch of samples for the test etch were generated as follows:

1. Arrays of 6×6 were chosen just enough to guarantee the uniformity of lenses within an array, and spacing was chosen to be 0.4 mm (arbitrary).
2. Lenses were made of three polymer types NOA 63, NOA 65, NOA 68 which have had fairly consistent dispensing characterization data (see Chapter 2).
3. Substrates used: Corning 7059F glass coated with a thin layer CVD-SiO_2 that allows dispensed optical adhesives spread evenly to form good microlenses easily and quartz pieces (available at AMC and are used for monitor windows of the RIE apparatus).
4. Lens sizes were in the diameter range from 0.2 to 0.3 mm. Figure 3.7 shows approximately what these lenses looked like. The shape of their cross sections should be about the same as those of the scanned cylindrical polymer profile shown in Fig. 3.7(b).

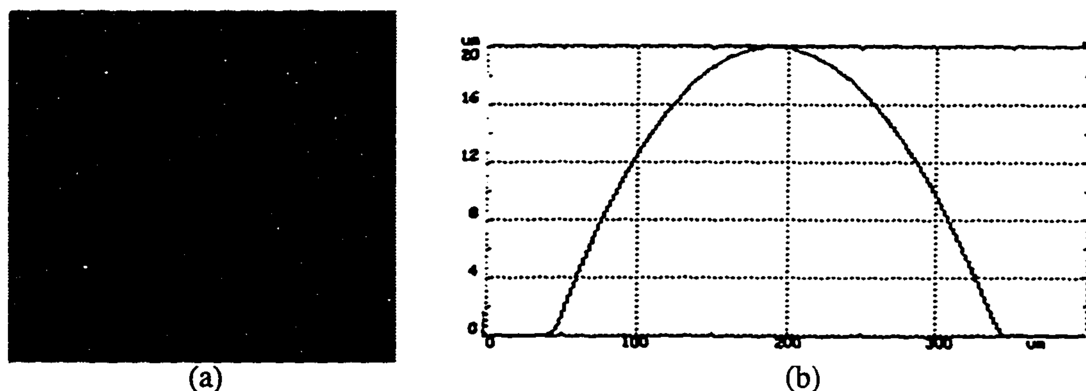

(a) Microscope picture of some polymer microlenses used for the initial etch.
(b) Approximate dimensions of polymer lenses for the initial etch.

Figure 3.7 Dispensed polymer microlenses which were initially etched.

5. The same substrate cleaning and the dispensing technique described in Chapter 2 was used. The top dispensing mode (the polymer was pushed out before being brought to contact with the substrate) which is believed to give better dispensing uniformity was applied. Dispensing parameters are given in Table 3.1.

Table 3.1 Dispensing parameters for initial etched samples

Polymer	Pressure (psi)	Time (second)	Tip Diameter (μm)
NOA 68	10	0.19	100
NOA 65	5	0.1	100
NOA 63	5	0.1	100

Etching: The prepared samples were tested by using the RIE equipment with a recipe previously developed at AMC for quartz etching. The scanning electron microscope (SEM) pictures of the etched profiles are shown in Fig. 3.8. To save time required by a full etch, in this test the dispensed polymer patterns were first partially etched for about 45 minutes (Fig. 3.8(a)), then the unetched polymer was partially stripped (Fig. 3.8(b)) to reduce the amount of polymer. Finally, the sample was etched again until no polymer was left (Fig. 3.8(c)). These pictures indicated promising successful results for the tested approach although a number of small pits were observed. This problem will be discussed again in Section 3.2.4.

The same etching test for samples of Corning 7059F glass substrates was done but the results seemed to show that this material was not etched. Later, the conditions of the previous run were repeated. The etching time was 5 hours. Both the microscope pictures and scanned profile in Fig. 3.9 indicate that this glass was not etched. Figures 3.9(b) and 3.9(c) show a very slightly etched profile whose scanned height of only 2.5 μm is about the thickness of CVD-SiO_2 layer deposited on the substrate surface. It is very likely that these profiles were patterns of dispensed polymer microlenses etched into the oxide layer.

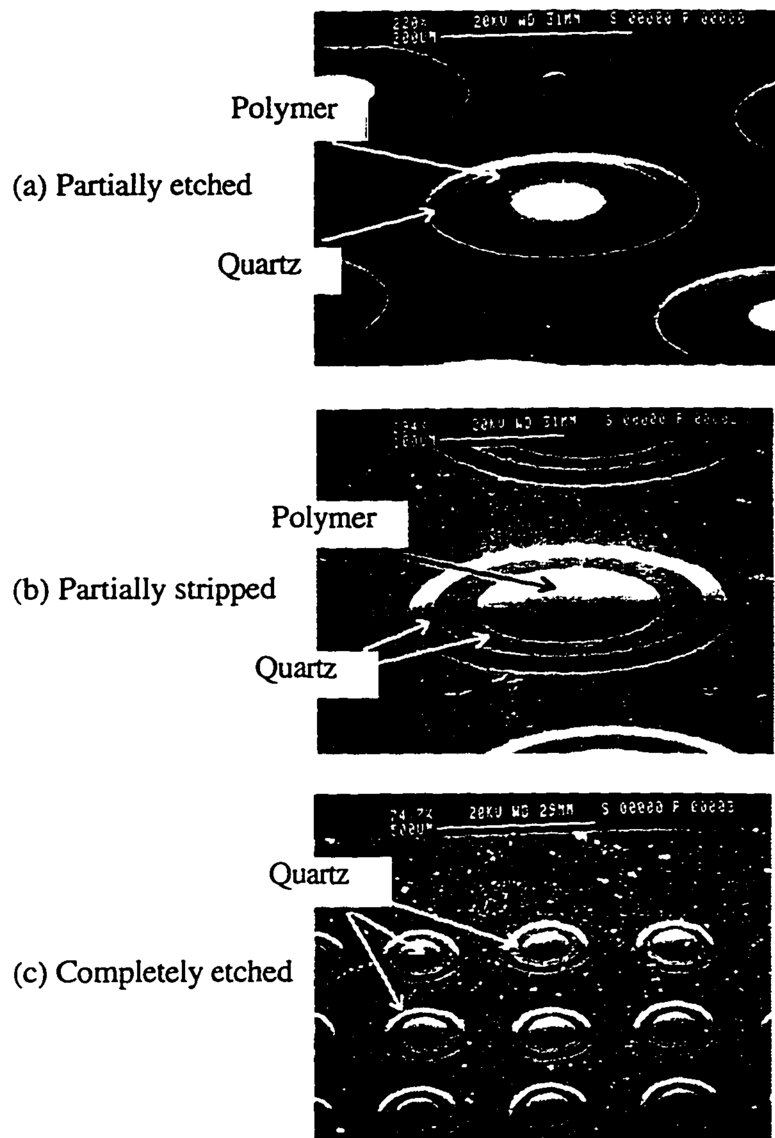

Figure 3.8 SEM pictures of the initially etched quartz sample.

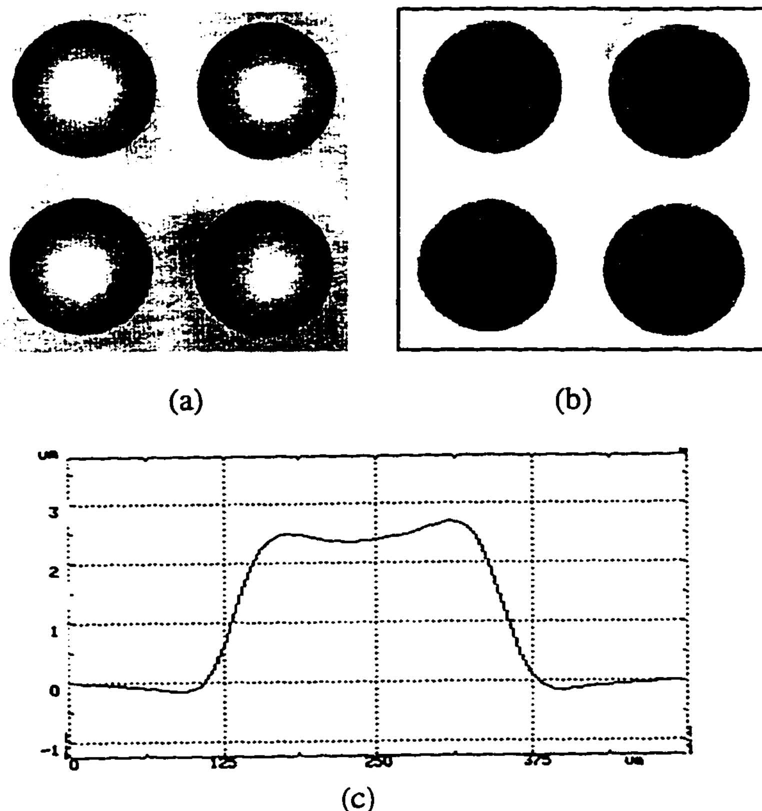

(a) Polymer Lenses before etching, magnification 153×
(b) Picture of vaguely etched profiles, magnification 153×
(c) A scanned profile of slightly etched patterns.

Figure 3.9 Corning 7059F glass was not etched by RIE.

3.2.3 Scanning Accuracy with the Profilometer

In the characterization process, the measuring tools and the way of using them have certain effects on measurement results. In this work, etch rates and etched profiles are determined by using the mechanical scanning profilometer which is a very commonly used tool in microfabrication for the measurement of etched depths in materials. Thus, its accuracy needs to be examined for the etch selectivity characterization which is crucial for the fabrication process of etched lenses.

Figure 3.10 shows the profiles of an etched sample at one spot scanned with different speeds which gave significant discrepancies between measured results. At the

scanning speed of 0.01 mm/s (0.25 mm is scanned in 25 seconds shown in the legend of Fig. 3.10(a)) more details of profile can be recorded. Less details are taken at the speed of 0.05 mm/s (Fig. 3.10(b)) and the speed of 0.25 mm/s gives the least details of the profile (Fig. 3.10(c)). Therefore, the slower the scanning speed is, the more reliable the scanning results will be.

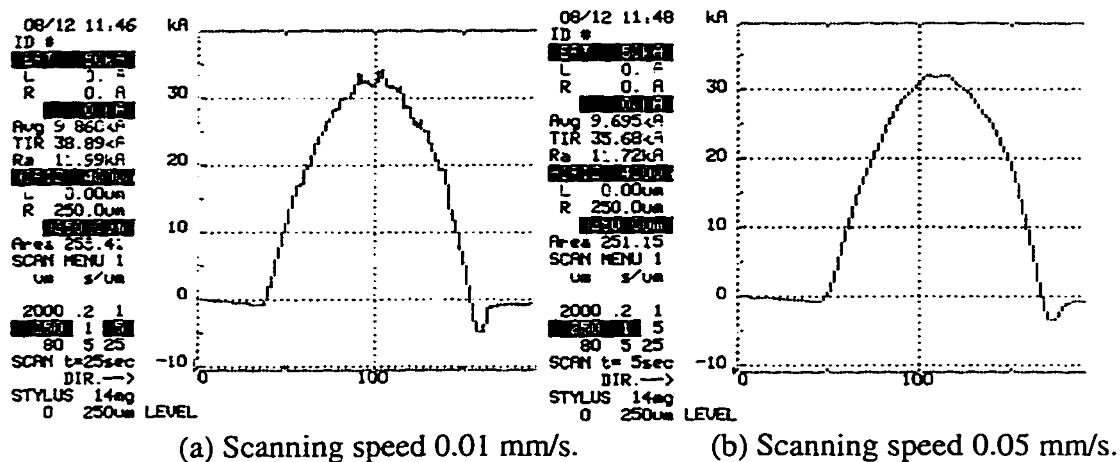

(a) Scanning speed 0.01 mm/s. (b) Scanning speed 0.05 mm/s.

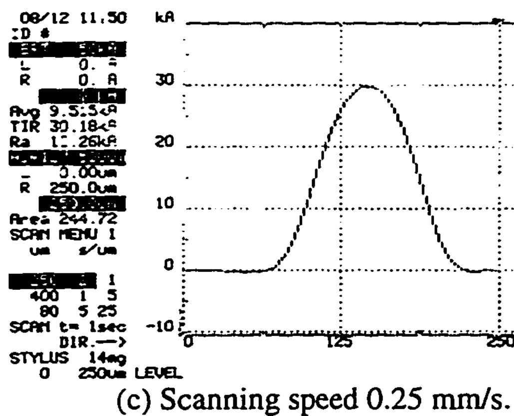

(c) Scanning speed 0.25 mm/s.

Figure 3.10 The effect of scanning speed on the accuracy.

3.2.4 The Role of Cleaning Process

RIE, as in other clean room techniques, requires some standard procedures to be followed. The way the substrate is cleaned before processing is very critical. In this project it has been found that any substrate cleaning process with methanol or acetone in the last

step that might cause some residues to react with polymer is fatal to RIE. This section will discuss why it had taken some time until this conclusion was arrived at.

After the initial etch had been done, the results were analyzed to plan the development of a fabrication process for etched microlenses. First of all, it was assumed that the pits on the surface of the test etch sample were a consequence of using a low quality quartz substrate (Corning glass was not etched after the first test). Therefore, the work after the first test concentrated on

1. producing the first complete etch of microlens arrays in quartz and silicon;
2. doing trials with Corning glass etching to confirm the previous result;
3. analyzing the effect of etch selectivity on F# and spherical aberration of the final etched lens shapes;
4. carrying out the recipe characterization work (the investigation of the etch selectivity range).

Details of the first step are given in this section while those of the last two are presented in Section 3.3. NOA 68 was chosen for the dispensed polymer microlenses to limit the investigation to a reasonable time period. Using other adhesives could be the subject of further work.

The first complete etch: A similar lens sample of a 10×10 array and the same recipe as the one used for the initial etch (see Section 3.2.2) were tested to produce a completely etched microlens array in quartz pieces which were originally used for monitor windows of the RIE apparatus. The total etching time was 4 hours. The SEM picture of this quartz lens array is shown in Fig. 3.11(a), and as is a close-up picture of two lenses in Fig. 3.11(b). Table 3.2 compares specifications of some dispensed polymer microlenses to those of their etched counterparts of the array shown in Fig. 3.11.

After the first complete etch had been done, the F# control of the etched lens fabrication process with dispensed polymer microlenses as masks seemed ready to be characterized for the following reasons:

1. The surface quality problem in the previous etches was still believed due to substrate quality (quartz of monitor windows).
2. Some characterization samples that had been made up to this point did not show any evidence of this problem because their substrates were silicon coated with CVD-SiO_2, but were not cleaned with methanol or acetone before etching.

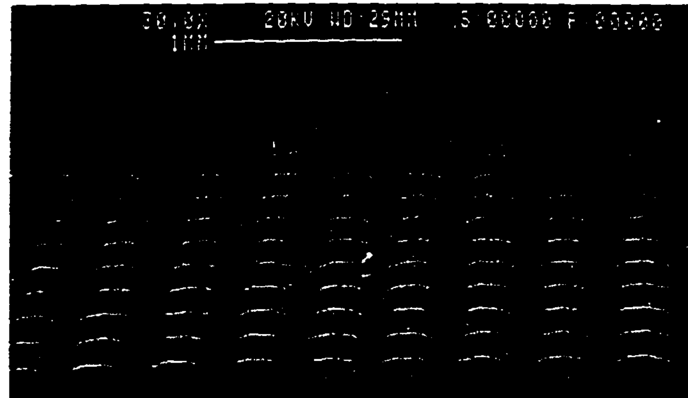

(a) Picture of the etched microlens array.

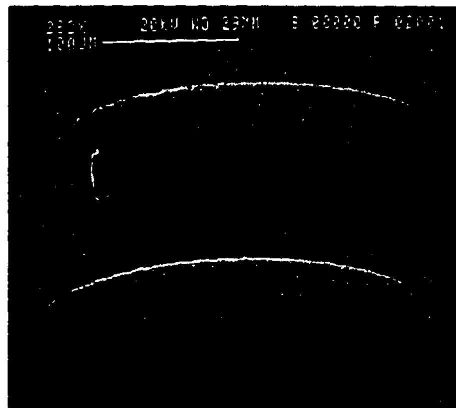

(b) Close-up picture

Figure 3.11 The first completely etched quartz microlens array.

Table 3.2 Lens characteristics comparison.

Lens parameter	Polymer lens (before etching)				Quartz lens (after etching)			
Ø (μm)	297.0	295.0	298.0	298.0	297.0	295.0	301.0	298.0
Focal length (mm)	1.37	1.44	1.38	1.41	2.42	2.40	2.43	2.38
F#	4.61	4.87	4.62	4.72	8.15	8.12	8.07	7.97

However, not until the first cylindrical glass microlens design failed was it realized that the damaged etched surfaces shown in Fig. 3.12 were caused by something other than just the material quality of the substrates. In this design, the etched surfaces on Corning 7059F glass substrates were layers of CVD-SiO_2 which was coated on the silicon substrates used before that for recipe characterization. The only difference was that the silicon substrates were not cleaned with methanol or acetone and no surface damages were observed with these samples. Therefore, more efforts were required to identify the cause of this problem.

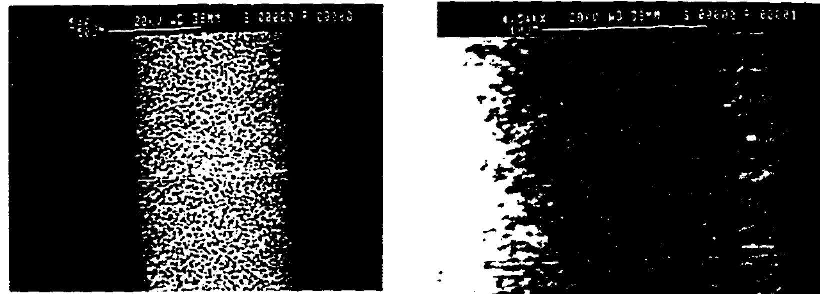

Figure 3.12 Damaged etched surfaces before surface correction.

<u>**Correction of surface problem:**</u> Different trial processes were utilized to identify the problem including

1. Baking the polymer NOA 68 at temperature up to 250°C for 4 hours. The surface of a cylindrical microlens looked the same before and after baking (Fig. 3.13). No surface damage due to thermal expansion of polymer was observed.

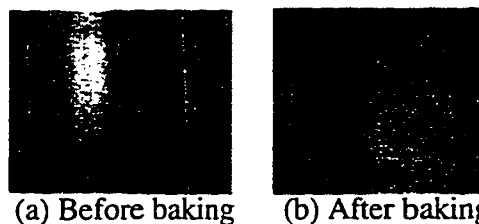

(a) Before baking (b) After baking

Figure 3.13 No thermal effect on cylindrical polymer surface by baking; Magnification 153×.

2. The substrate was cleaned using the piranha process (see Appendix II). After that, dispensing was done manually in a clean room and the samples were etched without leaving the clean room. This process eliminated all surface damages.
3. In another trial, the substrate was cleaned using piranha process then kept tightly closed until dispensing which was done with the set up in the lab at TRLabs, and that was successful as well.

(a) CVD-O_2. Magnification of 153×

(b) CVD-O_2. Magnification of 118×

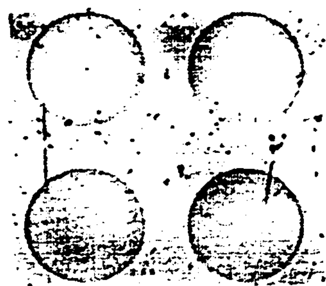

(a) Quartz. Magnification of 153×

(b) Quartz. Magnification of 153×

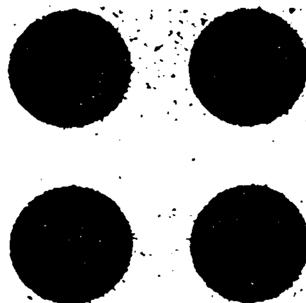

(a) Silicon. Magnification of 153×

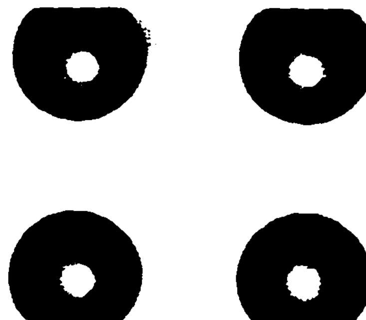

(b) Silicon. Magnification of 153×

Figure 3.14 Microscope pictures of similar microlens arrays between damaged surfaces (a) and corrected surfaces (b).

Fig. 3.14 compares the corrected surfaces with damaged surfaces of etched samples. Since then, the method of trial 3 has been applied successfully to produce different prototypes.

3.3 PROCESS CONTROL

Once the process was proved to be working for the substrate microlens fabrication, the remaining question was how to control the process to meet requirements of a particular lens design. That is the focus of discussions in the next subsection.

3.3.1 F# and Selectivity Analysis

Normally, the two main parameters for a particular lens design are the lens diameter and F#. To simplify deriving the analytical relationship between the F#s of etched lenses and the etch selectivity S in the RIE processes, the analysis is based on the paraxial region of the lens with the same assumptions made in Section 3.2.1.

Assuming the specifications of a dispensed polymer microlens are known, it is desirable to derive the etch selectivity S for an F# of an etched lens design. First of all, due to the highly directional nature of RIE, the diameters of the etched lens is assumed to be the same as that of the polymer microlens before etching. By using Equation (3.7), the radius of curvature $R_s(0)$ at the vertex of the etched lens due to $y_s'(0) = 0$ is given by

$$\frac{1}{R_s(0)} = y_s''(0) \qquad (3.8)$$

Together with Equation (2.11) the required selectivity is

$$S = \frac{(n_p - 1)}{(n_s - 1)} \frac{F\#_p}{F\#_s} \qquad (3.9)$$

where in addition to $F\#_p$ and n_p defined previously,

$F\#_s$ = F-number of the etched lens.

n_s = refractive index of substrate material.

The necessary etch selectivity S will be given by the appropriate choice of an etch recipe (pressure, power and gas mixture) determined by characterization. Table 3.3 gives some examples of the cases for known S and F#s of polymer microlenses. The estimated $F\#_s$ values of etched lenses were determined by using Equation (3.9) and the measured ones were achieved after etching. For the estimation the refractive indices were taken n_p = 1.54 for NOA 68 and n_s = 1.46 for bulk quartz.

Table 3.3 Estimated and measured F#s of quartz microlenses

Selectivity S	F#s of Polymer Lenses	F#s of Etched Lenses		Deviation	
		Estimated	Measured	absolute	%
0.76	4.61	7.12	8.15	1.03	12.6
	4.87	7.52	8.12	0.60	7.4
	4.62	7.14	8.07	0.93	11.5
	4.72	7.29	7.97	0.68	8.5
0.16	3.91	28.69	28.00	- 0.69	- 2.4
1.00	3.14	3.69	3.70	0.01	0.3
1.78	4.40	2.89	2.00	- 0.89	- 44.5

Table 3.4 Examples of guessed recipes.

Prototype		F#s		
Array type	Lens type	Polymer lens	Etched lens	
			Achieved	Targeted
5×5	Spherical	2.83	15	20
5×5	Spherical	2.83	19.1	20
15×15	Spherical	2.8	39.5	40
15×15	Spherical	2.8	34	40
15×15	Spherical	2.8	33	40
1×24	Cylindrical	2.54	14.1	12.5 ± 5%

Based on the tendency of the F# of etched quartz microlenses to increase with the increasing O_2 content in the gas mixture, one can guess the etch recipe for a certain design based on the previously known recipes. Table 3.4 are examples of fabrication cases which

were done with estimated recipes because the profilometer for the measurement of the necessary selectivity was not available at the time of etching.

3.3.2 Etch Recipe Characterization

From the previous sections, it has been confirmed that dispensed polymer microlenses may be transferred into a substrate by RIE. In addition, Equation (3.9) may be used to estimate the required etch selectivity for a desired lens design. The next step is to carry out the etch recipe characterization which will determine the selectivity for each RIE recipe. Because of the large number of variable parameters and the length of time to process one sample, this work could take a long time to complete. It has been ongoing since the beginning of the project and is still unfinished. This section presents the main procedures of the characterization work and gives some preliminary results.

The substrates used in this work are (a) silicon wafer double-sided polished for etching silicon and (b) silicon wafers coated with a CVD-SiO_2 layer 2 to 5 μm thick for etching fused silica (quartz and CVD-SiO_2). The main variables which affect RIE are gas mixture, gas flow, pressure, and power. As well, there are a large number of polymers to choose from. Only NOA 68 has been used so far. The parameters are expressed as:

1. Gas flow in % opening of MFC.
2. Pressure in mTorr.
3. Driving power for plasma system in W.
4. Etch rate is given in μm.

The procedure order is as follows:

1. For substrates kept tight from the clean room, no cleaning is required except for dusting off. Otherwise, substrate cleaning by piranha process (Appendix II) should be applied.

2. Fabrication of dispensed cylindrical microlens profile of polymer (only NOA 68 used up to this point): For scanning with the profilometer, it is easy to get the heights of dispensed cylindrical microlenses although it is possible with the spherical lenses. The samples are made by using dispensing technique described in Chapter 2.

3. Etching and selectivity measurements:

3.1 Scanning the height h_p of the polymer lens profile using the profilometer before etching (for an example see Fig. 3.7(b)).

3.2 Partially etching the profile:

- Setting gas mixture for etching process from available gases (O_2, CHF_3, CF_4, SF_6). Commonly used gases are O_2, CHF_3, and CF_4 for fused silica whereas O_2, CF_4, and CF_4 for silicon.
- Normally, the etching time for fused silica is about 30 to 45 minutes and it is much shorter (about 10 minutes) for silicon.

3.3 Scanning the height h_{part} of the partially etched profile using profilometer. Typical scanned profiles for different ranges of selectivity S can be referred to Fig. 3.6.

3.4 Stripping polymer by etching the partially etched sample for 3 to 10 minutes again with a recipe developed at AMC.

3.5 Scanning the same sample after polymer was stripped (see Fig. 3.15).

3.6 Calculating etch rates and etch selectivity:

$$ER_s = (DE_s)/\, t_e \tag{3.10}$$

$$ER_p = [h_p - (h_{part} - DE_s)]/\, t_e \tag{3.11}$$

$$S = ER_s/\, ER_p = (DE_s)/\, [h_p - (h_{part} - DE_s)] \tag{3.12}$$

where

- Substrate etch rate = ER_s.
- Polymer etch rate = ER_p.
- Etch selectivity = S.
- Etched depth into substrate = DE_s (see Fig. 3.15) .

- Etching time = t_e.

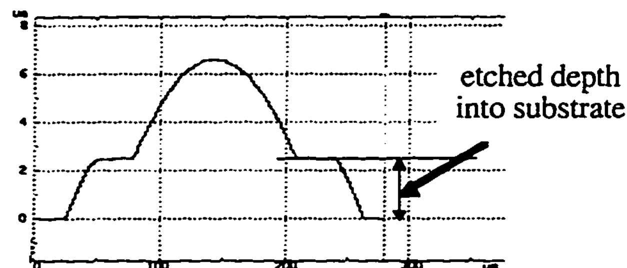

Figure 3.15 Polymer partially stripped after having been partially etched.

The preliminary characterization results have shown that CF_4-flow and O_2-flow have a similar effect on selectivity in both quartz and silicon etching. This effect of O_2-flow is shown in Fig. 3.16 with CHF_3-flow as parameter for quartz and SF_6-flow for silicon. In all recipes used throughout the project, gas concentration is measured as the percentage of the full open position of the mass flow controller (MFC) built into the system. Fig. 3.17 shows the effect of plasma power on substrate etch rates which are related to polymer etch rates by the selectivity. These etch rates can be used to determined the required times for full etches. During the characterization the following issues were addressed:

1. Baking polymer lens at 80°C to remove some residue, but no clear difference was found.
2. Time dependence of selectivity by using one recipe for a calibrated lens array: Because the scanning accuracy of profilometer is limited, no significant difference was measured.
3. Testing the loading effect by comparing runs of different sample numbers per batch: No difference between run of one sample and of eight samples was found, probably because the limited accuracy of scanning does not have enough resolution.

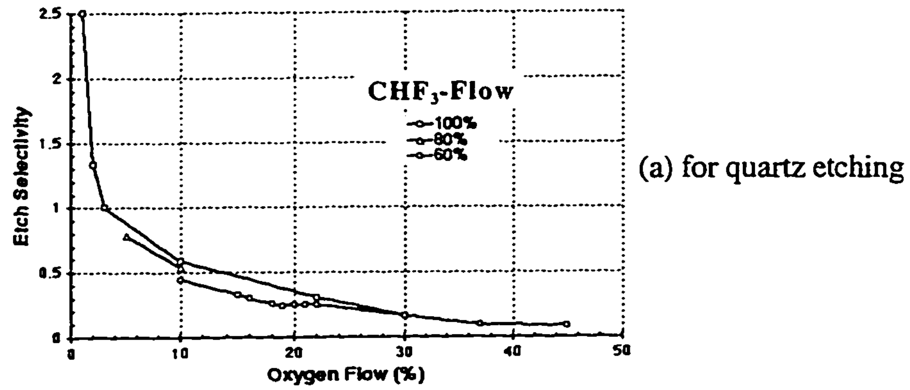

(a) for quartz etching

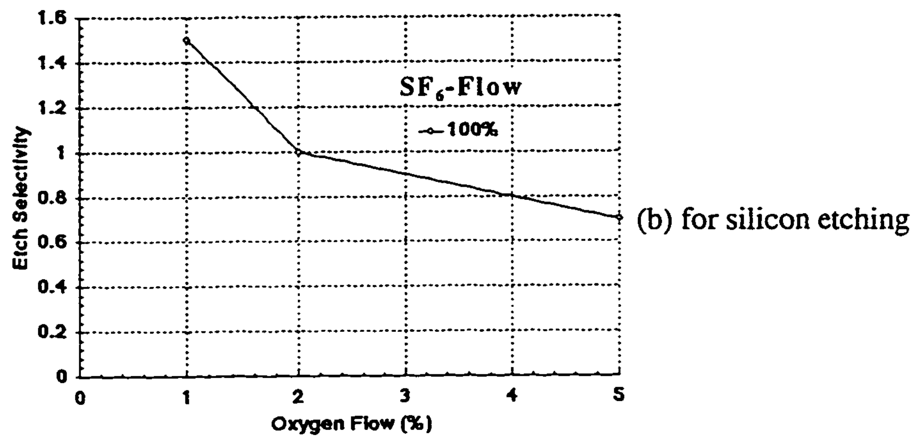

(b) for silicon etching

Figure 3.16 The effect of O_2-flow on etch selectivity.

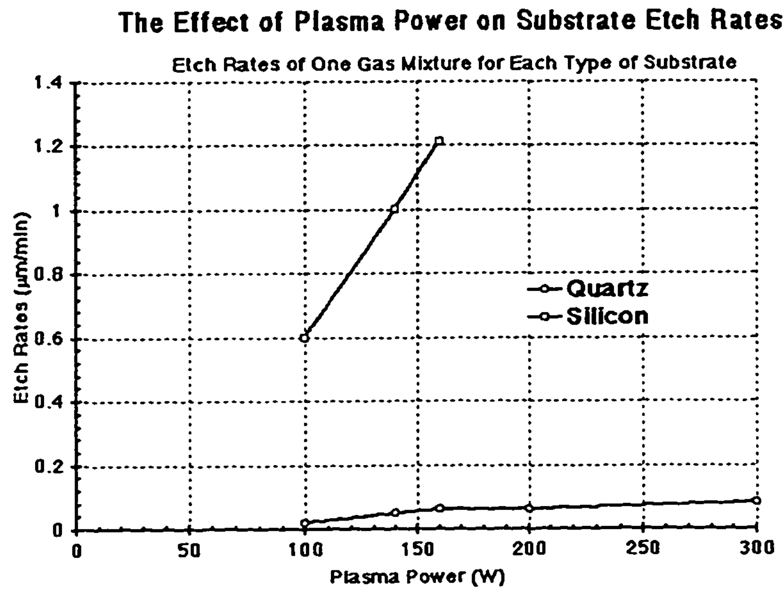

Figure 3.17 The effect of plasma power on substrate etch rates.

3.4 DISCUSSION

After a certain period of time, the processes that allow the transfer of patterns of dispensed polymer lenses into fused silica (quartz and CVD-SiO_2) and silicon were developed. The RIE process can be conveniently controlled to meet requirements of particular desired lens designs with a satisfactory accuracy. Characterization results have shown that varying contents of O_2 similar to that of CF_4 have a significant effect on the etch selectivity while the change in plasma power affect mainly the etch rates which determines the complete time of etching. Along with the development results of the process a number of etch recipes have been documented. The fabrication procedure is given in Appendix II.

This achievement is the result of work done in preliminary investigations, recipe characterization, and simplified analysis of lens shape as well as of the relationship between F# and the etch selectivity. After that, some lens prototypes were also fabricated to confirm the validity of the processes developed. Nevertheless, the poorly understood nature of RIE gives rise to the need for a better model of lens shape analysis and for more accurate tools for etch rate determination to meet more precisely the requirements of different applications. The work done in the past has shown the processing time with selectivity $S < 1$ (especially, for long focal length design) or with $S = 1$ is fairly reasonable (average 3 to 5 hours) whereas for $S > 1$ the etching time becomes enormously large and even much longer than that estimated from measured selectivity (it could be more than 20 hours). Therefore, improving the effectiveness of the etching process also needs further investigation.

4. MICROLENS TESTING

To ensure that application requirements are met, the microlens manufacturer and/or user must make measurements of design parameters [34]. Testing principles of microlenses are not different from those of other lenses. The measured parameters and techniques used are the same. However, very often the measurements of very small lenses make it difficult to use the standard equipment that is available for the testing of bulk optics [35].

This chapter discusses measurements of interest in this project, and also a way of using a Mach-Zehnder interferometer in the laboratory for different measurements, especially the simplifying of the interferogram generation procedure. Microlenses which are measured in this work have diameters between 0.1 mm and 5 mm, and focal lengths between approximately 0.1 mm and 10 mm. First, an overview on microlens measurements is given.

4.1 OVERVIEW ON MICROLENS MEASUREMENTS

A particular lens design will specify required parameters with their tolerances. In general, microlens measurements are done for geometrical properties such as surface profile, diameter, focal length, fill factor and for performance properties such as wavefront and wave aberration, modulation transfer function (MTF), point-spread function (PSF), Strehl ratio, and optical efficiency.

Measuring is actually a process of the comparison between the parameters of interest with those of an ideal. Some of them are of interest to the manufacturer, the others of interest to the user and they are vital in achieving a given optical performance. Some of these parameters are more difficult to measure than others. Diameter and fill factor are relatively simple to determine. The lens surface profile and the wavefront shape are related to each other; therefore it may not be necessary to measure both of them. Based on an accurate wavefront measurement, MTF and PSF can be determined [34]. The related theoretical fundamentals, different techniques and equipment of these measurements are

described in [9, 34-45]. However, at the present time, this project is interested in only measurements of diameter, focal length, spherical aberration (in terms of wave aberration), and focused spot size for positive plano-convex microlenses.

One useful result of this project is that a laboratory Mach-Zehnder interferometer may be used for all measurements of present interest. The practical work and related concepts of these measurements will be described in the next sections.

4.2 MACH-ZEHNDER INTERFEROMETER

The Mach-Zehnder interferometer is a very effective lab tool for microlens testing [9, 34-36]. The theoretical background of its operation and of its characteristics are given in [40-42]. However, the next subsection describes briefly some main concepts related to this equipment.

4.2.1 Main Concepts

It is known that interference of light is the result of radiation coming from its source to the point of detection with more than one path. The resultant intensity can be observed as light and dark bands, called interference fringes. The records or the mathematical descriptions of these fringes are called as interferograms. Practically, interferometers are the apparatus which is used to generate any desired interference. When two beams come from the same sufficiently small source with a sufficiently narrow bandwidth, they are coherent and will interfere. Otherwise, they are incoherent, their intensities will add directly and no interference is produced if they come from different sources. For test interferograms, it is desirable to maximize their contrast (or their visibility) which is defined by Michelson and given in [40] as

$$V = (I_{max} - I_{min})/(I_{max} + I_{min}) \tag{4.1}$$

where I_{max} is the maximum light intensity distribution (light fringes) and I_{min} is the minimum one (dark fringes).

The development of lasers has made available light sources that can produce beams that are highly coherent with each other for almost all interferometer arrangements [40]. Interferometers can be classified according to the number of interfering beams, methods used to separate these beams, etc. The Mach-Zehnder interferometer, whose operation principle is illustrated in Fig. 4.1, is a type of two-beam (one in each arm) interferometer with amplitude division (of the input beam field (1)). It is also called a single-pass interferometer because the interfering beams go through the system once. The straight fringes (5) shown in the same figure for circular apertures are the result of an alignment of the two plane mirrors (3) such that the output beams emerge in slightly different directions. Detailed discussions of this interferometer are given in [40-42].

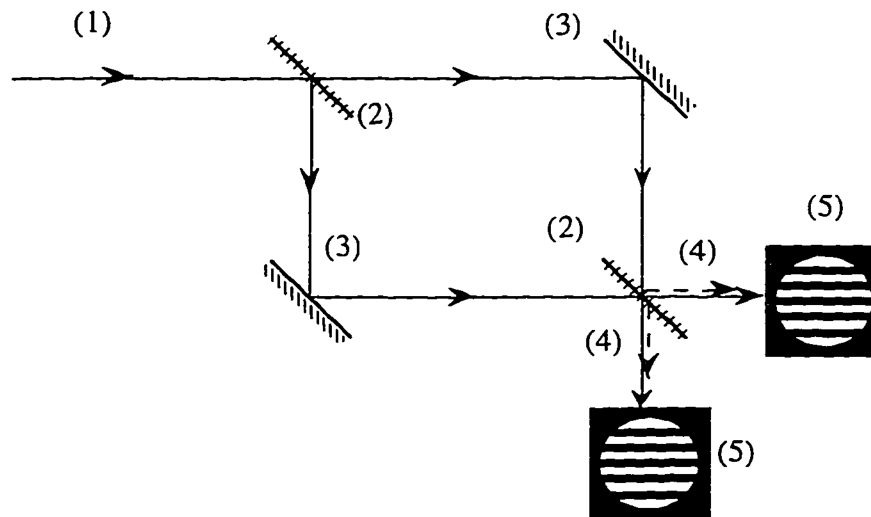

(1). Input beam; (2). Beamsplitters; (3). Plane mirrors; (4). Output beams; (5). Interferograms.

Figure 4.1 The operation principle of a Mach-Zehnder interferometer.

Using the concepts of wavefronts (contours of constant propagation phases) and rays (wavefront normals), Figure 4.2 describes two basic types of waves that are combined to generate interferograms of microlenses under test. In an isotropic medium, wavefronts of plane waves (Fig. 4.2a) propagate in the same direction whereas those of spherical waves spread in all directions (Fig. 4.2b).

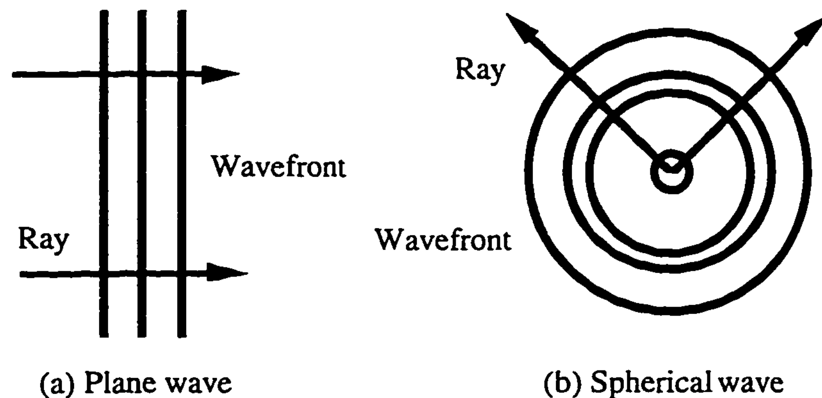

(a) Plane wave (b) Spherical wave

Figure 4.2 Concepts of light waves.

Theoretically, two spherical waves of point sources which are at a very large distance from the interfering plane (plane of interference fringes) will give interferograms of straight fringes (Young's fringes). As the limiting case (the sources at infinity), Figure 4.3(a) shows two plane waves with a tilt and their interference patterns of straight fringes (same as in Fig. 4.1). As the tilt between these two plane waves disappears, the fringes spread out [40] (Fig. 4.3(b)) until only one remains.

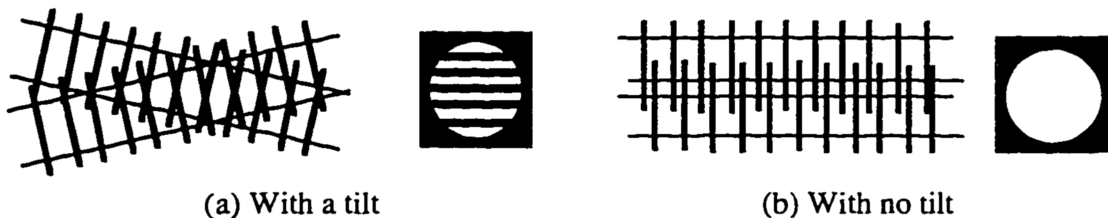

(a) With a tilt (b) With no tilt

Figure 4.3 Interference of two plane waves.

In contrast, non-plane waves will produce interferograms of non-straight fringes. Circular fringes will be generated if a spherical wave interferes with a plane wave (Fig. 4.4(a)). Similarly, interference fringes of a partially plane wave interfering with a plane wave are curved fringes for the case "with a tilt" (Fig. 4.4(b)) or a minimal number of circular fringes for the case "with no tilt" (Fig. 4.4(c)). Therefore, any optical element

placed in one arm of the apparatus in Fig. 4.1 can be analyzed by its effect on the fringe patterns at the output.

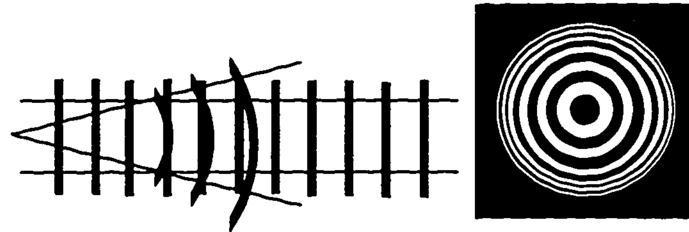

(a) Spherical wave

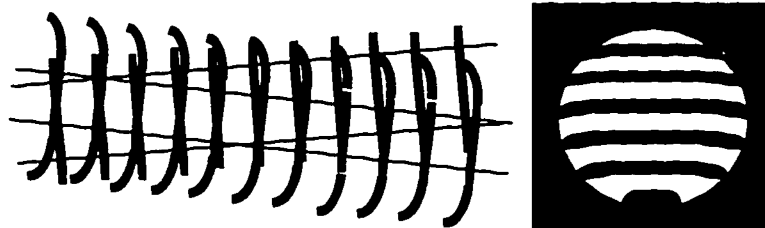

(b) Partially plane wave with a tilt

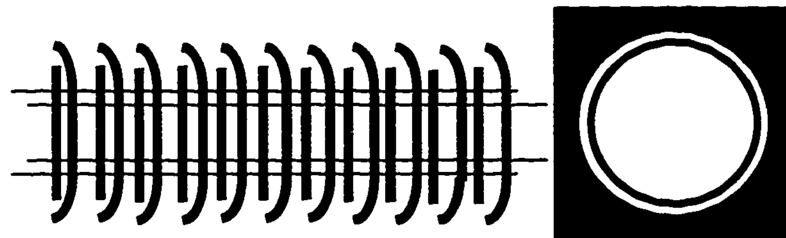

(c) Partially plane wave with no tilt

Figure 4.4 Interference of non-plane waves with a plane wave.

To be more specific, the above interpretation is now applied to the consideration of microlens testing. Ideally, a perfect lens should convert a plane wave into a perfect spherical wave and if the center of a perfect spherical wave is located in the focal plane of a perfect lens, then this wave will be converted into a perfect plane wave. Therefore, two perfect lenses can be aligned in such a way that a plane wave of light going through this arrangement will emerge as a plane wave again (Fig. 4.5). These two lenses can be axially parallel with offset (Fig. 4.5(a)) or without offset (Fig. 4.5(b)).

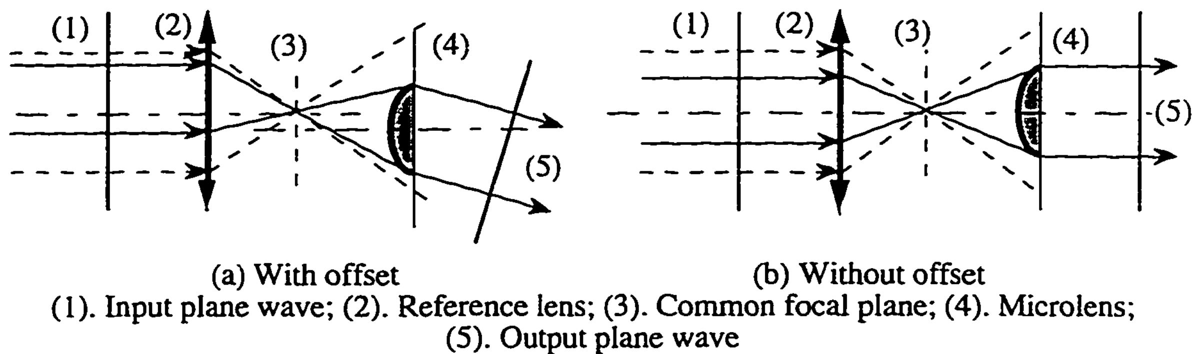

(a) With offset (b) Without offset
(1). Input plane wave; (2). Reference lens; (3). Common focal plane; (4). Microlens; (5). Output plane wave

Figure 4.5 The effect of perfect lenses for plane waves.

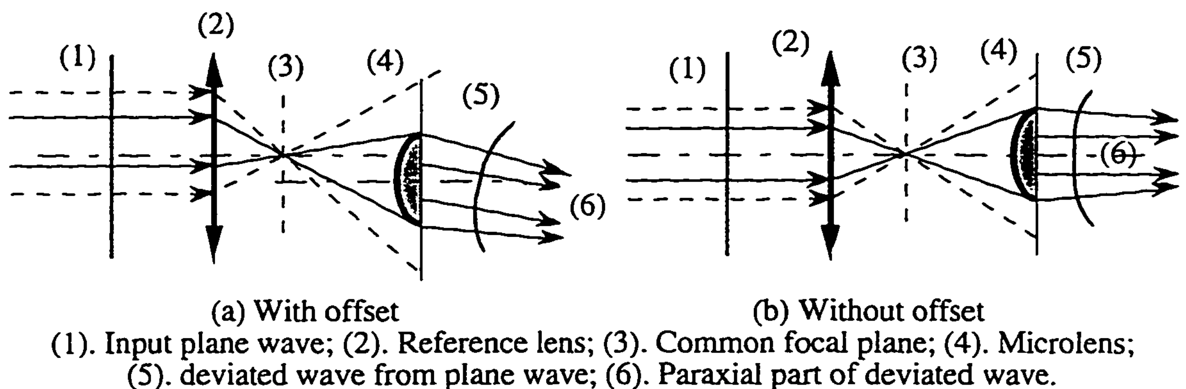

(a) With offset (b) Without offset
(1). Input plane wave; (2). Reference lens; (3). Common focal plane; (4). Microlens; (5). deviated wave from plane wave; (6). Paraxial part of deviated wave.

Figure 4.6 The effect of a nonperfect lens on plane wave.

If, however, one of the two lenses is perfect and the other is not, then the output wave will deviate from a plane wave. When this lens combination is put into one of the two arms of the Mach-Zehnder, interferograms will be generated that can be used to measure the deviations of the test lens from a perfect reference lens. It is also known in optics that for any lens, the paraxial region (very close to the optical axis) can be considered as a perfect reference. Similar to the perfect case, the arrangement in Fig. 4.6 shows one alignment with offset (Fig. 4.6(a)) and the other without offset (Fig. 4.6(b)). In practice, the reference region is taken as the small area in the middle of the lens. This is the underlying principle of microlens wave aberration measurements with a Mach-Zehnder interferometer: the interpretation of interferograms will be based on the assumption that the middle area (considered as paraxial) of the lens under test is ideal.

In practice, by adjusting laterally one of the two lenses in Fig. 4.5 and 4.6 one can vary the tilt of the output wavefront to generate the desired interferogram patterns of Fig. 4.3(a) (perfect lenses) or of Fig. 4.4(b) (aberrated lenses) because the circular and spread out fringes can not be used for lens evaluations. Since the phase difference of two consecutive light (dark) fringes is 2π the distance between these bands is taken as one wavelength for wave aberration measurements.

4.2.2 Set up Requirements

Before this project began, a Mach-Zehnder interferometer had been established in the laboratory for the measurements of small microlenses. A problem with the original configuration was that the set up for each measurement could take half an hour or more and was extremely difficult for lenses of diameters greater than 0.5 mm. Therefore, it was decided to develop a standard procedure simplifying and implementing the use of this tool. The details of the schematic layout of the apparatus is shown in Fig. 4.7.

The very first optical alignment of the apparatus (suggested in Appendix III1) can be fixed for all measurements. However, occasionally the alignment of the input beam at the first beamsplitter cube close to the laser source still needs to be checked to see if any adjustment is necessary. Since the main function of Mach-Zehnder interferometer is to generate interferograms for wave aberration measurement of microlenses under test with respect to reference lenses, the set up in Fig. 4.7 must fulfill the following simultaneous conditions:

1. The reference lens and the lens under test have to be so aligned that in the paraxial region (area in the middle of these lenses) would give an output plane wave if the input beam were a plane wave (collimated beam).
2. The test lens aperture (or perimeter) has to be in focus in the CCD camera.
3. The imaging of the test lens aperture must have the correct magnification such that the image fits into the TV screen without being cut off.

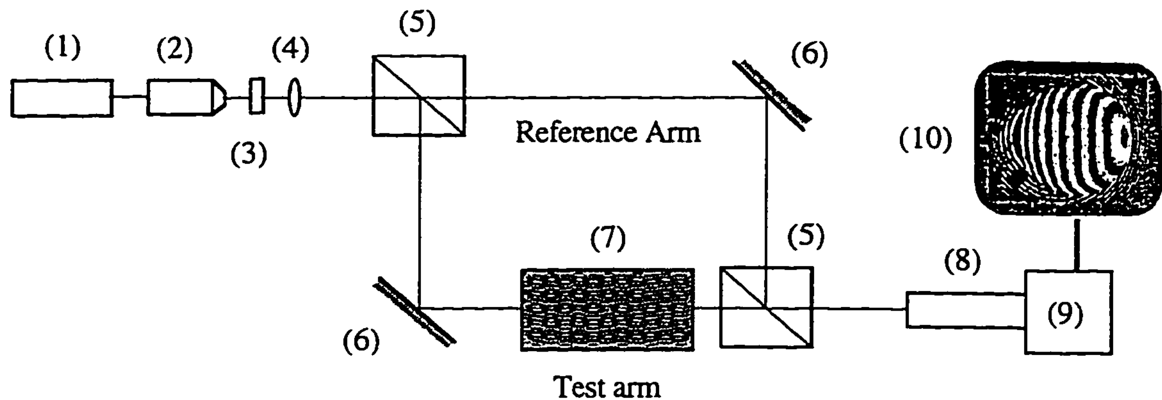

(a) System details

(1). He-Ne laser (λ = 632.8 nm) (2). Microobjectiv as beam expander
(3). Half wave plate for fringe contrast adjustment (4). Beam collimating lens
(5). Polarizing beamsplitter cubes (6). Plane-mirrors
(7). Test combination (Fig. 4.6b) (8). Zoom lens VZM
(9). CCD camera (10). TV monitor

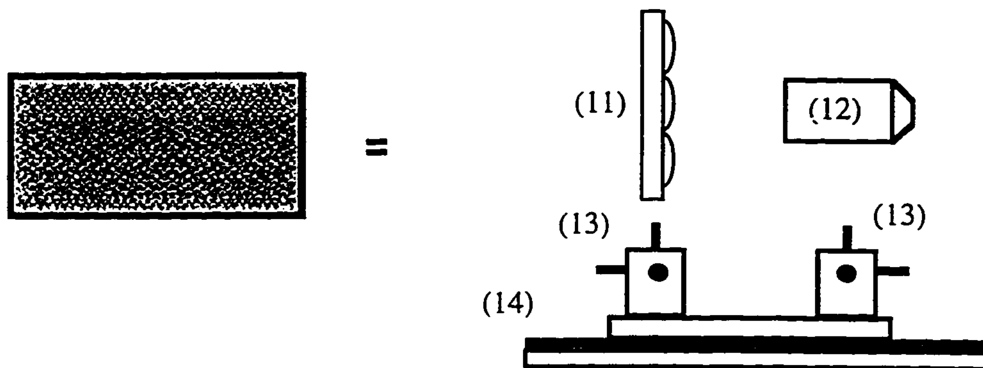

(b) Content of test combination

(11). Substrate with microlenses under test (12). Reference lens (microobjectiv)
(13). Micro-positioners (14). Measuring rail

Figure 4.7 The schematic layout of the Mach-Zehnder interferometer.

The actual views of the components in Fig. 4.7 are shown in Fig. 4.8.

The set up procedure becomes considerably simpler if these requirements are set in separate steps by using the configuration of the test combination in Fig. 4.9(a) for lens diameters less than 0.5 mm and that in Fig. 4.9(b) for those greater than 0.5 mm. For the estimation of the former configuration (refer to Fig. 4.9(a)), the required conditions can be formulated mathematically as follows:

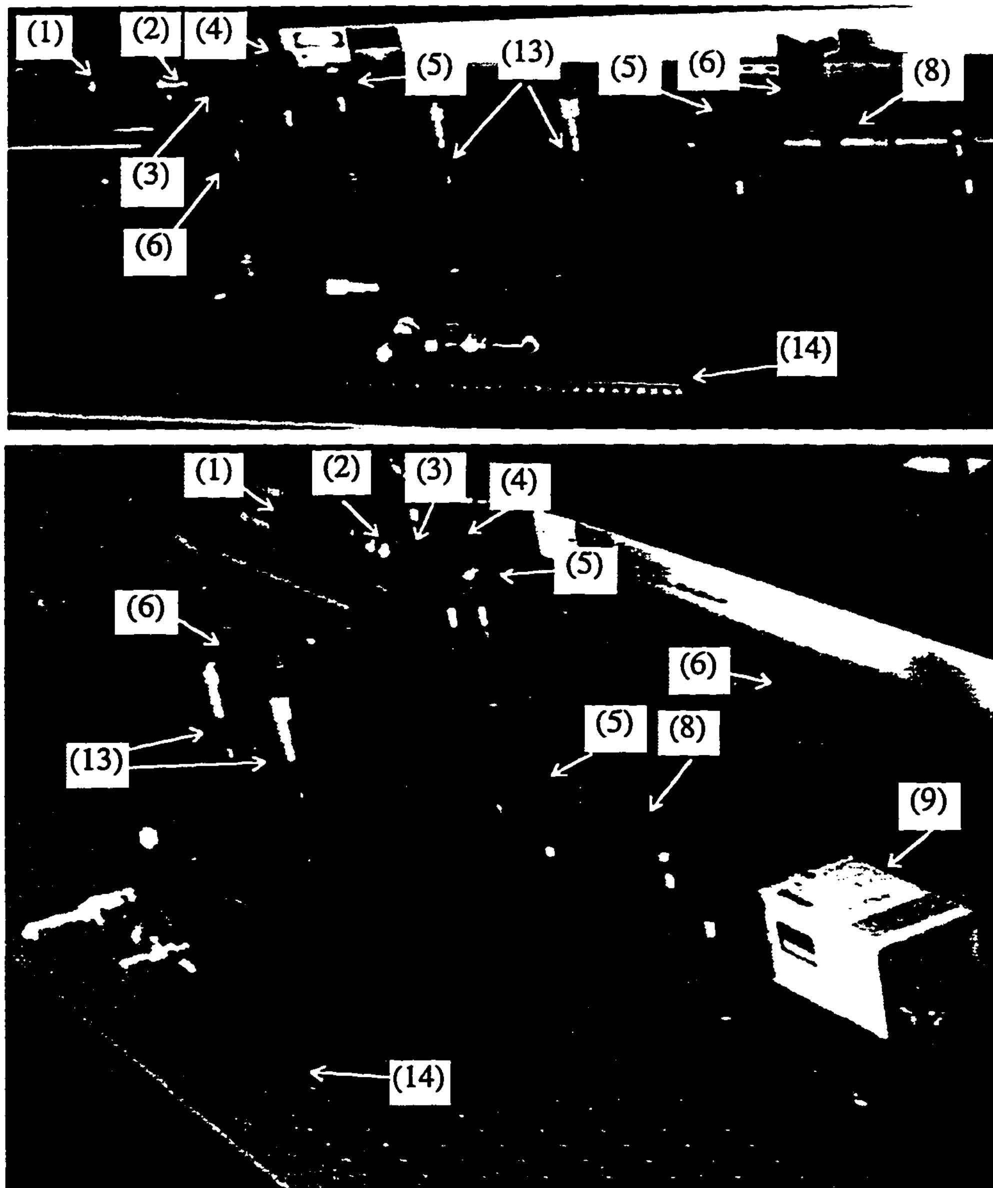

Figure 4.8 Two actual views of the schematic layout in Fig. 4.7 without components 10, 11 and 12.

1. The generation of a plane wave within the paraxial region of microlenses:

$$-s = f_T + f_B \tag{4.2}$$

2. The surface of the microlens aperture is imaged by the reference lens:

$$\frac{1}{s'} - \frac{1}{s} = \frac{1}{f_B} \tag{4.3}$$

3. The magnification is correct: $y_v \geq D_T \frac{s'}{-s}$ (4.4)

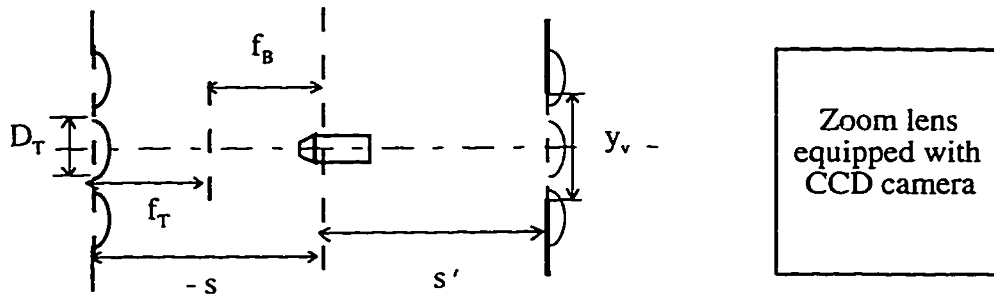

(a) For diameters ≤ 0.5 mm

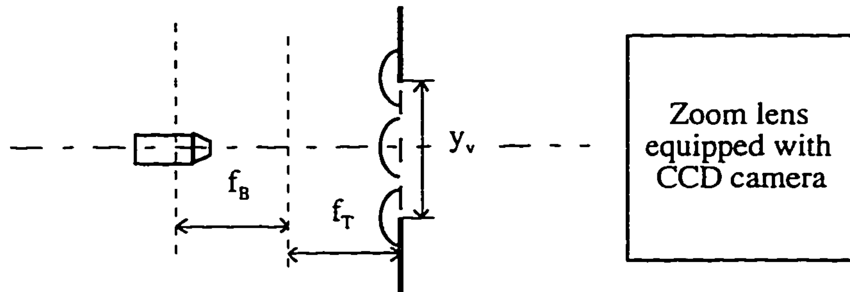

(b) For diameters ≥ 0.5 mm

Figure 4.9 Measurement configurations with Mach-Zehnder interferometer.

where

- s' = Distance from the image of test lens surface to the reference lens
- \- s = Distance from surface of test lens to the reference lens (Note: minus sign for sign convention in Equations (4.3) and (4.4); real object s > 0, virtual object distance s < 0 ; image upright = positive magnification, inverted = negative)
- f_B = Focal length of microobjectiv used as the reference lens
- f_T = Focal length of test lens
- D_T = Diameter of test lens
- y_v = Imaging field of zoom lens (maximum imaging size still displayed on the TV screen for smallest zoom)

For lenses whose diameters are greater than 0.5 mm (refer to Fig. 4.9(b)), these conditions become: $-s = f_T + f_B$ and $D_T \leq y_v$ (4.5)

The solution of the system of Equations (4.2-4) is

$$f_B = \frac{y_v f_T}{D_T} \tag{4.6}$$

$$-s = f_T \frac{(D_T + y_v)}{D_T} \tag{4.7}$$

$$s' = f_T \frac{(D_T + y_v)}{D_T} \frac{y_v}{D_T} \tag{4.8}$$

Finally, the understanding of the imaging mechanism in microlens testing with a Mach-Zehnder interferometer allowed us to develop a procedure for the set up of interferogram generation that presently takes as little as 2 to 5 minutes per measurement and can also be applied for the whole diameter range of interest (0.1 mm to 5 mm). Details of different measurements will be described in the next section.

4.3 TEST PROCEDURES

All different test procedures that have been used to measure the microlens parameters which are of interest are given in this section.

4.3.1 Diameter

The microlens diameter concept and its measurement are quite straightforward. Microlens diameter can be measured either with the Mach-Zehnder interferometer or with an imaging system equipped with a CCD camera as follows:

Mach-Zehnder Interferometer:

This measurement can be done by drawing a cross hair on the TV monitor screen, then the following steps are carried out:

1. Block the reference arm beam.

2. Use the micro-positioners to move the test lens laterally to two different positions (1) and (2) as shown in Fig. 4.10.
3. Diameter of test lens = the difference of two readings in positions (1) and (2).

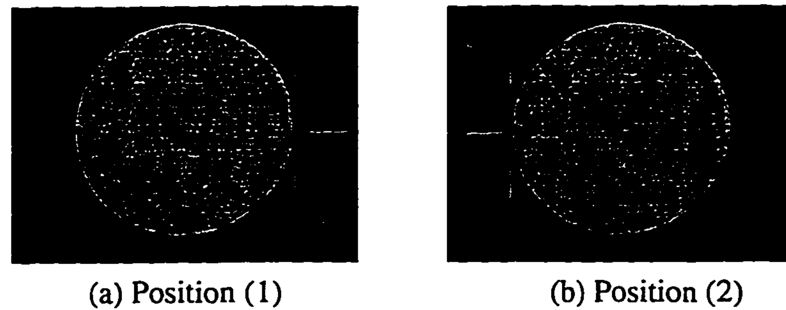

(a) Position (1) (b) Position (2)

Figure 4.10 Positions for lens diameter measurement.

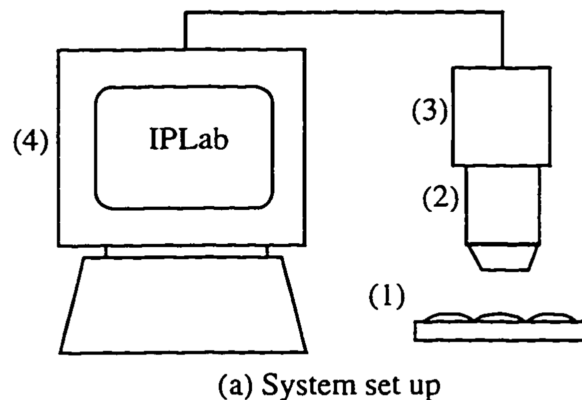

(a) System set up

(1). Substrate carrying microlens (2). Microscope
(3). CCD camera (4). Computer with IPLab software

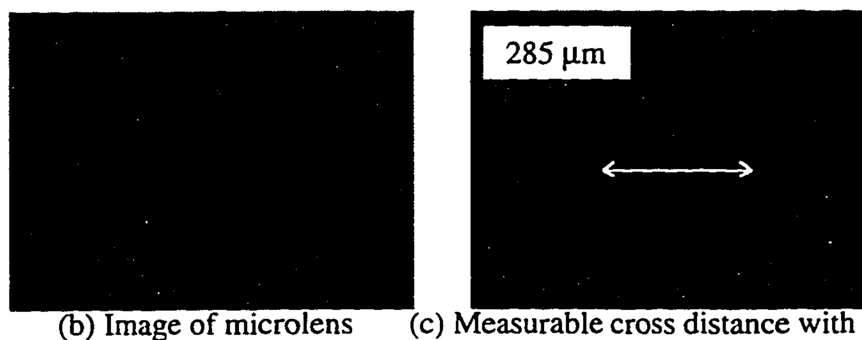

(b) Image of microlens (c) Measurable cross distance with IPLab

Figure 4.11 Set up for diameter measurement with IPLab software.

Imaging System Equipped with CCD Camera:

(a) - By using an imaging software package, IPLab, the set up shown in Fig. 4.11 can be utilized for this measurement in which the distance across the test lens diameter is measured in the number of pixels. The conversion of this number into length is given in Table 4.1.

(b) - Similar to the Mach-Zehnder interferometer the set up in Fig. 4.12 can be used for lens diameter measurements as well.

Table 4.1 Conversion factor for diameter measurement.

Microobjectv	50×	20×	10×	5×	3×
Conversion (pixel/mm)	6860	2713	1548	878	670

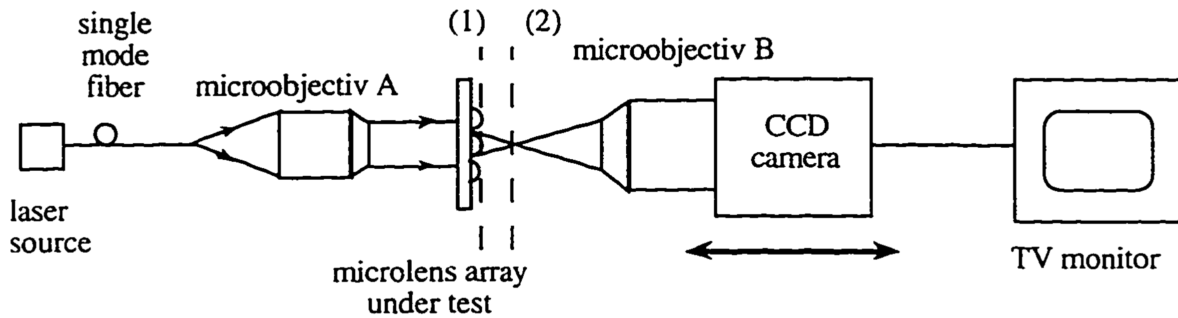

Figure 4.12 Set up for focal length measurement.

4.3.2 Focal Length and Spot Size

Practically, the focal length measurement can be considered as determining the relative position of a focal point from one of several reference points (e.g. lens vertex or lens perimeter) which might cause some confusion. In addition, apart from ideal ray theory, there is no real focal point, but rather a small focused spot of light. Therefore, it is necessary to clarify what is really meant by this measurement in this section.

As was mentioned earlier, all microlenses discussed here are plano-convex made of optical polymers on a substrate or etched into a substrate. The concept of focal points of

these lenses is illustrated in Fig. 4.13 using path of a parallel beam (collimated). The particular geometry makes their focal points different from one lens side to another. For polymer microlenses, the collimated beam is refracted once in (a) and three times in (b). Similarly, etched microlenses refract the incident collimated beam once in (c), but only twice in (d) since the refractive index does not change between the lens and the substrate. It is known in optics that the aberrations are worse when the convex side is nearest the focus (i.e., (a) and (c)). Therefore, the measurements of the focal length and of wave aberration are done on this side. Then, the measured focal length is defined as the distance from the focal point to the surface of the lens aperture (perimeter).

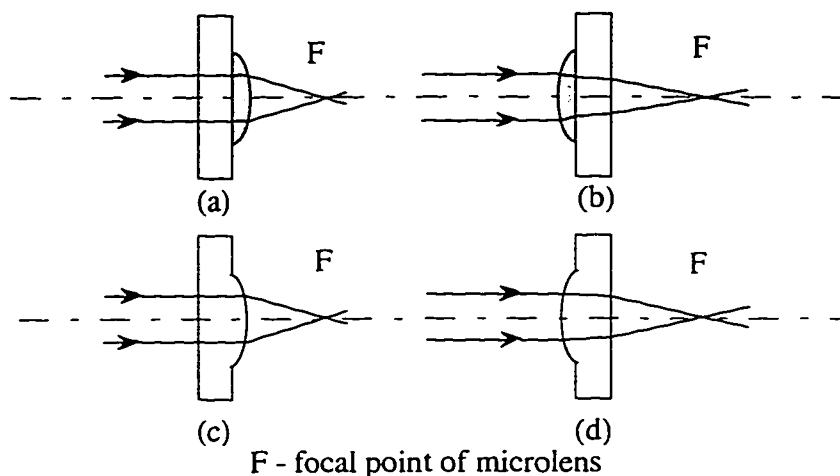

Polymer microlens: (a) light refracted once; (b) light refracted three times.
Etched microlens: (c) light refracted once; (d) light refracted twice.

Figure 4.13 the concept of focal point.

Now, it is necessary to clarify what is meant by the focal point for this measurement. It is also known in optics that the focused spot limited by diffraction (the "waist" of a focused gaussian beam such as a laser beam), and the paraxial focal point of ray theory are not identical. However, for microlenses measured here, the difference is not measurable for the following reasons:

1. The accuracy of the measurement instrument does not allow us to distinguish the difference.

2. The subjective human factor (e.g. deciding when the spot in minimum) is comparable with this difference.

Fortunately, the nature of the present applications allows us to not take this difference into account. Based on these reasons, the focal length and spot size measurements are taken at the position at which the focused spot barely starts to be diffracted. That means the reading of these measurements are taken just before the first diffraction ring of the spot starts to appear.

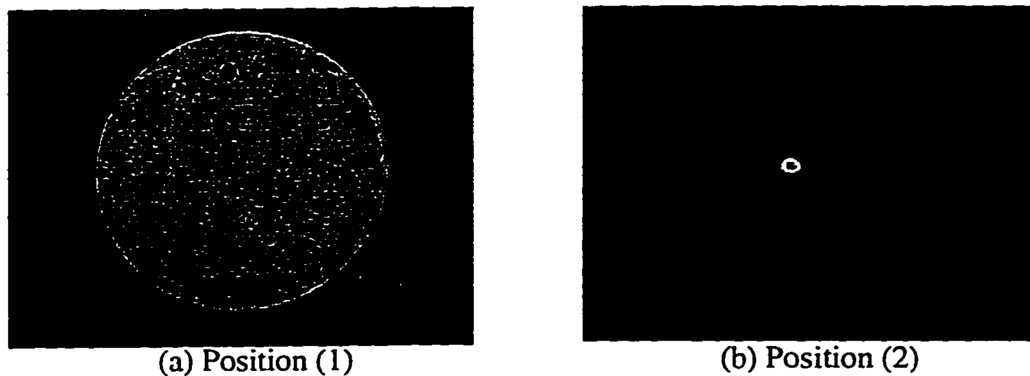

(a) Position (1) (b) Position (2)

Figure 4.14 Positions for focal length measurement.

Using the Mach-Zehnder interferometer (reference arm blocked) or the set up in Fig. 4.12, the focal length measurement can be done by moving the test lens on-axis. The reading will be the difference between positions (1) and (2) as illustrated in Fig. 4.14. At position (2), spot sizes can be measured in the same way as diameters. If the focal length and the diameter of a microlens (circular lenses) are given, the other two parameters commonly used in the practice can be determined:

1. F-number (F#) is sometimes called as the relative aperture, or speed

$$F\# = (\text{focal length})/(\text{ microlens diameter}) \tag{4.9}$$

2. Numerical aperture (NA) of a microlens in free-space is a measure of the half illumination cone

$$NA = \sin\left[\tan^{-1}\left(\frac{1}{2F\#}\right)\right] \tag{4.10}$$

4.3.3 Interferogram Generation and Interpretation

One of important results that can be extracted from interferograms of a microlens is quantitative lens wave aberration. Interferograms of microlenses under test can be generated by using the set up and procedure described in Section 4.2.2 and the following steps are suggested:

1. After the diameter and the focal length of lens under test are determined, one of the test configurations in Fig. 4.9 will be selected.
2. Estimate the necessary microobjectiv for the test combination (reference lens and lens under test). The specifications of system components are summarized in Appendix III2.
3. With the laser on, and no test combination, straight fringes are observed on the TV screen (Fig. 4.15(a)). With a reference lens or a test lens, centered circular fringes are observed (Fig. 4.15(b)).
4. Mount the microlens substrate under test and the reference microobjectiv system (schematically shown in Fig. 4.7) on the micro-positioners so that they are facing each other. If in the middle, centered circular fringes are still observed, move one of these two lenses a small distance laterally for a slight offset.
5. Adjust the microlens substrate under test and the reference microobjectiv system on-axis relatively to each other until interference fringes in the middle of aperture become least curved (the test beam becomes best collimated) and fix this relative position of the two micro-positioners on the part that is movable on the optical rail. Figure 4.15(c) illustrates an example of this display on the TV screen. By setting appropriate attenuators and adjusting the half wave plate, the desired fringe contrast (visibility) can be achieved.
6. Adjust the position of the fixed test combination on-axis along the rail until the aperture of the microlens under test is best imaged on the CCD camera (best displayed on the TV screen). Then fine adjustment is repeated for steps 5 and 6 until

the best result of the measured interferogram is obtained (sharpest image of microlens perimeter and fringes are straight in the middle of the interferogram). Figure 4.15(d) shows an example of an interferogram taken for a microlens under test.

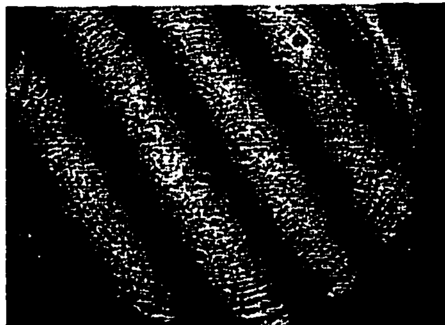

(a) Fringe pattern without test combination

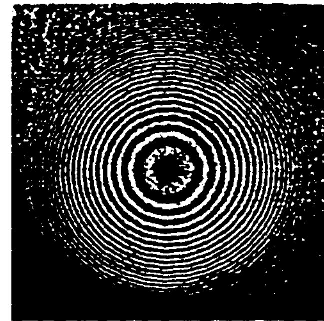

(b) Fringe pattern in presence of either reference or test lens

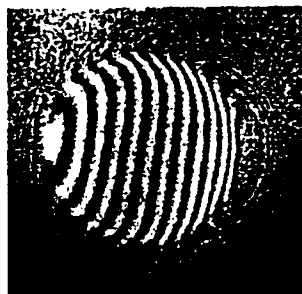

(c) An example for step 5

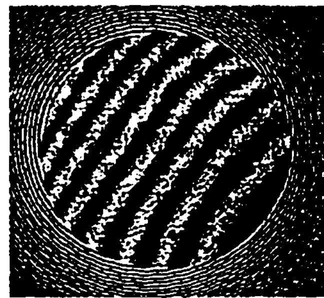

(d) An example of final fringe pattern

Figure 4.15 Display fringe patterns in interferogram generation procedure.

The theoretical background on interpretation techniques for acquired interferograms is given in [39, 44-51] and there are also commercial software packages. However, all wave aberration measurements were done in this project, especially for samples in Chapter 5, by a manual interferogram interpretation procedure given in [45, 46]. If desired, an equation given in [37] allows one to derive the conversion of wave aberration in number of waves, called the optical path difference (OPD), into longitudinal and transverse spherical aberration (LSA and TSA) according to

$$LSA = (OPD) /[(NA/4)^2] \quad (4.15)$$

and

$$TSA = (LSA)[\tan (\sin^{-1}(NA))] \quad (4.16)$$

where LSA for a lens is defined as the maximum deviation from its paraxial focus of the axial intersections of all rays going through this lens and parallel to its optical axis [37]. The wave aberration in length units can be given by multiplying the number of waves with the wavelength used in the measurement.

4.4 SUMMARY

Testing microlenses is an important and indispensable part of the microlens technology. The Mach-Zehnder interferometer is an effective tool for the measurement of microlens parameters, especially for generating interferograms to determine wave aberration. This chapter reviewed briefly characteristics of this equipment and some concepts related to the microlens testing in this project. A standard procedure that was developed simplifies the use of this tool and allows the set up time to be reduced from hours to between 2 and 5 minutes.

In principle, from the interferograms generated by a Mach-Zehnder interferometer, useful information can be extracted with different techniques and appropriate software. So far this apparatus has been used to measure diameter, focal length and wave aberrations of microlenses. To fully take advantage of it, an interferogram interpretation software package could be implemented. This might be an area for further work.

5. INVESTIGATION OF MICROLENS ABERRATION

There are different parameters that affect the wave aberration of microlenses fabricated by the techniques described in Chapters 2 and 3. Prior to this project, theoretical studies showed that negative gravity (defined in Chapter 2) could be used to improve the optical performance of dispensed polymer microlenses [52]. Similarly, changing the etch recipe judiciously during RIE processing (temporal etch selectivity) can also reduce wave aberration of quartz and silicon microlenses [6, 53].

In this chapter, experimental investigations of wave aberration of polymer and etched microlenses are reported. The former were tested for the effect of gravity and the latter for the effect of etch selectivity. Sample preparation is described together with the resulting interferograms that were taken at the wavelength of 632.8 nm and interpreted manually using the procedure mentioned in the previous chapter.

5.1 GRAVITY EFFECT TESTS

Wave aberrations of dispensed polymer microlenses depend strongly on lens shapes which are defined (as shown in Chapter 2) by surface tension and gravity if curing effects are considered separately. In addition, it is also known that the effect of gravity is negligible for small lenses. There is a transition range of diameters for which the aberration progresses from being negligible to being severe. The work in this section is to investigate how wave aberration depends on the lens size. For this work, samples of dispensed polymer lenses on Corning 7059F glass substrate coated with a thin layer of CVD-SiO_2 were prepared as follows:

1. A series of sizes ranging between 0.28 mm and 2 mm (for the transition region investigation) and approximately 2, 3, 4, 5 mm (for large size investigation).
2. Two sets for each size, one of negative and one of positive gravity.

Both sets were dispensed with drops of optical adhesives in sessile position (lens side up). For the set with positive gravity, the lenses were covered for 30 minutes and then cured

with UV-light for 30 minutes. For negative gravity, the lenses were covered and cured in the pendant position for the same time.

5.1.1 Aberrations in the Transition Region

Figure 5.1 shows a series of interferograms of sample lenses in the diameter range from 0.28 mm to about 1.5 mm. Wave aberration gradually gets more severe with increasing lens diameter and becomes very severe for lens diameters of 1.5 mm and higher. There was no difference observed between the effect of positive and of negative gravity.

5.1.2 Aberration of Large Diameter Microlenses

For lens diameters of 2, 3, 4, and 5 mm, wave aberration is very severe even with negative gravity. Figure 5.2 is a series of interferograms taken for these lenses. Various ways of dispensing and of curing were also investigated, but the gravity effect was still very small compared to other distortions. The same effects were observed with polymer lenses dispensed on thin polymer films spun on glass substrates. Figure 5.3 shows interferograms of NOA 63 polymer lenses dispensed on thin films (approximately 0.011 mm) of NOA 63 polymer which were initially spun on Corning 7059F glass substrate for 50 seconds at 500 revolutions per minute (rpm), then at 5000 rpm for 50 seconds. The interferograms in Figures 5.1, 5.2, and 5.3 show some unknown effects which are more dominant than the effect of gravity and make the control of these lens shapes very difficult. Based on conditions under which these lenses were fabricated, some reasons for this wave aberration can be thought of as follows:

1. For large lenses, the localized curing might cause microdistortions of lens shapes. As a result, very severe wave aberration has been observed.
2. Also the curing mechanism might cause variations of refractive index in polymer lenses.

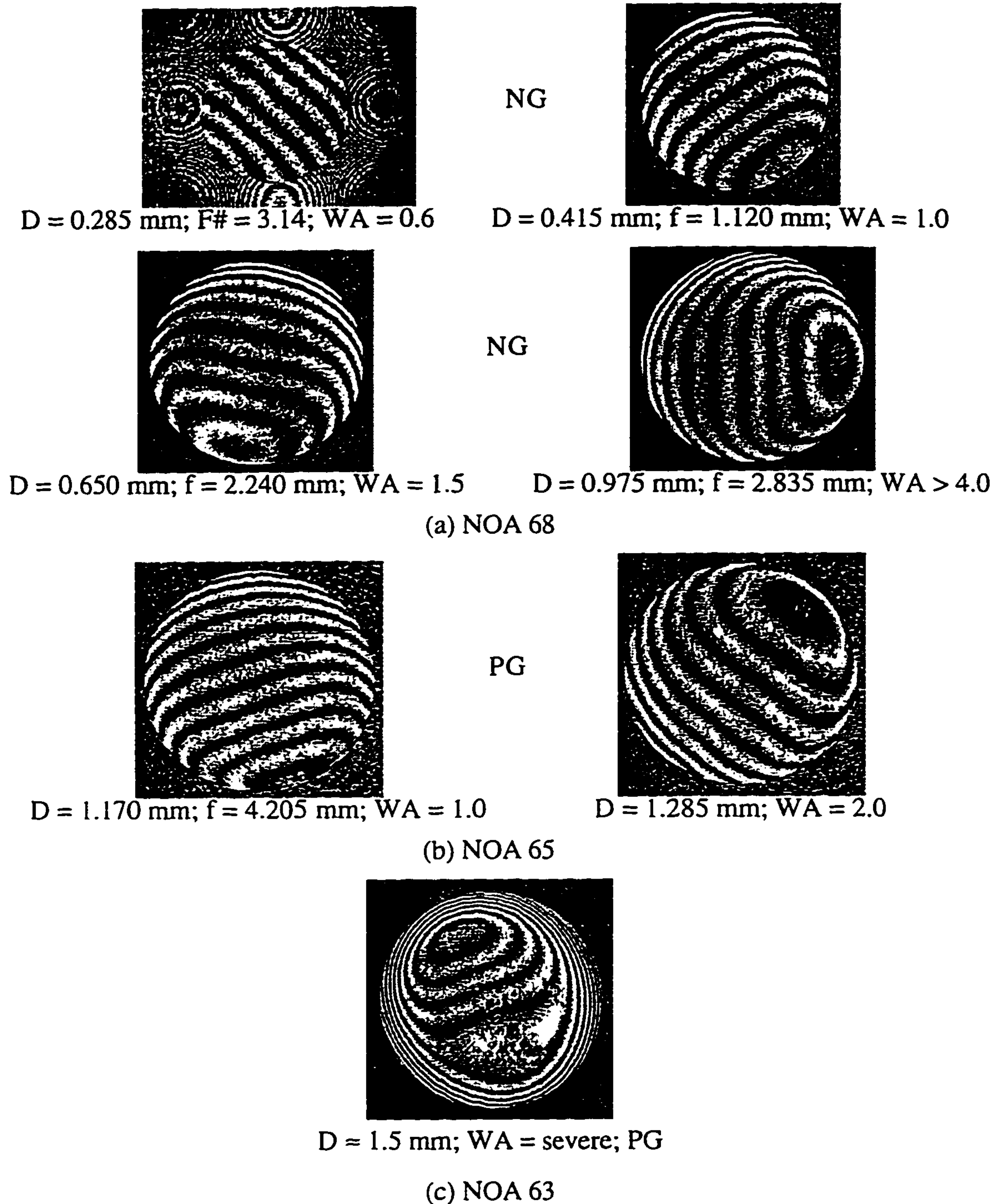

D = Diameter; NG = Negative gravity; PG = Positive gravity;
WA = Wave aberration (in wavelength λ); f = Focal length; F# = f/number

Figure 5.1 Wave aberration of polymer lenses in the transition range.

Negative gravity **Positive gravity**

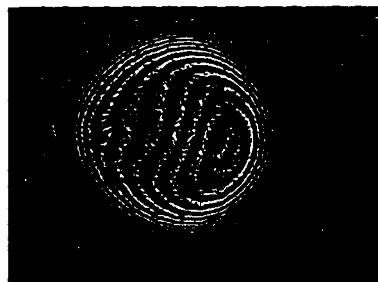

(a) Diameter ≈ 2 mm

(b) Diameter ≈ 3 mm

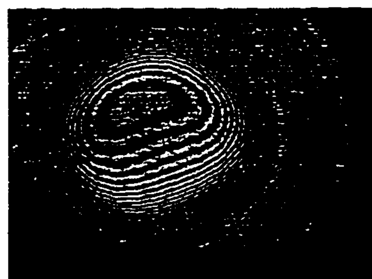

(c) Diameter ≈ 4 mm

(d) Diameter ≈ 5 mm

Figure 5.2 Severe wave aberration of large polymer (NOA 63) lenses.

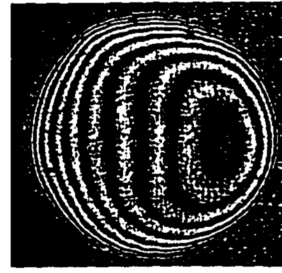

D = 3.600 mm; f = 10.640 mm; NG D = 4.910 mm; f = 15.120 mm; PG

D = Diameter; f = Focal length; PG = Positive gravity; NG = Negative gravity

Figure 5.3 Large polymer lenses dispensed on polymer film (NOA 63 on NOA 63).

5.2 ETCH SELECTIVITY EFFECT TESTS

It is shown in Chapter 3, with the assumptions made in Section 3.2.1, that shapes of etched microlenses can be described in terms of etch selectivity by Equation (3.7). For selectivities not equal 1, this equation describes an arc on the cross-section of an ellipsoid. Based on the preliminary prediction, etched microlenses fabricated with S greater than 1 should show the reduced, but non-optimized, wave aberration. Therefore, an experiment was designed to test the effect of varying S over a large range on the wave aberration of etched quartz microlenses. The samples prepared for this experiment are dispensed polymer microlenses (NOA 68) on quartz substrates. Fig. 5.4 shows the interferograms of three different samples which were etched with different selectivities S = 0.16, 1.00, and 1.78.

In this experiment, the first sample (S = 0.16) shows an immeasurable amount of wave aberration due to the very high F# of the etched lens. The second sample (S ≈ 1.00) shows a measurable amount of aberration which seems to live up to the expectation that wave aberration will go down slightly due to a little higher F# of the quartz lens (same diameter). Only the last sample (S = 1.78) shows a result that seemed unreasonable for two reasons:

1. The height of the etched lens was 40 μm instead of 30.3 μm which is expected for the dispensed polymer microlens height of 17 μm before etching.
2. The etched lens shows that the wave aberration is increased instead of decreased.

Polymer lenses (before etching)	**Quartz lenses (after etching)**
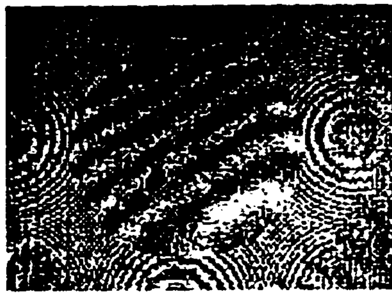	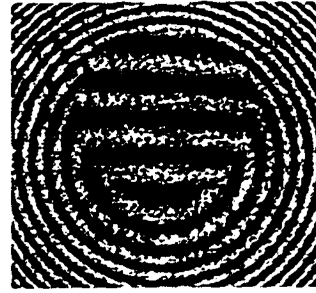
D = 0.291 mm; F# = 3.91; WA = 0.6	D = 0.291 mm; F# = 28; WA = 0.0 S = 0.16
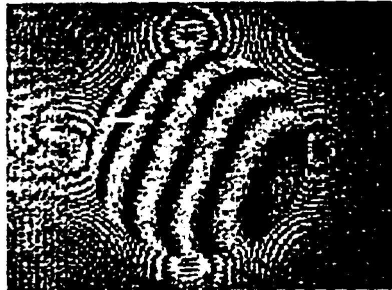	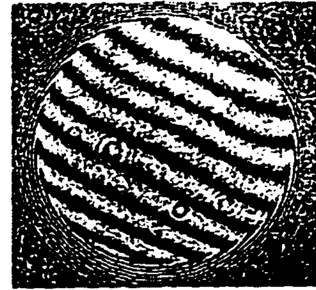
D = 0.285 mm; F# = 3.14; WA = 1.0	D = 0.285 mm; F# = 3.7; WA = 0.6 S ≈ 1.00
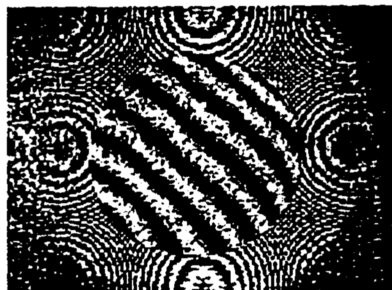	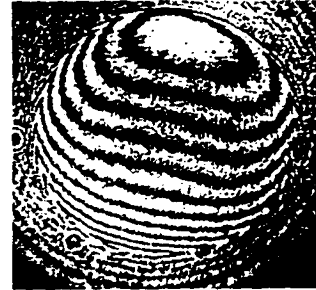
D = 0.305 mm; F# = 4.1; WA = 0.6	D = 0.305 mm; F# = 2.0; WA = 2.5 S = 1.78

D = Diameter; F# = f/number; S = Etch selectivity;
WA = Wave aberration (in wavelength λ).

Figure 5.4 Effect of etch selectivity on wave aberration of quartz microlenses.

Further study, based on ideal lens shapes known in optics as "Cartesian ovals" [54], has shown that for a certain substrate material, the "ideal" cross section profile of an etched microlens has to be either a hyperbola or an ellipse whose eccentricity is a function of the refractive indices (e.g., those of air and the substrate for lenses in free-space). This issue can be the subject of further investigation to test these "ideal" etched microlenses. This work might also need a better understanding of the etch mechanism. At the same time, varying the etch selectivity during the RIE processing (S(t)) is a possible method for generating the desired aspheric shapes of microlenses for more precise applications.

6. CONCLUSION

This chapter summarizes the work completed in this project and concludes with some suggestions for further work.

Work completed

Extending the capability of polymer micro-optics, especially dispensed polymer microlenses, requires characterization work. Based on the study of the liquid lens formation theory, the contact angle of optical polymers was chosen to be measured. A sample series of cylindrical microlenses made of eleven different optical polymers was generated on silicon wafers coated with CVD-SiO_2 by using the dispensing technique. Polymer lens profiles were scanned by the Alpha Step 2000 profilometer. Despite some irregularities of samples, a set of contact angle data was acquired by a selective computation. The relation between the experimental measurements (lens sizes and calculated angles) and the viscosity of the investigated optical adhesives indicates that some of apparent dynamic effects are still observable. Some optical adhesives such as NOA 60, NOA 61, NOA 81, OG 112 and OG 113 which showed unpredictable behaviors while being cured might not be appropriate to the fabrication of dispensed polymer microlenses.

By using dispensed polymer microlenses as an etching mask, the fabrication of fused silica and silicon microlenses was investigated. A process that allows the control F# for a certain microlens design was developed and the etching recipes have been documented.

For microlens testing, the Mach-Zehnder interferometer has been shown to be a very effective tool. To make this apparatus become more useful in the laboratory, a standard operating procedure was developed to simplify its use in different measurements for a wide range of microlens sizes (between 0.1 mm and 5 mm) and to reduce significantly the set up time for each wave aberration measurement. Previously, a minimum of 30 minutes was required, but now these measurements can be completed in 5 minutes or less.

Attempts to reduce microlens wave aberration were made. A number of microlens samples were generated to investigate the change in optical performance of dispensed polymer microlenses due to effect of gravity while curing and of etched microlenses with the effect of etch selectivity. It was found that for large lenses where gravity was expected to affect the lens shape, other curing effects dominate. For etched microlenses, deviations of the etching process from the ideal results in microlenses that still show appreciable aberration.

Further work

The study of the unknown effects on dispensed polymer microlens profiles requires further investigations. A more effective characterization of the dispensed polymer microlens fabrication might be necessary. A fully automated dispensing process is possible by developing the connection between the monitoring system and the control system. The more precise control of etched lens design requires better understanding of the RIE mechanism and probably better etch rate characterization tools as well. However, the change of etch selectivity which results in the change of original lens shapes (dispensed polymer shapes) in a substrate can be used to develop RIE processes with temporal etch selectivity for the fabrication of desired aspheric microlenses. Moreover, looking for better etch rates that can improve the processing effectiveness, especially for S greater than 1, is certainly desirable. It might be worthwhile to carry on the investigation to fabricate etched microlenses of "Cartesian oval" shapes for different application designs. In microlens testing, a versatile interferogram analysis requires the implementation of a software package which can also be used to investigate different types of lens shapes for aberration reduction designs.

REFERENCES

[1] Huey-Daw Wu, F. S. Barnes, **Microlenses** ***Coupling Light to Optical Fibers***, pp 149-214 and pp 279-310, The Institute of Electrical and Electronics Engineers, Inc., New York, 1991.

[2] S. Sinzinger, *et al.*, *Appl. Opt.*, v 34 n 29 pp 6626-6632, Oct. 1995.

[3] W. Singer, *et al.*, *Appl. Opt.* , v 34 n 13 pp 2165-2171, May 1995.

[4] F. A. P. Tooley, *et al.*, *Appl. Opt.*, v 34 n 28 pp 6471-6480, Oct. 1995.

[5] R. Grunwald, *et al.*, *SPIE Proc.*, v 2383 pp 324-333.

[6] M. Eisner, J. Schwider, " Transferring resist microlenses into silicon by reactive ion etching ", *Opt. Eng.* **35**(10), pp 2979-82, Oct. 1996.

[7] M. B. Stern, T. R. Jay, " Dry etching for coherent refractive microlens arrays ", *Opt. Eng.* **33**(11), pp 3547-3550, Nov. 1994.

[8] P. Savander, " Microlens Arrays Etched into Glass and Silicon ", *Optics and Lasers in Engineering*, **20**, pp 97-107, 1994.

[9] K. Mersereau, " Fabrication and measurement of fused silica microlens arrays ", *SPIE Vol. 1751 Miniature and Micro-Optics*, pp 229-33, 1992.

[10] B. P. Keyworth, *et al.*, Single-Step Fabrication of Refractive Microlens Arrays, TRLabs Edmonton, Alberta, Canada T5K 2P7, *Applied Optics*, v 36 n 10 pp 2198-2201, Apr. 1997.

[11] D. J. Corazza, H. Nguyen, *Recent Developments in TRLabs Microlens Technology*, HyPIC semi-annual meeting, TRLabs Edmonton, Alberta, Canada, T5K 2P7, October 28, 1996.

[12] B. P. Keyworth, *et al.*, " Beam Extractor Card for Free-Space Optical Backplanes", *Proc. SPIE*, Vol. 2692, pp 109-113, 1996.

[13] R. Nagarajan, **Diffractive Optics in Optoelectronic Switching**, PhD Thesis Presentation, Department Electrical and Computer Engineering, University of Alberta, Canada, February 24, 1997.

[14] J. C. Berg, **Wettability**, pp 251-301, Marcel Dekker, Inc., 1993.

[15] C. A. Miller, P. Neogi, **Interfacial phenomena *Equilibrium and Dynamic Effects***, surfactant science series vol. 17, Marcel Dekker, Inc., 1985.

[16] R. Defay, et al., **Surface Tension and Adsorption** , John Wiley & Sons, Inc., 1966.

[17] J. T. Davies, E. K. Rideal, **Interfacial Phenomena**, 2nd ed., Academic Press, 1963.

[18] E. Matijevi'c, **Surface and Colloid Science**, Vol 2, John Wiley & Sons, Inc., 1969.

[19] E. Matijevi'c, **Surface and Colloid Science**, Vol 1, John Wiley & Sons, Inc., 1969.

[20] R. J. Stephenson, **Mechanics and Properties of Matter**, 3rd ed., pp 299-321, John Wiley & Sons, Inc., 1969.

[21] R. A. Heidemann, et al., **An Introduction to the Properties of Fluids and Solids**, pp 264-267, The University of Calgary Press, 2500 University Drive, Calgary, Alberta, Canada T2N 1N4, 1984.

[22] J. Bauer, G. Drescher, M. Illig, " Surface tension, adhesion and wetting of materials for photolithographic process", *J. Vac. Technol.* B 14(4), pp 2485-2492, Jul/Aug 1996.

[23] A. H. Cottrell, **The Mechanical Properties of Matter**, John Willey & Son, Inc., 1964.

[24] J. F. Holzman, Optical and RF Developments in Hybrid Integrated Opto-Electronic Device, coop-student report at TRLabs, Edmonton, Alberta, Sept. 1996.

[25] Norland Products Inc., Tel. (908) 545-7828, 695 Joyce Kilmer Ave., New Brunswick, N. J. 08902 USA.

[26] Z. D. Popovic, et al., " Technique of monolithic fabrication of microlens arrays ", *Appl. Opt.*, **27**(7), pp1281-1284, 1988.

[27] D. Daly, et al., " The manufacture of microlenses by melting photoresist ", *Meas. Sci. Technol.*, **1**, 1990.

[28] N. F. Borelli, et al., " Photolythic technique for producing microlenses in photosensitive glass ", *Appl. Opt.*, **24**, pp 2520-5, 1985.

[29] M. Oikawa, et al., " Array of distributed-index planar micro-lenses prepared from ion exchange technique ", *Jpn J. Appl. Optics*, **20**, pp 296-8, 1981.

[30] G. Nakagawa, et al., " High Efficient Coupling Between LD Array and Optical Fiber Array Using Si Microlens Array ", *IEEE Photon. Technol. Lett.*, **5**(9), pp 1056-58, Sept. 1993.

[31] M. A. Lieberman, A. J. Lichtenberg, **Principles of Plasma Discharges and Materials Processing**, John Wiley & Sons, Inc., 1994.

[32] J. W. Corburn, **Plasma Etching and Reactive Ion Etching**, The American Vacuum Society, 1982.

[33] Ch. Steinbruechel, et al, "Mechanism of Dry Etching of Silicon Dioxide", *J. Electrochem. Soc.*, Solid-State Science and Technology, Vol.132, No. 1, 1985.

[34] K. Mersereau, et al., " Testing and measurement of microlenses ", pp 210-215, *SPIE Vol. 1992 Miniature and Micro-Optics and Micromechanics*, 1993.

[35] M. C. Hutley, et al., " The testing of microlens arrays ", *Microlens Arrays*, M. C. Hutley, Ed., Institute of Physics Short Meetings Series **30**, pp 67-87, 1991.

[36] N. Lindlein, J. Schwider; *Interferometric Test for Micro-Optics*, Vol. 5, pp 288-291, Technical Digest Series (Optical Society of America, Washington DC),OSA , 1996.

[37] W. J. Smith, **Modern Optical Engineering the design of optical systems**, 2nd ed., McGraw-Hill, Inc., pp 281-286, 1990.

[38] H. Haferkorn, **OPTIK: physikalisch-technische Grundlagen und Anwendungen**, VEB Deutscher Verlag der Wissenschaften, Berlin DDR, 1981.

[39] H. Haferkorn, **Bewertung optischer Systeme**, VEB Deutscher Verlag der Wissenschaften, Berlin DDR, 1986.

[40] W. H. Steel, **Interferometry**, Cambridge University Press, 2nd ed., 1983.

[41] G. Schulz, " Zweistrahlinterferenz in Planspiegelanordnung I und II ", *Opt. Acta* **11**, pp 43-60 and pp 131-143, 1964.

[42] G. Schulz, J. Schwider, " Zweistrahlinterferometer, Lichtquellenbild-Transformation als Schraubung und neue Effekte an Interferenzstreifen ", *Optik* **21**, pp 587-597, 1964.

[43] J. Schwider, et al., " Twyman- Green interferometer for testing microspheres ", *Opt. Eng.* **34**(10), pp 2972-75, Oct. 1995.

[44] H. Sickinger, et al., "Characterization of microlenses using a phase-shifting shearing interferometer", *Opt. Eng.* **33**(8), pp 2680-86, Aug. 1994.

[45] D. Malacara, **Optical Shop Testing**, John Wiley & Sons, 1978.

[46] A. H. Guenther, D. H. Liebenberg, **Optical interferograms-reduction and interpretation**, American Society for Testing and Materials, 1978.

[47] J. Schwider, " Advanced evaluation techniques in interferometry ", in **Progress in Optics**, vol. XXVIII, pp 273-353, E. Wolf editor, Elsevier Science Publishers B. V., 1990.

[48] K. Creath, " Phase-Measurement Interferometry Techniques ", in **Progress in Optics**, vol. XXVI, pp 351-393, E. Wolf editor, Elsevier Science Publishers B. V., 1990.

[49] J. Schwider, et. al., " Digital wave-front measuring interferometry: some systematic error sources ", *Appl. Opt.*, **22**(21), pp 3421-32, 1983.

[50] J. Bruning, et al., "Digital Wavefront Measuring Interferometer for Testing Optical Surface and Lenses", *Appl. Opt.*, **13**(11), pp 2693-2703, 1974.

[51] D. Nyyssonen, J. M. Jerke, " Lens Testing with a Simple Wavefront Shearing Interferometer ", *Appl. Opt.*, **12**(9), pp 2061-70, 1973.

[52] B. P. Keyworth, *et al.*, **OSA Annual Meeting & Exhibit**, paper WVV52, Oregon Convention Center, Portland, Oregon, USA, Sept. 10-15, 1995.

[53] K. Mersereau, et al., **Diffractive Optics and Micro-Optics**, paper DMB1, Technical Digest Series, Vol. 5, April 29 - May 2, 1996.

[54] E. Hecht, **Optics**, 2nd ed., pp 129-32, Addison-Wesley Publishing Company, 1990.

APPENDIX I

Profilometer Scans of Cylindrical Polymer Lenses:

Axes: Measured in µm

Graph notation:

- Negative gravity (**a**)
- Positive gravity (**b**)

NOA 60: Viscosity 300 cps @ 25 degrees C

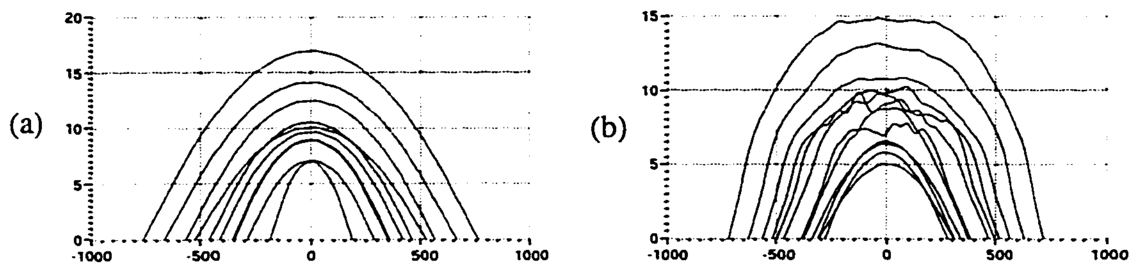

NOA 61: Viscosity 300 cps @ 25 degrees C

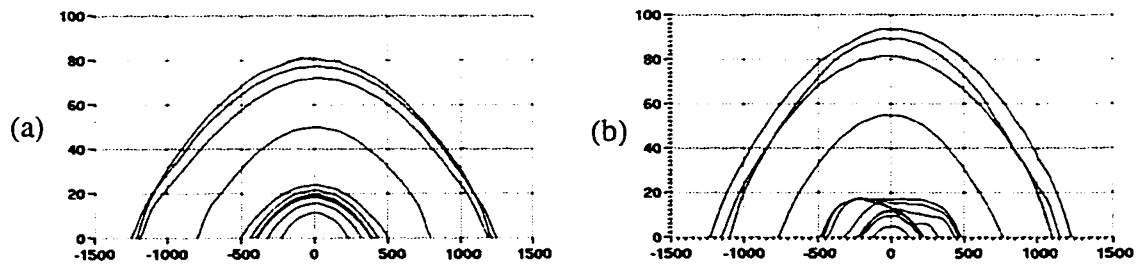

NOA 81: Viscosity 300 cps @ 25 degrees C

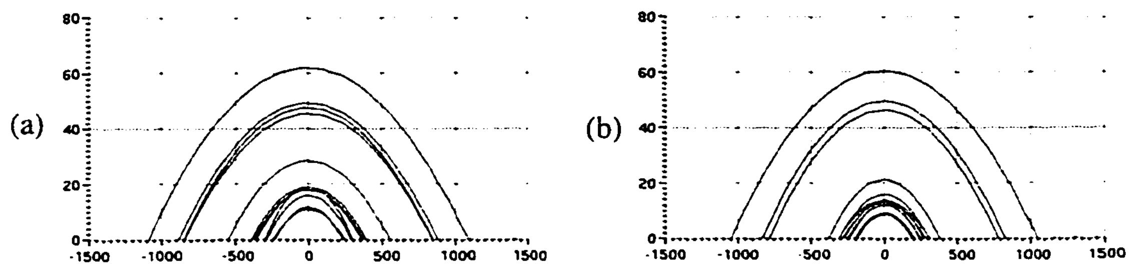

OG 112: Viscosity 965 cps

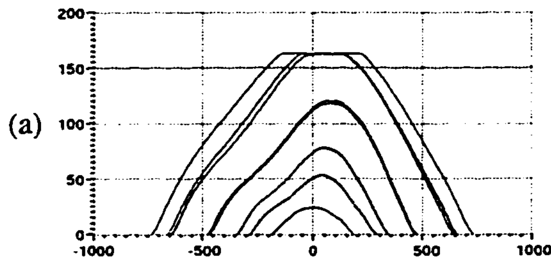

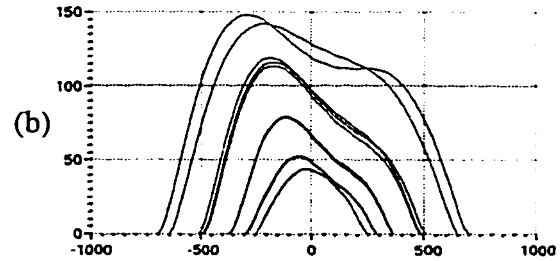

OG 113: Viscosity 143 cps

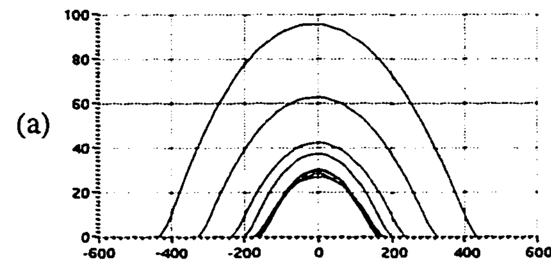

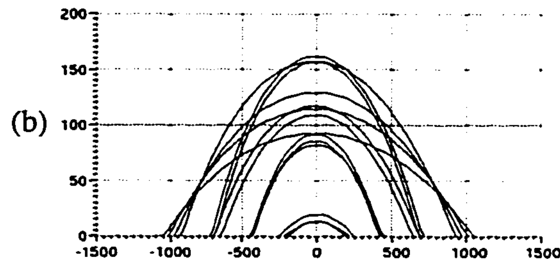

OG 115: Viscosity 4900 cps

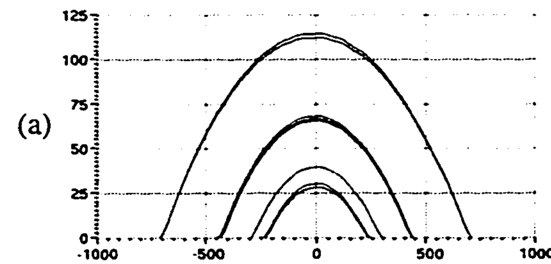

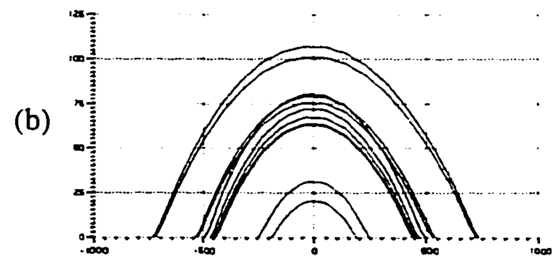

OG 116: Viscosity 34000

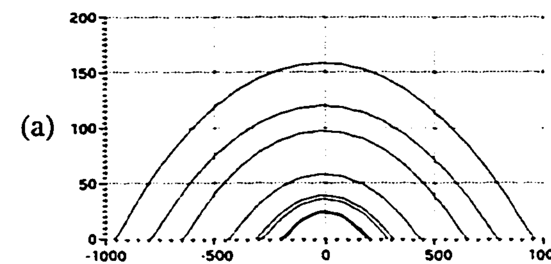

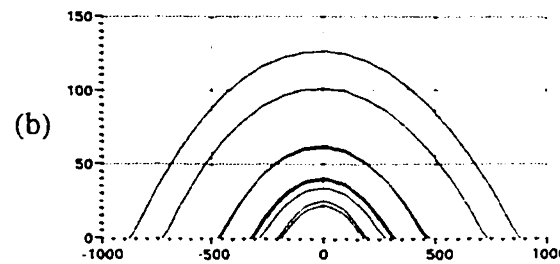

UVO 114: Viscosity 300 - 700 cps (23 degrees C @ 100 rpm)

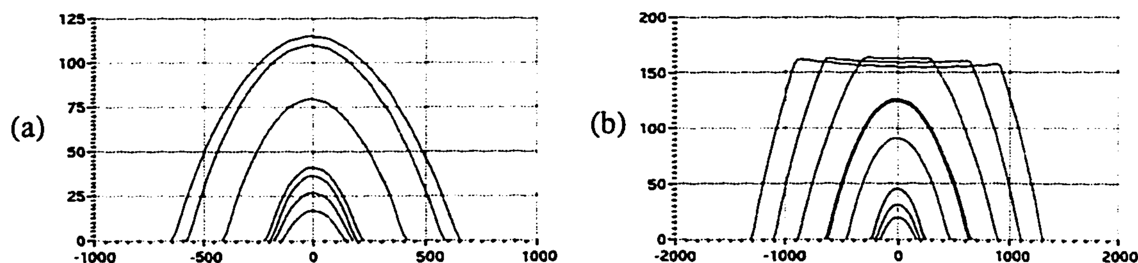

Table I.1 Measurement results for various polymers.

W/2 = Half width of the cylindrical microlens in μm

α = Experimental contact angles in (°)

NG = Negative gravity; PG = Positive Gravity

cured	NOA 60		NOA 61		NOA 63		NOA 65	
	W/2	α	W/2	α	W/2	α	W/2	α
NG	185.9	3.6	228.2	5.7	153.1	13.0	642.0	2.1
	288.5	2.4	320.9	5.7	160.0	14.6	644.1	2.1
	348.8	2.5	387.7	6.2	165.6	15.1	927.0	2.7
	357.5	2.4	397.6	5.9	166.3	14.6	946.1	2.8
	415.7	2.3	398.4	5.9	224.0	15.6	965.1	2. 6
	523.0	1.9	434.1	6.1	231.3	13.4	1079.5	3.2
	564.9	2.2	503.2	5.8	240.7	15.6	1105.1	3.3
	662.4	2.1	795.7	11.0	297.0	15.9	1105.5	3.1
	759.0	2.2	1186.2	9.9	320.9	16.7	1129.1	3.4
			1208.7	12.1	418.1	16.4	1200.4	3.7
			1246.5	9.3	420.9	17.2	1243.1	3.9
					444.6	17.2		
					724.8	17.2		
					892.2	18.3		
PG	282.3	2.1	203.3	4.7	149.3	12.0	649.7	2.6
	308.8	1.5	216.0	5.8	150.3	12.3	649.8	2.6
	313.2	2.0	225.7	5.2	154.0	12.3	650.5	2.6
	340.4	1.8	255.2	3.5	246.2	13.7	662.4	2.6
	374.7	2.2	322.5	5.8	265.1	14.1	940.6	2.8
	385.6	2.7	439.3	8.6	324.3	14.5	970.1	2.7
	466.4	2.7	465.7	9.9	340.8	14.8	1103.2	3.1
	496.7	3.5	480.1	9.4	448.1	15.6	1113.0	3.3
	516.7	3.5	763.0	9.8	478.31	15.7	1164.8	3.7
	563.7	3.7	1098.7	13.9	509.0	16.0	1242.1	3.6
	626.4	4.3	1155.8	11.4	617.3	16.4	1370.9	3.9
	718.4	4.3	1230.9	13.7	771.4	16.6	1459.9	4.2
					943.9	17.7		

(see pages 88 and 89 for the rest of the table)

cured	NOA 68		NOA 81		OG 112		OG 113	
	W/2	α	W/2	α	W/2	α	W/2	α
NG	172.6	14.8	230.6	5.1	183.5	12.6	157.2	17.5
	264.2	16.2	244.7	4.4	185.5	13.1	163.2	17.7
	274.9	15.6	286.5	5.8	283.3	16.9	163.9	17.1
	313.8	16.2	298.6	6.7	286.5	17.0	172.3	15.4
	387.3	15.0	354.7	5.5	340.3	21.1	198.3	19.2
	470.2	15.5	373.2	5.1	341.0	21.6	233.9	18.8
	499.1	15.6	392.0	5.2	462.9	24.1	325.4	20.7
	537.5	15.9	554.2	5.7	474.7	24.3	432.9	23.9
	729.1	16.5	841.0	6.0	640.2	24.6		
	769.2	16.3	846.1	6.4	657.7	23.9		
			882.6	6.3	729.8	24.5		
			1088.2	6.5				
PG	246.5	15.9	188.0	4.5	245.7	17.5	184.3	7.0
	259.1	16.4	206.9	4.1	245.8	18.2	211.8	6.0
	277.3	16.4	241.0	5.2	288.8	17.6	249.1	8.0
	304.7	17.2	251.0	5.0	292.0	17.9	428.0	21.6
	385.1	17.2	274.8	5.0	360.6	26.3	442.5	27.1
	486.9	17.2	284.5	4.7	365.2	25.9	448.8	19.8
	471.1	17.7	308.2	5.4	484.3	30.2	648.6	19.5
	531.0	17.5	383.4	5.9	487.6	30.6	694.7	25.1
	725.9	18.0	783.3	6.6	507.0	30.7	695.8	19.5
	763.9	17.7	830.2	6.7	647.5	29.1	719.7	25.6
			1047.8	6.2	696.6	31.4	933.1	20.2
							975.0	15.7
							1016.1	13.4
							1051.0	10.5

cured	OG 115		OG 116		UVO 114			
	W/2	α	W/2	α	W/2	α		
NG	230.8	12.6	186.3	12.6	145.1	11.0		
	235.9	13.4	197.9	11.9	178.3	15.1		
	294.9	14.5	201.3	12.3	196.3	19.1		
	433.5	17.0	286.0	13.1	220.9	19.7		
	437.3	17.1	313.2	13.1	413.5	22.0		
	439.3	16.7	437.5	14.5	583.1	22.1		
	443.7	17.3	649.0	17.1	653.4	20.8		
	706.6	18.4	792.6	17.3				
	708.4	18.8	959.3	19.3				
	846.6	17.5						
	850.6	17.5						
PG	189.2	10.8	184.0	11.8	164.1	11.7		
	246.3	13.3	198.5	12.5	200.0	15.8		
	440.3	16.0	277.9	12.8	236.4	20.5		
	445.0	16.0	310.0	13.5	243.1	19.9		
	454.5	16.6	321.5	13.3	467.7	22.5		
	466.9	17.5	460.1	15.1	637.8	23.2		
	493.4	18.7	471.9	14.4	655.4	23.1		
	526.7	16.3	730.1	16.3	890.0	24.9		
	536.6	16.7	876.5	16.9	1105.3	26.8		
	722.3	16.2			1311.4	27.9		
	733.5	16.8						

APPENDIX II

FABRICATION PROCEDURE FOR ETCHED LENSES

1. Substrate Cleaning by Piranha Process

the safety procedures are strictly applied

- **Piranha mixture:** mix 1800 ml of H_2SO_4 (sulfuric acid) with 600 ml of H_2O_2 (hydrogen peroxide) using Teflon container.
- **Cleaning steps:** as an option substrate can be cleaned by ultra sonic process before these steps are carried out.
    1. Put substrate into Teflon holder.
    2. Rinse substrate with acetone.
    3. Wash the substrate with deionized water for 2 or 3 cycles.
    4. Dry the substrate with dry air.
    5. Immerse the substrate deep into container of piranha solution for 15 to 20 minutes.
    6. Wash the substrate with deionized water again for 2 or 3 cycles.
    7. Dry with dry air.

2. Dispensing Polymer Patterns

Use the dispensing technique in Chapter 1.

3. Etching by RIE

Steps used in etching

1. Estimate the complete time-to-etch from the ratio of lens height and the polymer etch rate of selected etch recipe. The actual running time is usually 10% longer than the estimated one.

2. Before running any etching process the RIE chamber needs to be cleaned for about 10 to 30 minutes depending on previous condition of RIE chamber.
3. Put the substrate into the RIE chamber and run the system with the selected recipe. As an option, the system can be preconditioned by running the desired recipe without substrate.
4. Inspect for complete etch using transmission microscope.

APPENDIX III

1. OPTICAL ALIGNMENT FOR MACH-ZEHNDER INTERFEROMETER

The following steps are suggested for the alignment of optical components (refer to Fig. 4.7 for number codes):

1. Turn on the He-Ne laser (1) and mark its spot at a distance (usually on a wall)
2. Insert and adjust the beam expander (microobjectiv (2) and bulk lens (4)) so that the new spot falls with the originally marked spot together.
3. Insert one of two plane-mirrors (6) between the lens (4) the and first marked spot, then align the reflected beam from this mirror approximately perpendicular to the beam from the laser. Make second mark for the beam from the mirror (again another wall can be used).
4. Insert one of the polarizing beamsplitter cube (5) between the lens (4) and the mirror just inserted. Adjust the cube until the spot of the laser beam from the first mirror covers the second mark.
5. Insert the second polarizing beamsplitter cube (5) between the first mirror and the second mark and adjust the cube so that the beam spot covers the mark again.
6. Insert the second mirror (6) into the path of the reflected beam from the first cube to reflect this beam to the second cube.
7. There will be two spots of laser light observed. Adjust the second mirror until these spots approximately overlap each other. Double check and do some fine adjustment on cubes or mirrors if it is necessary.

This alignment can be kept the same for all measurements. Occasionally, the beam quality after the beam expander needs to be checked, usually only minor adjustments will be required.

2. OPTICAL ELEMENTS FOR INTERFEROGRAM GENERATION

Table III.1 Zoom lens VZM 0.7× – 4.5×.

Specifications	Unit
Magnification Primary Objective	0.7× – 4.5×
Magnification (1/2" CCD/13" Monitor)	28 - 180×
Working distance	95 mm
Field of view (1/2" CCD/Diag.)	11.4 mm - 1.7 mm
Resolution	18 LP/mm @ 0.7× and 90 LP/mm @ 4.5×
Length	236 mm
Diameter	40 mm
Weight	15 oz.

Table III.2 Microobjectives

Model	Focal length (mm)	Working distance (mm)	Clear aperture (mm)	Numerical aperture
M - 5×	25.5	15.0	7	0.1
M - 10×	14.8	6.0	8	0.25
M - 20×	8.3	1.9	7	0.40
M - 40×	4.3	0.4	6	0.65
M - 60×	2.9	0.3	5	0.85